

SENSITIVITY ANALYSIS OF PRODUCTION VARIABLES OF GEOPOLYMER
CEMENT CONCRETE TO MECHANICAL AND DURABILITY
CHARACTERISTICS

by

Maria Beci Yesenia Trejo

A thesis submitted to the faculty of
The University of North Carolina at Charlotte
in partial fulfillment of the requirements
for the degree of Master of Science in
Civil Engineering.

Charlotte

2016

Approved by:

Dr. Brett Tempest

Dr. Janos Gergely

Dr. Tara Cavalline

©2016
Maria Beci Yesenia Trejo
ALL RIGHTS RESERVED

ABSTRACT

MARIA BECI YESENIA TREJO. Sensitivity Analysis of Production Variables of Geopolymer Cement Concrete To Mechanical and Durability Characteristics. (Under the direction of DR. BRETT Q. TEMPEST)

Geopolymer cement is an alternative binder manufactured from fly ashes that can fully replace portland cement in traditional reinforced concrete applications. As a viable material for precast components, geopolymer features very rapid strength development and the ability to be prepared using typical concrete equipment. This study focused on a sensitivity analysis of three base mixture designs of geopolymer cement concrete (GCC) with compressive strengths ranging from 1500-6000 psi (10.3-41.4 MPa). The fresh concrete properties including slump flow, air content, and temperature were measured and correlated to the mechanical properties including the compressive strength, modulus of rupture, and modulus of elasticity. The main purpose of the sensitivity analysis is to determine the level of influence of typical production variables on the resulting mechanical properties of the concrete. The production variables, such as, water to cementitious materials ratio (w/cm), curing temperature, and curing duration are each known to impact the compressive strength and elastic properties of GCC. Regression analysis was used to determine the level of influence of each production variable on mechanical properties. The interactions between changes in the production variables were also studied to determine if a combination of variables may have a greater net impact on the mechanical properties of the concrete. From the analysis, we find that as we adjust production variables we can influence the resulting compressive strength. These relationships have been illustrated with the regression models. This study also

characterized the freeze thaw durability of GCC. The study resulted in improved freeze-thaw durability of GCC for a 2% to 3% air content range compared to the same range in portland cement concrete (PCC).

DEDICATION

Para mi Mamá y Papá, a quienes les debo el origen de todas mis oportunidades.

Gracias.

ACKNOWLEDGEMENTS

This thesis and study could not have been completed without the support, direction, and input of my faculty advisor (Dr. Brett Tempest), faculty advisors, the Precast/Prestressed Concrete Institute (PCI) Daniel P. Jenny Fellowship Committee, Georgia-Carolinas PCI, Metromont, Inc., research assistants, countless friends, and my family. Thank you.

TABLE OF CONTENTS

LIST OF TABLES	xi
LIST OF FIGURES	xiv
CHAPTER 1: INTRODUCTION	1
1.1 Background	1
1.2 Scope of Research	2
1.3 Thesis Arrangement	2
CHAPTER 2: GEOPOLYMER CEMENT CONCRETE BACKGROUND	4
2.1 Development Background	4
2.2 GCC Preparation	5
2.2.1 Source Material	5
2.2.2 Activating Solution	5
2.2.3 Curing Process	6
2.3 Sustainability Benefit	7
2.4 Economic Progress	10
2.5 U.S. Department of Energy Solar Decathlon: UNC Charlotte 2013	14
2.5.1 GCC Development and Production Process	16
2.5.2 Activating Solution	19
2.5.3 Concrete Mixing and Casting	19
2.5.4 Concrete Curing	21
2.5.5 Industry Perspective	21
2.5.5.1 Interviews with Metromont, Inc. Employees	22

	viii
2.5.5.2 Economic Analysis	23
CHAPTER 3: PREPARATION, MIXING, AND CASTING OF SAMPLES	25
3.1 Mixture design	25
3.1.1 Fly Ash	27
3.1.2 Activating Solution	27
3.1.3 Aggregates	29
3.2 Sample Breakdown	29
3.3 Mixing	31
3.4 Casting	32
3.5 Curing Regimen	32
3.6 Fresh Concrete Properties	32
3.6.1 Temperature After Mixing	33
3.6.2 Slump Flow	34
3.6.3 Air Content	39
CHAPTER 4: MECHANICAL PROPERTIES OF HARDENED CONCRETE	41
4.1 Literature Review	41
4.1.1 Hardjito et al. (2004)	42
4.1.2 Khale and Chaudhary (2007)	45
4.1.3 Hardjito and Rangan (2005)	46
4.1.4 Vora and Dave (2013)	47
4.1.5 Tempest et al. (2016)	50
4.2 Specimen Preparation	51
4.3 Parameters of Analysis	51

	ix
4.3.1 Water To Cementitious Materials Ratio (<i>w/cm</i>)	52
4.3.2 Curing Temperature	52
4.3.3 Curing Duration	52
4.4 Mechanical Properties Affected	53
4.4.1 Compressive Strength	53
4.4.2 Modulus of Rupture	60
4.4.3 Modulus of Elasticity	63
4.4.3.1 Calculations	64
4.4.3.2 Design Equations	64
4.4.3.3 Modulus of Elasticity Results	65
 CHAPTER 5: SENSITIVITY ANALYSIS	 69
5.1 Statistical Analysis Methodology	69
5.1.1 Multiple Regression Analysis of All Data	73
5.1.2 Multiple Regression Analysis of Data by Concrete Age	79
5.1.3 Interaction plots	87
5.1.4 Main Effects Plots	89
5.1.5 Optimization Analysis	95
5.2 Sensitivity Analysis Conclusion	99
 CHAPTER 6: FREEZE THAW DURABILITY	 102
6.1 Freeze-Thaw Study Methodology	102
6.2 Literature Review	104
6.2.1 FHWA (2006) and Kosmatka and Wilson (2011)	104
6.2.2 Mindness et al. (2002)	109

	x
6.3 Freeze Thaw Testing	110
6.4 Specimen and Material Preparation	110
6.5 Chamber Temperature Calibration	111
6.6 Testing Procedure	112
6.6.1 Testing Procedure Calibration	116
6.6.2 Freeze Thaw Cycles and Measurements	116
6.6.3 Calculations	119
6.7 Air Content: Additional Testing	120
6.8 Results	124
6.8.1 Physical Deterioration	124
6.8.2 Mass Change	125
6.8.3 Mechanical and Durability Properties	127
6.9 Discussion	132
CHAPTER 7: CONCLUSIONS	137
REFERENCES	141
APPENDIX A: INTERVIEW TRANSCRIPT	145
APPENDIX B: COMPRESSIVE STRENGTH DATA	147
APPENDIX C: SENSITIVITY ANALYSIS	156
APPENDIX D: FREEZE THAW DATA	158
APPENDIX E: FREEZE THAW SAMPLE PICTURES	168

LIST OF TABLES

TABLE: 2.1 Cost data for the Solar Decathlon home, Urban Eden, as detailed by Tempest et. al. (2015).	24
TABLE: 3.1 Mixture designs used for samples, pounds per cubic yard (kilograms per cubic meter).	26
Table: 3.2 Chemical composition of fly ash used in study.	27
TABLE: 3.3 Sample breakdown and labeling scheme.	29
TABLE: 3.4 Batches B and C sample types and testing purpose.	30
TABLE: 3.5 Batch A sample types and testing purposes.	30
TABLE: 3.6 Measured temperature of GCC batches following mixing.	33
TABLE: 3.7 Average reading of slump flow, in. (mm), over a minute and a half interval.	36
TABLE: 3.8 Acceptance criteria of self consolidating concrete workability as produced by the University of Texas Center for Transportation Research (Koehler, 2007).	39
TABLE: 3.9 GCC fresh concrete air content values measured with procedures from ASTM C173 and ASTM C231.	40
TABLE: 4.1 Average compressive strength of batch 1.60.	54
TABLE: 4.2 Average compressive strength of batch 2.60.	55
TABLE: 4.3 Average compressive strength of batch 3.60	56
TABLE: 4.4 Average compressive strength of batch 1.70.	56
TABLE: 4.5 Average compressive strength of batch 2.70.	57

	xii
TABLE: 4.6 Average compressive strength of batch 3.70.	58
TABLE: 4.7 Average compressive strength of batch 1.80.	58
TABLE: 4.8 Average compressive strength of batch 2.80.	59
TABLE: 4.9 Average compressive strength of batch 3.80.	60
TABLE: 4.10 Average modulus of rupture results, psi (MPa).	61
TABLE: 4.11 Average modulus of rupture results, psi (MPa).	62
TABLE: 4.12 Sample 28 day modulus of elasticity measurements and comparison with ACI 318-14 (2014) and Tempest et al. (2016)	67
TABLE: 5.1 Multiple regression models and optimization results of analysis of all data.	74
TABLE: 5.2 Multiple regression models analyzed by concrete age.	79
TABLE: 5.3 Optimization analysis of samples tested at 0-days with compressive strength goal maximized.	96
TABLE: 5.4 Optimization analysis of samples tested at 14-days with compressive strength goal maximized.	96
TABLE: 5.5 Optimization analysis of samples tested at 28-days with compressive strength goal maximized.	97
TABLE: 5.6 Optimization analysis of all samples tested with compressive strength goal maximized.	97
TABLE: 5.7 Optimization analysis of samples tested at 28-days with compressive strength goal set at 4000 psi (27.6 MPa).	98
TABLE: 6.1 Freeze thaw sample series and quantities.	119
TABLE: 6.2 Recorded count values for air content analysis.	121

	xiii
TABLE: 6.3 ASTM C457 calculated values for air content of selected samples.	123
TABLE: 6.4 Average compressive strength of freeze thaw specimens (psi, MPa).	127
TABLE: 6.5 Calculated values per ASTM C666 (2008) and ASTM C215 (2008) including final durability factors.	128
TABLE: 6.6 Summary of measured and calculated values associated with the freeze-thaw durability of the samples.	136

LIST OF FIGURES

FIGURE: 2.1 Projected increase in annual cement production (Hasanbeigi et al. 2012).	8
FIGURE: 2.2 Carbon dioxide emissions comparison of GCC and OPC concrete per Turner et. al.'s study (Turner and Collins 2013).	10
FIGURE: 2.3 Development steps diagram for geopolymer cement concrete as outlined and detailed by Van Deventer et al. (2012).	11
FIGURE: 2.4 Urban Eden precast geopolymer cement concrete home produced by UNC Charlotte for the 2013 U.S. Dept. Energy Solar Decathlon.	15
FIGURE: 2.5 Standard wall cross section used for the walls of Urban Eden.	15
FIGURE: 2.6 Activating solution pouring into concrete mixing truck.	20
FIGURE: 2.7 Geopolymer cement concrete placing using standard concrete equipment.	20
FIGURE: 2.8 Water heaters set up for heat curing of concrete.	21
FIGURE: 3.1 Slump flow test setup using Procedure B of ASTM C1611.	35
FIGURE: 3.2 Slump flow test sample once allowed to flow completely per ASTM C1611.	36
FIGURE: 3.3 Graph depicting average slump flow over 1:30 of reading.	37
FIGURE: 3.4 Graph depicting average slump flow reading and slump flow speed for each w/cm value.	38
FIGURE: 4.1 Experimental data showing the change in compressive strength as samples aged as shown by Hardjito et al. (2004).	43
FIGURE: 4.2 Experimental data showing the change in compressive strength with varying curing duration as noted by Hardjito et al. (2004).	43

	xv
FIGURE: 4.3 Experimental data showing the change in compressive strength with varying water:solids ratio as noted by Hardjito et al. (2004).	44
FIGURE: 4.4 Standard testing setup for compressive strength testing per ASTM C39.	54
FIGURE: 4.5 Strength development with specimen age of batch 1.60, Mix 1 cured at 140°F (60°C).	55
FIGURE: 4.6 Strength development with specimen age of batch 2.60, Mix 2 cured at 140°F (60°C).	56
FIGURE: 4.7 Strength development with specimen age of batch 3.60, Mix 3 cured at 140°F (60°C).	56
FIGURE: 4.8 Strength development with specimen age of batch 1.70, Mix 1 cured at 158°F (70°C).	57
FIGURE: 4.9 Strength development with specimen age of batch 2.70, Mix 2 cured at 158°F (70°C).	58
FIGURE: 4.10 Strength development with specimen age of batch 3.70, Mix 3 cured at 158°F (70°C).	58
FIGURE: 4.11 Strength development with specimen age of batch 1.80, Mix 1 cured at 176°F (80°C).	59
FIGURE: 4.12 Strength development with specimen age of batch 2.80, Mix 2 cured at 176°F (80°C).	60
FIGURE: 4.13 Strength development with specimen age of batch 3.80, Mix 3 cured at 176°F (80°C).	60
FIGURE: 4.14 Testing setup for modulus of rupture per ASTM C78.	61
FIGURE: 4.15 Graph illustrating the comparison between measured modulus of rupture values and those calculated from ACI 318-14 (2014).	63
FIGURE: 4.16 Graph illustrating method of determining MOE of measured data	65

for direct comparison to alternate methods.

FIGURE: 4.17 Graph illustrating the comparison between measured modulus of elasticity values and those calculated from Tempest et al. (2016), and ACI 318-14 (2014).	66
FIGURE: 5.1 Multiple regression model building by the Minitab statistical processor.	72
FIGURE: 5.2 First-order linear equation model showing values for curing durations of 48, 36, 24, and 12 hours.	76
FIGURE: 5.3 Full quadratic model equation showing the trend for curing durations of 48, 36, 24, and 12 hours at the three curing temperatures.	77
FIGURE: 5.4 Quadratic model and linear model with experimental data w/cm 1 shown.	77
FIGURE: 5.5 Quadratic model and linear model with experimental data w/cm 2 shown.	78
FIGURE: 5.6 Quadratic model and linear model with experimental data w/cm 3 shown.	78
FIGURE: 5.7 Full quadratic models for samples tested directly following curing.	80
FIGURE: 5.8 Full quadratic models for samples tested at 14 days following curing.	80
FIGURE: 5.9 Full quadratic models for samples tested at 28 days following curing.	81
FIGURE: 5.10 Trend in “Incremental increase in R^2 , %” of each parameter.	82
FIGURE: 5.11 Full quadratic model equation showing the model and experimental data for the three curing temperatures for w/cm 1; concrete age is zero days.	82
FIGURE: 5.12 Full quadratic model equation showing the model and experimental data for the three curing temperatures for w/cm 2; concrete age is zero days.	83
FIGURE: 5.13 Full quadratic model equation showing the model and experimental	83

data the three curing temperatures for w/cm 3; concrete age is zero days.	
FIGURE: 5.14 Full quadratic model equation showing the model and experimental data for the three curing temperatures for w/cm 1; concrete age is fourteen days.	84
FIGURE: 5.15 Full quadratic model equation showing the model and experimental data for the three curing temperatures for w/cm 2; concrete age is fourteen days.	84
FIGURE: 5.16 Full quadratic model equation showing the model and experimental data for the three curing temperatures for w/cm 3; concrete age is fourteen days.	85
FIGURE: 5.17 Full quadratic model equation showing the model and experimental data for the three curing temperatures for w/cm 1; concrete age is twenty-eight days.	85
FIGURE: 5.18 Full quadratic model equation showing the model and experimental data for the three curing temperatures for w/cm 2; concrete age is twenty-eight days.	86
FIGURE: 5.19 Full quadratic model equation showing the model and experimental data for the three curing temperatures for w/cm 3; concrete age is twenty-eight days.	86
FIGURE: 5.20 Interaction plot of compressive strength as affected by w/c ratio, curing temperature, curing duration, and sample age.	88
FIGURE: 5.21 Main effects plot for compressive strength of all data collected.	91
FIGURE: 5.22 Main effects plot for compressive strength of 0-day aged samples.	92
FIGURE: 5.23 Main effects plot for compressive strength of 14-day aged samples.	93
FIGURE: 5.24 Main effects plot for compressive strength of 28-day aged samples.	94
FIGURE: 6.1 Relative dynamic modulus to freeze thaw cycles of samples with varying air content as reported by SHRP. (FHWA 2006)	108
FIGURE: 6.2 Freeze-thaw durability factor parameters against total air content (Cordon and Merrill 1963).	109

FIGURE: 6.3 Temperature output of environmental chamber calibration.	111
FIGURE: 6.4 Resonant frequency testing set up of sample.	115
FIGURE: 6.5 Set up for transverse frequency testing.	115
FIGURE: 6.6 Dynamic frequency readout of sample 1.80.24.2 prior to freeze thaw cycling.	115
FIGURE: 6.7 Samples after being removed from environmental chamber.	118
FIGURE: 6.8 Sample weight measurement following removal from environmental chamber.	118
FIGURE: 6.9 Chart used to find spacing factor per ASTM C457 (2012).	122
FIGURE: 6.10 Sample 3.80.48.2 at 66 of 132 cycles.	124
FIGURE: 6.11 Sample 3.80.48.2 at 132 of 132 cycles.	125
FIGURE: 6.12 Mass change chart of $w/cm:1$ samples.	125
FIGURE: 6.13 Mass change chart of $w/cm:2$ samples.	126
FIGURE: 6.14 Mass change chart of $w/cm:3$ samples.	126
FIGURE: 6.15 Relative dynamic modulus of samples with the base water content in the mixture design, notated as Series 1.	129
FIGURE: 6.16 Relative dynamic modulus of samples with a 10% water content increase in the mixture design, notated as Series 2.	130
FIGURE: 6.17 Relative dynamic modulus of samples with a 20% water content increase in the mixture design, notated as Series 3.	131
FIGURE: 6.18 Freeze-thaw durability factor parameters against total air content (Cordon and Merrill 1963) with results from study shown in box.	134

FIGURE: 6.19 Summary Durability Factors against air content of samples with a linear trend line applied.	xix 134
FIGURE: 6.20 Summary of measured air content per ASTM C173, ASTM C231, and ASTM C457.	135

CHAPTER 1: INTRODUCTION

1.1 Background

Geopolymer cements can make use of any highly alkali and silicate materials many of which are produced as industrial waste. Fly ash, a waste product of coal burning electric plants has become one of the most popular materials and the source material upon which this study focuses. The use of fly ash is highly encouraged by many academics as it provides numerous benefits for the construction industry in terms of comparable properties to portland cement concretes (PCC) and the sustainable benefits, which indicate a reduced carbon dioxide emissions associated with geopolymer cement concrete (GCC).

Geopolymers differ greatly in chemistry processes to PCC's primarily in that geopolymers create a three dimensional chemical structure of alkalis and silicates which harden over time. The hardening of the product is encouraged and sped up through the addition of heat to the curing process. GCC as presented in this study makes use of Class F fly ash (a low calcium fly ash), an alkaline activating solution (sodium hydroxide and sodium silicate), coarse and fine aggregates, and water.

This thesis explores the commercial use of GCC by characterizing a series of production variables for construction at a precasting facility. The production variables are the water to cementitious materials ratio (w/cm), high heat curing temperature, and high

heat curing duration. These are analyzed based on the mechanical properties of three *w/cms*.

1.2 Scope of Research

The research presented in this thesis focuses on the mixture design characteristics, fresh concrete properties, mechanical properties, and durability properties of GCC mixes. A sensitivity study and analysis was performed on a total of thirty-six mixture designs with varying combinations of three different *w/cms*, three heat curing temperatures, and four heat curing durations. The study analyzed the effects of the noted changes in mixture design on the fresh concrete properties (temperature, slump flow, and air content), mechanical properties (compressive strength, modulus of rupture, and modulus of elasticity), and the durability property of freeze thaw resistance. These properties and parameters are commonly used as metrics for describing the quality of PCC. This research seeks to correlate these properties to the appropriate use of GCC, particularly in the precast concrete industry. A further goal of this research is to provide a basis for specifications establishing the guidelines for producing this type of concrete in precast plants by creating metrics and tolerances for the quality control of the concrete.

1.3 Thesis Arrangement

A literature review of GCC origins and a background is outlined in Chapter 2 along with some of the sustainability and economic discussions in recent literature. This chapter is designated to establish the reasoning for the increased interest in fly ash based GCC's and leverages fly ash as the binder with the most potential in the industry. The chapter also discusses, as a case study, the 2013 U.S. Department of Energy Solar Decathlon entry of a residential home constructed of precast GCC walls. The case study

focuses on the development and production of the structural components for residential construction in the industrial setting of a precast concrete plant.

In chapter 3, the mixture designs, preparation, mixing, and casting of specimens used in this study are discussed. The fresh concrete properties are also tabulated and discussed in the chapter. Chapter 4 follows up with a literature review of studies dealing with the mechanical properties of GCC's. A summary of the selected factors for analysis is described and the proposed effects on the mechanical properties. The chapter also tabulates the results for the following mechanical properties: compressive strength, modulus of rupture, and modulus of elasticity. The sensitivity analysis is presented, analyzed, and discussed in Chapter 5 with numerous regression analyses of the mechanical properties including portions of the study focusing on the age of the concrete. The chapter also includes an optimization analysis that seeks to use all available data to determine the most appropriate combinations of mixture design properties to optimize the compressive strength.

Lastly, Chapter 6 provides results of a durability study on the freeze thaw resistance of a selected group of GCC mixture designs. A literature review covering selected durability studies is included as well as a background on the importance and currently understood mechanisms in PCC. Very few studies dedicated to characterizing the durability properties of any GCC's have been performed, and therefore the literature review provided is broadened to include studies that have outlined the mechanics and acceptance guidelines of PCC.

In conclusion, Chapter 7 provides a synopsis and summary of all tests and results with a discussion of significant findings and recommendations for further studies.

CHAPTER 2: GEOPOLYMER CEMENT CONCRETE BACKGROUND

2.1 Development Background

Joseph Davidovits is credited as the grandfather of GCC. Geopolymer cements are composed of an alumina silicate material combined with a silicate solution used to “activate” cementitious characteristics. A commonly used alumina silicate source material is the coal combustion product, fly ash. However, other materials exist which can be used to produce geopolymer products. Davidovits has identified four categories of geopolymer cements; slag-based, rockbased, fly ash-based, and ferro-sialate based (Davidovits 2013). These categories encompass a wide range of possibilities for using alternative materials to portland cement in concrete construction. While these may present a great number of opportunities for the development and the production of new, high quality products, they also present new challenges because they will require product-specific specifications and usage parameters. The long term and ubiquitous use of portland cement in the concrete industry across the globe has built a deep understanding of the behavior of portland cement and PCC.

While all of the categories Davidovits (2013) mentioned in “Geopolymer Cement: A review” are relevant to the industry, the focus on fly ash-based geopolymers is of great interest due to the abundance of the source material. Fly ash based geopolymer cement makes use of either Class F or C fly ashes as categorized by ASTM C618 (2008). Class F fly ashes are usually desired for their low calcium contents and, therefore, are the main

focus of discussion in this thesis. As a concrete, fly ash based geopolymer, makes use of waste ashes produced by coal burning power plants. Other ingredients in the concrete include typical coarse and fine aggregates, water, and an activating solution. The activating solution typically consists of an alkaline solution (such as sodium hydroxide NaOH or potassium hydroxide KOH), and a source of readily soluble silicate (such as sodium silicate). In this research, sodium hydroxide and sodium silicate make up the activating solution. Research has determined that mixing procedures of the ingredients can occur just as it would for PCC.

2.2 GCC Preparation

GCC may be prepared from any number of sources and may use various combinations of chemicals for ash activation. In order to properly focus this thesis the following is a summary of fly ash characteristics and preparation procedures referenced in this study.

2.2.1 Source Material

Fernández-Jiménez and Palomo (2003) have outlined a number of characteristics of fly ash which make it adequate for activation as a concrete. One of the main points discussed is the chemical composition of the ashes, namely the amount of material in the fly ash that is unburned in the coal burning process. A portion of the unburned material must be reactive silica in order for the subsequent reactions to take place with the activating solution (Fernández-Jiménez and Palomo 2003).

2.2.2 Activating Solution

The activating solution of GCCs typically consists of an alkaline solution and a soluble silicate. Many studies have focused solely on combinations of chemicals and

types of chemicals to use in these studies and have led to alternative paths for GCC development. Fernández-Jiménez and Palomo (2005) discuss the use of the following three types of activating solutions:

- Sodium hydroxide (NaOH)
- Sodium hydroxide (NaOH) with sodium silicate (Na₂SiO₃)
- Sodium carbonate (Na₂CO₃)

The study performed by Fernández-Jiménez and Palomo (2005) focuses on the differences between the activating solutions and the respective conditions associated with each in order to activate the fly ashes and create a cementitious paste. The study indicates the varying chemical compositions, which result when mixing the fly ash with each solution. Most notably, the presence of the sodium ion is key in order to create the structure. The hydroxide in the first two types of solutions aids in the speeding up of the reactions. Of the three types of solutions the sodium hydroxide and sodium silicate provides additional elements for the reaction process (Fernández-Jiménez and Palomo 2005).

2.2.3 Curing Process

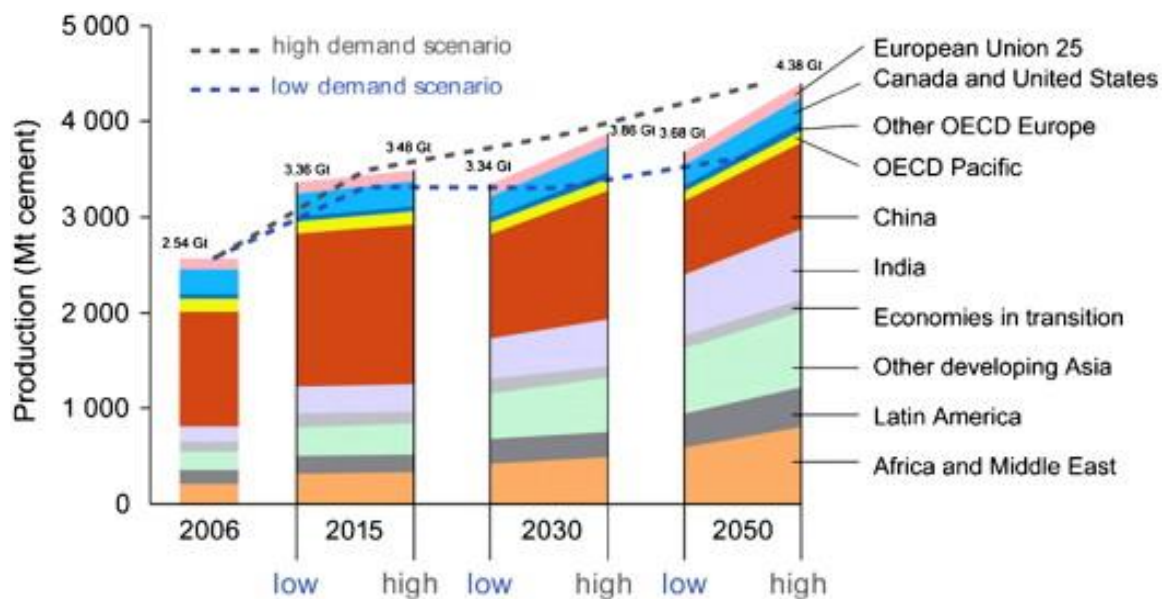
The curing process associated with GCC can vary in the amount of high heat curing temperatures and curing durations. Generally, curing temperatures can range from room temperature to 194°F (90°C) and curing durations can range from a few hours up to 48 hours. Alonso and Palomo (2001) have noted that increased temperatures above 140°F (60°C) are necessary in order to drive the polymerization reactions. Higher strengths and longer curing times are associated with higher compressive strengths (Alonso and Palomo 2001).

2.3 Sustainability Benefit

A significant benefit of GCC in comparison to PCC, which greatly motivates the use of GCC, involves the decreased greenhouse gas emissions associated with the start to finish production of the concrete. The carbon dioxide emissions associated with construction are an important consideration in many sustainably oriented projects and engineers and designers worldwide are seeking means to lower the impact of projects. Portland cement is one of the largest contributors to carbon dioxide emissions, which in turn cause a detrimental greenhouse effect. In their “Concrete CO₂ Fact Sheet” report, the National Ready Mixed Concrete Association (NRMCA 2008), has indicated that approximately 1,984 to 2,425 pounds of CO₂ are emitted for every 2,205 pounds of portland cement produced in the US alone. Much of these emissions are associated with the production of the cement through the calcination of limestone. Other CO₂ emissions are attributed to the extracting, grinding, milling, and transportation productions.

Hasanbeigi et al. (2012) in the report, “Emerging Energy-efficiency and CO₂ Emission-reduction Technologies for Cement and Concrete Production,” have provided a condensed summary of numerous technologies aimed at curbing or reducing the associated carbon dioxide emissions with portland cement. The researcher noted that concrete “is used worldwide as a building material and is the second-most-consumed substance on earth after water” (Hasanbeigi et al. 2012). This in turn makes portland cement a material which the world greatly depends on. Concrete production is expected to increase in much of the developing world, as a result of growing economies and necessary infrastructure. Figure: 2.1 shows the projected increases in Portland cement demand based on the information produced by the Organisation for Economic Co-

operation and Development (OECD). It is important to note, once again, the growth in countries with growing economic interest in infrastructure development. Hasanbeigi et al. (2012) have outlined numerous research and commercial endeavors to curb the associated carbon emissions with Portland cement or concrete in general. Besides the kiln improvements and carbon dioxide capture technologies is the growing field of cement alternatives where geopolymer cements are cited as a “current innovative technology” which is showing research and production interest and potential.



Note: OECD is an acronym for the Organization for Economic Co-operation and Development

Figure: 2.1 Projected increase in annual cement production (Hasanbeigi et al. 2012).

In their study, “Carbon dioxide equivalent (CO₂-e) emissions: A comparison between geopolymer and OPC cement concrete,” Louise K. Turner and Frank G. Collins (2013) offer insight into the sustainable attraction behind GCC. The study provided by Turner and Collins (2013), compares the carbon dioxide equivalent (CO₂-e) emissions of PCC and GCC. The comparison is based on a thorough analysis of the origin to in-place construction of 35.3 cubic feet (1 cubic meter) of concrete used to construct a crosshead

beam as part of a bridge near Melbourne, Australia. This study provides a unique side-by-side comparison of both types of concretes with an emphasis on the entire process of manufacturing including the mining, processing, and transportation of all materials. The authors have collected data from several audits of the production processes associated with each concrete or have received data from industry manufacturers. Seven primary categories are taken into account for the comparisons between PCC and GCC, these include the following:

- Sodium hydroxide production including the primary chlor-alkali process
- Sodium silicate manufacturing through the melting of silica sand and sodium carbonate
- Portland cement manufacture through the calcination of limestone
- Fly ash manufacturing as a waste by product of coal burning power plants
- Coarse and fine aggregate quarrying and transportation to concrete manufacturers
- Construction of the crosshead beam used as the product goal in the study
- Curing of the GCC by elevated temperatures of 140°F (60°C) to 176°F (80°C) for 24 hours

This study proactively focuses on the distinction between manufacturing processes of both concretes and discredits the common misconception of a highly attractive and dramatically reduced emissions GCC (Turner and Collins 2013). The study estimates a reduction in carbon dioxide equivalent (CO₂-e) emissions by 9%. The reduction is presented as a broad array of contributing factors shown in Figure: 2.2 The authors note the significant differences in their study with others, which have indicated a

range of 26% to 80% reductions in carbon dioxide emissions and attribute the discrepancy to differences in analyses. The most important differences are attributed to lack of thorough studies, which have not included complete analyses of transportation emissions for all materials, energy usage for the production of the activating solution materials, and the elevated temperature curing component of GCC.

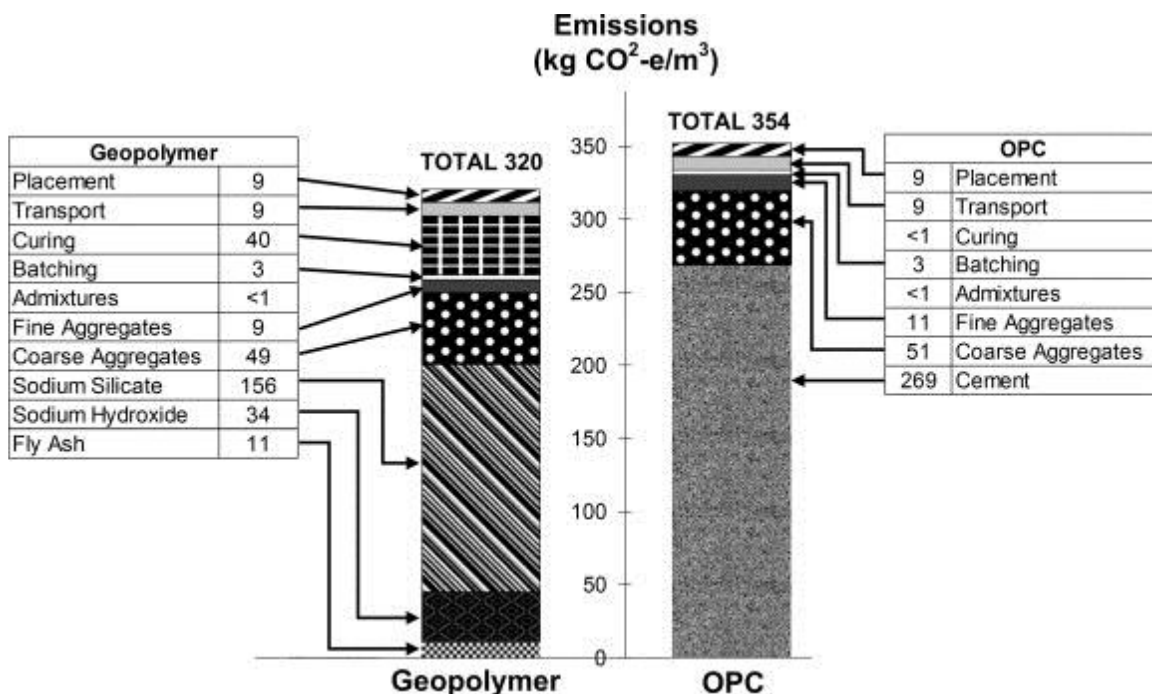


Figure: 2.2 Carbon dioxide emissions comparison of GCC and OPC concrete per Turner et. al.'s study (Turner and Collins 2013).

2.4 Economic Progress

The importance behind the appealing nature of a sustainable and environmentally friendly product such as GCC is what is categorized as “major drivers” by Van Deventer et al. (2012) for the adoption of geopolymers. Van Deventer et al. (2012) have determined a thorough program for the commercial adoption of GCC. This model is what may define the growing interest by organizations, companies, and countries in GCC’s.

Figure: 2.3 outlines this procedure as presented in the study.

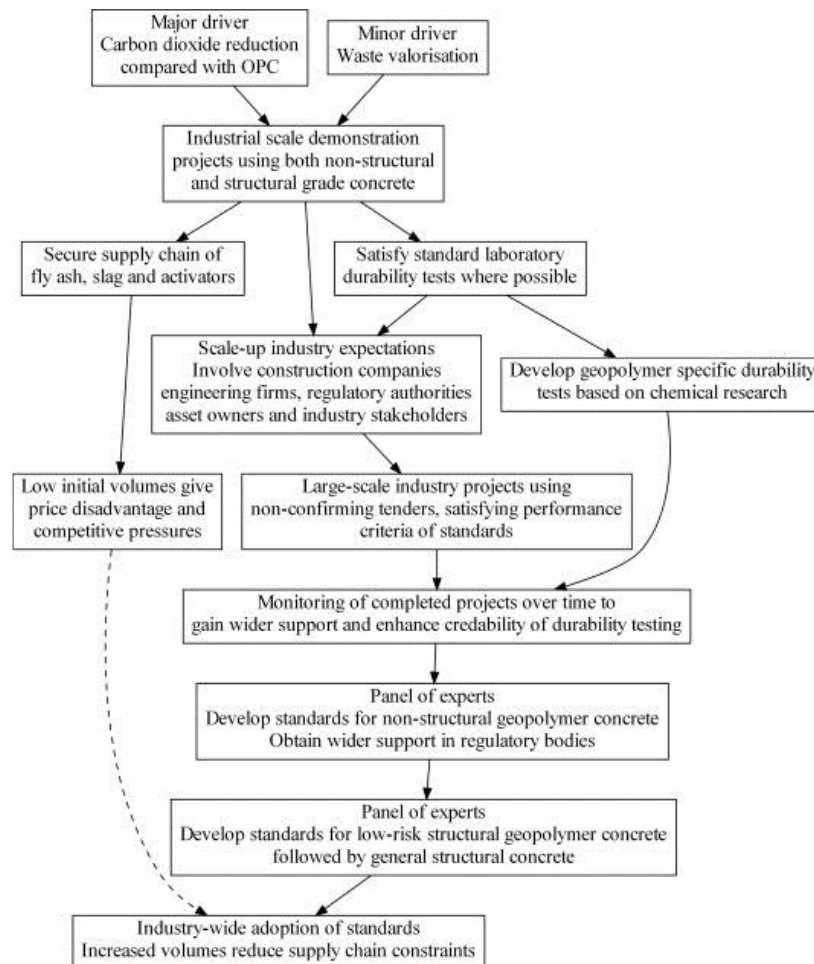


Figure: 2.3 Development steps diagram for geopolymer cement concrete as outlined and detailed by Van Deventer et al. (2012).

Van Deventer et al. (2012) have indicated the deliberate progress in the industry in order to make GCC a viable and appropriate material in the construction industry. With the use of fly ash, the desire for a more sustainable product is granted through the carbon dioxide emissions reduction and the waste reuse. Aside from examining the carbon dioxide emissions reduction Van Deventer et al. (2012) have indicated the importance of geopolymer paste rheology, the creation of standards, the concrete durability properties, and the further commercial acceptance of the concrete.

Among those finding great potential in GCC are researchers in the Australian industry. McLellan et al. (2011) performed an analysis of the “Costs and carbon emissions for geopolymer pastes in comparison to OPC” and have found that the costs of geopolymers could be up to two times the cost of OPC but the greenhouse gas emissions were reduced by 44% to 64% (McLellan et al. 2011). The analysis performed by McLellan et al. (2011) examines the energy use, greenhouse gas emissions, and costs associated with both geopolymer cement concrete and OPC concrete in the Australian market (McLellan et al. 2011). Their assessment focuses on the differences in the concrete up to the mixing and casting of the concretes as these are assumed to be equal for both concretes. In this way, McLellan et al. (2011) have compared the creation of Portland cement and the creation of geopolymer cements which takes into account the production of the activating solution (McLellan et al. 2011). Through their analysis, it was found that the transportation component of material from stocks tends to vary for each component and creates a skewed analysis because the wide availability of the geopolymer material stocks is not as wide spread as those of portland cement (McLellan et al. 2011).

A second location where researchers are looking into the use of geopolymer concretes is the United Kingdom (UK). Heath et al. (2013) offer a case for geopolymer concrete as a substitute for PCC in some applications. As with other countries, the authors note that the availability of fly ash is widespread in the UK with about three million tonnes ending up in landfills (Heath et al. 2013). However, the UK is reducing its dependence on coal for energy generation. This goal of transitioning to non-coal fuels is

shared by many countries and contributes to the further development of alternatively sourced geopolymers (Heath et al. 2013).

Even with considerations for the availability, costs, and environmental benefits of fly ash based GCC's very few commercial productions exist. To date, there are no examples of large-scale production of GCC. This may be attributed to the conservative nature of engineers and designers where comfort in the reliability of PCC is accepted. James Aldred and John Day (2012) present some small scale unique applications of GCC in a publication entitled, "Is geopolymers concrete a suitable alternative to traditional concrete?" Among the applications are pavements, a retaining wall, a water tank, a boat ramp, precast bridge decks, and most notably precast beams (Aldred and Day 2012). While most of the applications have been under uniquely driven and typically in singular applications, the thirty-three precast geopolymers concrete beams used in the construction of the Global Change Institute (GCI) building in Queensland, Australia are a significant accomplishment. A branded GCC, Earth Friendly Concrete, produced by Wagners of Australia is the constructor of the precast beams. Rod Bligh and Tom Glasby (2014) illustrate the steps taken to produce the precast panels. The primary incentive for using the GCC was the innovative and sustainable nature of the material. In order to properly document the GCC use the constructors requested preliminary research be performed to confirm the viability of the concrete for the project. Loading tests of full-scale panels were also conducted and the concrete was produced by Wagners working in conjunction with Precast Concrete (Bligh and Glasby 2014). It is important to note the use of regular concrete mixing machinery and casting methods for this project. A second large-scale production example of GCC can be found in residential infrastructure. The University of

North Carolina at Charlotte between 2012 and 2013 produced a residence made up of five precast geopolymer cement concrete wall panels. The production of these panels is detailed in the next section.

2.5 U.S. Department of Energy Solar Decathlon: UNC Charlotte 2013

Between 2011 and 2013, the University of North Carolina at Charlotte (UNC Charlotte) participated in an international competition hosted by the U.S. Department of Energy called the Solar Decathlon. The Solar Decathlon is a bi-annual competition that was first held in 2002. The competition serves as a means for universities to create innovative residences which can educate the public in novel energy-saving, money-saving, and sustainable ideas for their homes. The competition, currently held in Irvine, California, requires full scale homes be produced by designing universities.

UNC Charlotte as a participant of the 2013 decathlon elected to construct a precast concrete home named “Urban Eden.” More importantly, in order to utilize innovative technologies, GCC sourced from fly ash was used to construct the continuously insulated precast wall panels. The development of the GCC used for the purpose of constructing fully insulated double-wythe precast concrete wall panels was based on previous geopolymer research at UNC Charlotte. The residential home consisted of the five walls as shown in Figure: 2.4 All walls were produced according to the cross section shown in Figure: 2.5.



Figure: 2.4 Urban Eden precast geopolymer cement concrete home produced by UNC Charlotte for the 2013 U.S. Dept. Energy Solar Decathlon.

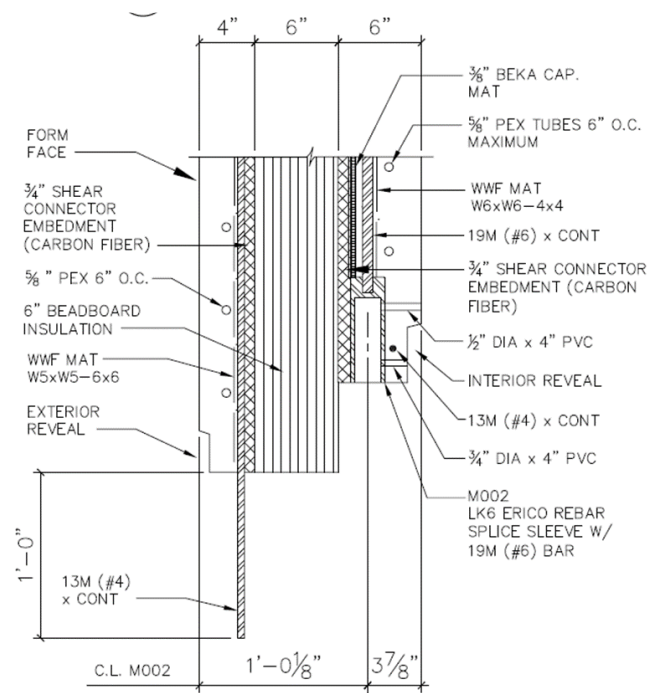


Figure: 2.5 Standard wall cross section used for the walls of Urban Eden.

2.5.1 GCC Development and Production Process

The development of the precast concrete wall panels used for UNC Charlotte's Solar Decathlon home, "Urban Eden," began in the Fall of 2012. A trial and adjustment procedure was used to develop the mixture design and to fine tune the following characteristics of the concrete:

- Finishing aesthetics
- Unique forms
- Final Coloring/ Color additives
- Workability
- Compressive Strength
- Water cement ratios
- Activating solution
- Curing duration
- Curing temperature

The textured forms were developed by architecture students who experimented with many materials to create rough, smooth, and unique finishes. During this process it was determined that improving the workability of the concrete would be crucial to the final product because the viscous nature of GCC did not allow it to be easily cast into the forms. Control over the color of the concrete was also identified as an important factor in the manufacturing process because of the variation in fly ash color. Because of the typically dark color of the ash, samples would attain a similar dark gray tint. With sandblasting, the surface color faded into lighter tones. Powder and liquid pigments were used for experimentation to determine the best option for controlling the color; through

this process, titanium dioxide was determined to be the most effective in creating a uniform and consistent, light gray coloring across samples. Through the trial and adjustment process the mixture design was further improved to create a mix with ideal workability, appropriate water content, and an activating solution combination which provided ideal compressive strengths. The ideal workability allowed for casting and finishing of the concrete in a timely fashion of the walls. A better workability was typically desired as explained in Section 2.5.5. The target compressive strength for the wall panels was that of approximately 4,800 psi (33 MPa). The curing temperature and duration were determined according to previous research.

Further development of the mixture design required creating three trial pours to scale up the mixing procedures from lab-scale to plant-scale and to try potential forming and heating methods. Two of the trial pours were conducted at the precast concrete plant, Metromont, Inc., and one was conducted at UNC Charlotte's Energy Production Infrastructure Center (EPIC) high bay research facility. These panels were used to introduce Metromont, Inc. employees to the unique characteristics of the GCC material and to trial the casting, finishing, and curing procedures of the concrete at-scale. The employees at the Metromont, Inc. plant provided very useful feedback during this calibration process. The most contrasting aspect of geopolymer cement concrete to Portland cement concrete as found by Metromont, Inc. employees involved the need to apply heat to the concrete for approximately 48 hours. This process required panels to remain on the casting bed for approximately three times as long as PCC. This initially reduced the appeal of GCC within a production setting that depends on rapid turnover of casting beds. The first method used by the team to cure the concrete in the trial process

consisted of using kerosene-fueled, forced air heaters to warm a tarp tent around the panels. This procedure was quickly abandoned because it required a heavy use of fossil fuel and created potential fire hazards for the surrounding area. Further development led to use of the hydronic heating system (visible in Figure: 2.5) embedded in the walls for curing purposes. The system was set up in such a way that pumping hot water through the embedded tubes created sufficient heat to warm the entire concrete mass to the desired curing temperature. Two iterations of this procedure using modified residential water heaters resulted in an adequate solution to the curing regimen at the precast plant.

Final mixing, casting, and curing procedures for the GCC walls were a product of lessons learned during the trial iterations. Some of the most significant conclusions, both positive and negative, from the trials included:

- Standard PCC mixing and finishing tools could be used to cast the GCC.
- The coloring of the concrete could be controlled through the use of titanium dioxide to lighten concrete that appeared dark due to the ash content.
- The lack of workability in comparison to PCC required more time on the part of the finishers to place and compact GCC.
- The embedded hydronic heating system was a suitable method to cure the GCC.
- The curing methods applied would result in a 48-hour cycle of turning over the beds.

2.5.2 Activating Solution

The preparation procedure for the activating solution for the double-wythe panels consisted of mixing a solution of sodium silicate and sodium hydroxide in 55-gallon drums. In order to minimize opportunities for error and simplify the process of dosing them into the truck mixers, the 55-gallon drums were filled to contain the correct amount of activator for a truck-load of GCC. The student team prepared the activating solution at least five days ahead of a scheduled pour date in order to equilibrate the temperature of the activating solutions before mixing.

2.5.3 Concrete Mixing and Casting

The dry materials for the concrete were batched into rotary drum mixing trucks by Concrete Supply, Inc. and arrived at the precast plant prior to mixing. It is important to note that all materials were already on hand at Concrete Supply, Inc. Because Class F fly ash is widely used as a secondary cementitious material in PCC, the availability of the fly ash at the batch plant was not a barrier to production. Once the mixing truck arrived at the plant with all the dry ingredients (fly ash, coarse aggregate, and fine aggregate) the activating solution (Figure: 2.6) was added to the drum and the material was mixed for 150 revolutions at high speed to allow for uniform mixing. Once mixed, the concrete was poured into large concrete buckets allowing for the concrete pouring in the panels (Figure: 2.7). Once poured, a team of finishers worked on the concrete to create a semi-smooth interior finish (later, plaster was used to create the finished surface). The process of mixing, casting, and finishing a wall panel lasted approximately four to five hours.



Figure: 2.6 Activating solution pouring into concrete mixing truck.

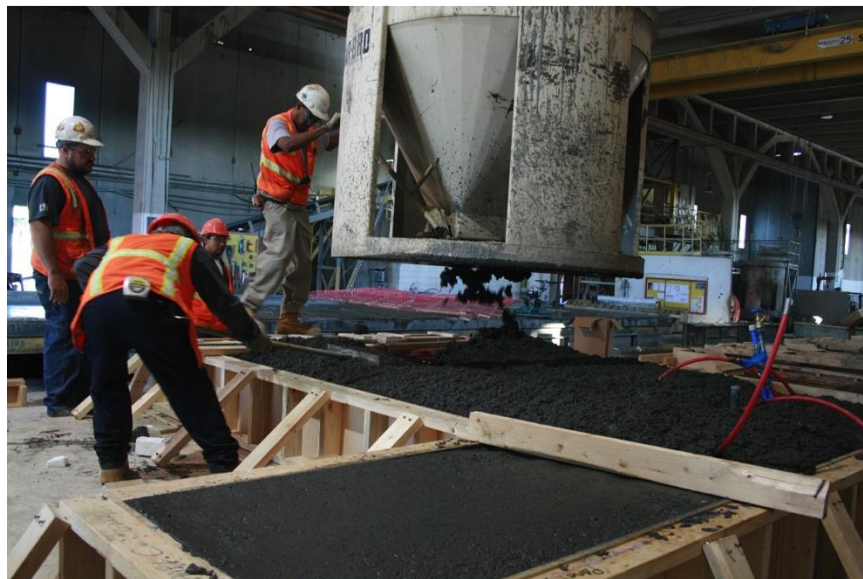


Figure: 2.7 Geopolymer cement concrete placing using standard concrete equipment.

2.5.4 Concrete Curing

The concrete was allowed to age for 24 hours at ambient temperatures while covered with plastic sheathing to prevent the upper surfaces from drying out or cracking from excessive shrinkage. After the aging period, heat was applied by passing heated water through the embedded hydronic heating system and two standard water heaters which raised the temperature of the concrete to the desired 167°F (75°C) (Figure: 2.8). Once cured, the panels were removed by and finished with typical precast concrete detailing methods of patching bug holes, sandblasting, and pressure washing.



Figure: 2.8 Water heaters set up for heat curing of concrete.

2.5.5 Industry Perspective

Following the mixing, casting, and finishing of the five precast geopolymer cement concrete walls a number of Metromont, Inc. employees were interviewed for their opinions regarding the material. The interview responses were primarily focused on the workability of the concrete with a great concern for the ability to make the concrete look nice, an important factor in precast concrete. Although dealing with a novel material

presented some challenges, the enthusiasm of the employees proved their interest in trying a new material. The construction industry is very comfortable with the Portland cement concrete and has rarely, if ever, altered the mixing procedures and methods in its journey to becoming one of the most consumed material in the world (Hasanbeigi, 2013).

2.5.5.1 Interviews with Metromont, Inc. Employees

Short interviews were conducted with plant managers, quality control managers, workers, and finishers to gain some perspective on the first impressions and thoughts on geopolymer cement concrete. The general consensus was that the workability and finishing characteristics of the concrete required improvement prior to acceptance for routine usage. In spite of the fact that employees had critiques on the material (outlined below), it became clear that they would not be opposed to using the material again after a little more progress is made. The areas of further investigation and research included the following characteristics with a list of possible methodologies to approach each characteristic.

- Workability (i.e. water content) – a very stiff concrete was typically produced, making it difficult for finishers to create a clean and smooth surface.
 - Sensitivity analysis of water content.
 - Analysis of the use of chemical additives.
- Coloring – the need for consistent coloring created uncertainty and required consistent use of similar fly ash sources.
 - Analysis of pigmentation compatibility geopolymer cement concrete.
- Curing temperature – the need for minimum compressive strengths required high heats in short periods.

- Sensitivity analysis of the curing temperature required to meet minimum mechanical properties.
- Curing duration – precast concrete plants revolve around a quick turnaround and repeatable product products, the longer time period required to achieve desirable mechanical properties can create hesitation.
 - Sensitivity analysis of the curing duration to determine minimum time frame for curing.
- Quality control methodology – because of the novel nature of geopolymer cement concrete, quality control procedure applicability is not explicit and requires further standardization.

2.5.5.2 Economic Analysis

The costs associated with GCC were also monitored during this case study and discussed by Tempest et al. (2015). The discussion focuses on the overall material costs associated with producing GCC in a precast setting. The discussion notes that while these costs are associated with the materials, the costs associated with the energy required to cure the material are in addition to the already high comparative cost. The energy costs to produce a cubic yard of GCC are estimated at \$2.49 (Tempest et al. 2015). Table: 2.1 outlines the associated costs with the material costs of the Urban Eden home. The final cost of GCC is estimated at \$160.83 compared to \$50.88 for PCC, per cubic yard.

Table: 2.1 Cost data for the Solar Decathlon home, Urban Eden, as detailed by Tempest et. al. (2015).

Material	Cost per 100 lb	GCC, lb (kg)	Cost per 1 yd ³ (0.765 m ³) GCC	PCC, lb (kg)	Cost per 1 yd ³ (0.765 m ³) PCC
Sodium Silicate	\$42.00	277 (125.76)	\$116.34	0	\$0
Sodium Hydroxide	\$64.00	36 (16.34)	\$23.04	0	\$0
Fly Ash	\$1.13	787 (357.30)	\$8.92	0	\$0
Fine Aggregate	\$0.42	1370 (621.98)	\$5.79	1250 (567.5)	\$5.28
Coarse Aggregate	\$0.49	1370 (621.98)	\$6.73	1800 (817.2)	\$8.84
Water	\$0.02	75	\$0.02	260 (118.04)	\$0.06
Portland Cement	\$5.64	0	\$0.00	650 (295.10)	\$36.69
Total		3915 (1777.41)	\$160.83	3960 (1797.84)	\$50.88

CHAPTER 3: PREPARATION, MIXING, AND CASTING OF SAMPLES

The samples prepared for this study included a combination of cylinders and prisms to characterize the mechanical and durability properties of twenty-seven GCC mixture designs. Samples used for this study were prepared over a five-month period. Three mixture designs were used for a comparative analysis of effects of w/cm on the mechanical properties and freeze-thaw durability properties of the concrete. The combined effects of the mixture design as well as three curing temperatures and four curing durations led to a matrix of twenty-seven mixture designs (outlined in Section 3.2). A standard three cubic foot capacity concrete mixer was used to prepare all the mixes. For the purposes of this study, the term, “mixture design,” refers to the chemical, aggregate, and water quantities. Additional production variables included the curing temperature and curing, which also significantly change the properties of the concrete. Further discussion on the effects of the curing temperature and duration can be found in Chapter 5.

3.1 Mixture design

- The mixture design used in this study primarily made use of the mixture design used in the Solar Decathlon entry by UNC Charlotte. The initial mixture design was developed with trial and test adjustment methods for workable ash:activator ratios and cement:aggregate ratios. Traditional methods were used to proportion the coarse and fine aggregates into the

overall mixes. The method used for determining the mixture design development and aggregate proportioning involved the Fuller Method, a particle packing method which is used to select an aggregate combination that will make the most efficient use of the space in the concrete matrix.

Table: 3.1 details the three mixture designs used in this study. The variable ingredient of mixes 1, 2 and 3 is the water content with a 10% and 20% increase on the original mix. The below significant ratios are noted:

- Sodium silicate to sodium hydroxide ratio of 7.65
- Activator liquids to fly ash ratio of 0.40
- Aggregates at 70% by mass of mix
- Water to solids ratios as follows:
 - $w/cm: 1 = 0.0954$
 - $w/cm: 2 = 0.1049$
 - $w/cm: 3 = 0.1145$

Table: 3.1 Mixture designs used for samples, pounds per cubic yard (kilograms per cubic meter).

Mix	$w/cm: 1$	$w/cm: 2$	$w/cm: 3$
Water, lb./yd. ³ (kg/m ³)	75.10 (44.6)	82.60 (49.0)	90.10 (53.5)
Sodium Silicate, lb./yd. ³ (kg/m ³)	277.0 (164.3)	277.0 (164.3)	277.0 (164.3)
Sodium Hydroxide, lb./yd. ³ (kg/m ³)	36.20 (21.5)	36.20 (21.5)	36.20 (21.5)
Fly Ash, lb./yd. ³ (kg/m ³)	786.8 (466.8)	786.8 (466.8)	786.8 (466.8)
Fine Aggregate, lb./ yd. ³ (kg/m ³)	1,370.3 (813.0)	1,370.3 (813.0)	1,370.3 (813.0)
Coarse Aggregate, lb./ yd. ³ (kg/m ³)	1,370.3 (813.0)	1,370.3 (813.0)	1,370.3 (813.0)
Total, lb./yd. ³ (kg/m ³)	3915.7 (2323.1)	3923.2 (2327.5)	3930.7 (2332.0)

3.1.1 Fly Ash

The fly ash used for this study was Class F fly ash from the Rogers Energy Complex (formerly known as the Cliffside Steam Station) in North Carolina. The ash was marketed as Class F (ASTM 2013). The breakdown of the chemical composition is shown in Table: 3.2.

Table: 3.2 Chemical composition of fly ash used in study.

Chemical	% by mass
Al ₂ O ₃	28.09
BaO	0.06
CaO	2.03
CuO	0.01
Fe ₂ O ₃	7.00
K ₂ O	1.06
MgO	1.08
MnO	<0.01
MoO	<0.01
Na ₂ O	0.47
NiO	0.01
P ₂ O ₅	0.26
PbO	<0.01
SiO ₂	55.23
SrO	0.09
TiO ₂	2.00
ZnO	0.02
ZrO ₂	0.02
LOI	2.98

3.1.2 Activating Solution

The activating solution is composed of 88% Type O sodium silicate and 12% sodium hydroxide. The sodium silicate was produced by Univar and is their Sodium Silicate O product with a 62.5 percentage by weight of water and a 37.5 percentage by weight of sodium silicate (Univar 2013). The sodium hydroxide is produced by PPG

Industries and is their PELS Anhydrous Sodium Hydroxide product (PPG-Industries 2011).

The activating solution was prepared a week in advance of mixing and allowed to equilibrate at 175°F (80°C) for 24 hours. Following the heating process, the activating solution was allowed to cool to ambient room temperature prior to mixing the concrete. Typically, the solution was prepared in a bucket and mixed with a hand drill fitted with a paint mixing attachment. The following steps were used to prepare the activating solution:

1. Add all of the sodium silicate in a bucket
2. Mix in one-third (1/3) of sodium hydroxide
3. Mix for five (5) minutes
4. Mix in one-third (1/3) of sodium hydroxide
5. Mix for five (5) minutes
6. Mix in one-third (1/3) of sodium hydroxide
7. Mix for five (5) minutes
8. Heat solution for 24 hours at 175°F (80°C)

The indicated eight-step process for mixing the activating solution is such that the sodium hydroxide in pellet form can dissolve in the sodium silicate a little at a time. The process allows for a consistent mixing of the solution so that the sodium hydroxide pellets do not remain in solid form. A second consideration taken into account for the mixing process involves the excess heat and fumes produced by the solution mixing process. The separation of the mixing process into three iterations allows for a steady and, most importantly, a safe mixing process. Among safety equipment used for mixing

these solutions are gloves, gas masks, and a chemical resistant apron. Prior to mixing the concrete, the activating solution was placed in an oven overnight at approximately 140°F (60°C) to maintain a viscous solution, otherwise the solution thickened.

3.1.3 Aggregates

The aggregates used in this study originated from Charlotte, North Carolina and were #78 granite stone and sand. All coarse aggregate was prepared to saturated-surface dry (SSD) condition and fine aggregates were prepared to oven-dry (OD) conditions.

3.2 Sample Breakdown

Given the variety of factors to be analyzed for this study and the limited mixer capacity, a total of twenty-seven batches were produced for full analysis. Table: 3.3 details the batch breakdown. Three *w/cms* were analyzed, four elevated curing temperatures, and four elevated temperature durations. In this document, the *w/cm* is defined as the weight ratio of the mixing water and water contained in the sodium silicate solution to the weight of the sodium silicate solids, the fly ash, and the sodium hydroxide, as illustrated in Equation 3.1.

$$\frac{\text{water} = \sum(\text{water in sodium silicate, mixing water, moisture content of aggregates})}{\text{cement solids} = \sum(\text{solids in sodium silicate, fly ash, sodium hydroxide})} \quad \text{Equation 3.1}$$

Table: 3.3 Sample breakdown and labeling scheme.

Mix	Curing duration, hr.	Temperature		
		140°F (60°C)	158°F (70°C)	176°F (80°C)
<i>w/cm: 1</i>	12 and 24	1.60.C	1.70.C	1.80.C
	36 and 48	1.60.B	1.70.B	1.80.B
	24 and 48	1.60.A	1.70.A	1.80.A
<i>w/cm: 2</i>	12 and 24	2.60.C	2.70.C	2.80.C
	36 and 48	2.60.B	2.70.B	2.80.B
	24 and 48	2.60.A	2.70.A	2.80.A
<i>w/cm: 3</i>	12 and 24	3.60.C	3.70.C	3.80.C
	36 and 48	3.60.B	3.70.B	3.80.B
	24 and 48	3.60.A	3.70.A	3.80.A

The batches were prepared in smaller quantities to optimize the mixer capacity and the specimen relationships. The batch-labeling scheme references labels A, B, and C. The types of samples associated with each label are detailed in Table: 3.4 and Table: 3.5; these tables provide the quantity of specimens associated with each type of batch given the w/cm , curing temperature, and curing duration combination. Two curing durations were associated with all batches in order to optimize the oven capacity and allowed for removal of specimens at the first time and at twelve hours later.

Table: 3.4 Batches B and C sample types and testing purpose.

Sample Type	Quantity per curing temperature	Description of Evaluation	Test Method
4"x8" (101mm x 203mm) cylinder	3	Test for compressive strength, f'_c immediately after heat curing	ASTM C39
		Test for modulus of elasticity	ASTM C469
4"x8" (101mm x 203mm) cylinder	3	Test for f'_c after 14 days	ASTM C39
		Test for modulus of elasticity	ASTM C469
4"x8" (101mm x 203mm) cylinder	3	Test for f'_c after 28 days	ASTM C39
		Test for modulus of elasticity	ASTM C469
Small beam, 20"x6"x6" (508mm x 152mm x 152mm)	2	Test for modulus of rupture at 28 days	ASTM C78

Table: 3.5 Batch A sample types and testing purposes.

Sample	Quantity per curing temperature	Description of Evaluation	Test Method
Prism, 11.25"x4"x3" (286mm x 102mm x 76mm)	2	Test for F/T after 14 days	ASTM C666
4"x8" cylinder	3	Test for f'_c after 14 days	ASTM C39
4"x8" cylinder	3	Test for f'_c after 28 days	ASTM C39

3.3 Mixing

Batches were mixed in the early morning, typically, over a five to six hour period with prior setup and collection of materials. The morning mixing time was crucial for proper mixing as ambient temperatures were in the range of 80°F (27°C) to 90°F (32°C) during the mixing period. The consistent mixing prior to the highest heat of the day was important to maintain a mixing procedure preventing the concrete from drying out too quickly. The following mixing process was used for each batch to achieve uniform mixing at each batch:

1. Add half of the total coarse aggregate.
2. Add half of the total fine aggregate.
3. Mix concrete for five (5) minutes.
4. Add half of the total fly ash.
5. Allow the mixer to mix for 12 revolutions.
6. Add half of the total fly ash.
7. Allow the mixer to mix for 12 revolutions.
8. Add the total activating solution.
9. Add the total water.
10. Add the last half of the total fine aggregate.
11. Add the last half of the coarse aggregate.
12. Allow to mixer to mix for 15 minutes.
13. Pour and cast concrete accordingly.

The mixing procedure was organized such that consistency between batches could be achieved and it allowed the mixers to handle the large quantities of materials. The

basic regimen consisted of mixing a portion of the aggregates followed by a portion of the fly ash; this process minimized the material lost after each addition. The fly ash tends to escape out of the mixer very easily when mixing and can create significant losses and changes in the mix if too much is lost. The possibility of losing fly ash is also the key reason for adding the activating solution and water in steps eight and nine, this process allows the fly ash to settle and mix into the proper paste and concrete.

3.4 Casting

The casting of samples was performed within thirty minutes of final mixing. Plastic 4" x 6" (101.6mm x 203.2mm) cylinders were used to cast the samples for compressive strength, steel molds were used for the large prisms and freeze thaw samples, and wooden molds lined with plastic sheeting were used to create the freeze thaw prism specimens. The plastic sheeting was used in order to create a smooth surface on the sample. Following casting, the samples were placed on a vibrating table for consolidation.

3.5 Curing Regimen

The curing regimen for the samples was such that after casting, samples were covered and aged at room temperature for twenty-four hours and then moved to an oven to be heat cured at the designated temperatures. Samples were removed from the oven after they reached the appropriate curing duration. The curing duration for each type of sample can be found in Section 3.2 and Table: 3.3.

3.6 Fresh Concrete Properties

Several fresh concrete properties were measured as part of the correlation to the durability test procedures. The fresh properties measured were the temperature of the

concrete following mixing, the slump flow of the concrete per ASTM C1611 (2014), and the air content of the concrete per ASTM C231 (2014) and ASTM C173 (2014). All of these properties were measured on mixes with an “A” designation; the description of the type “A” mixes can be found in Section 3.2 and Table: 3.5.

3.6.1 Temperature After Mixing

The temperature of the concrete directly after mixing was recorded to determine whether high heat following mixing should be expected. Table: 3.6 shows the measured temperatures after mixing of batches.

Table: 3.6 Measured temperature of GCC batches following mixing.

<i>w/cm</i> Batch	Concrete Temperature, °F (°C)	Ambient Temperature, °F (°C)
1	79.7 (26.5)	Not measured
2	82.4 (28.0)	Not measured
3	79.4 (26.3)	Not measured
3	80.1 (32.3)	Not measured
3	80.8 (27.1)	Not measured
3	83.2 (27.9)	Not measured
1	87.8 (31.0)	Not measured
2	80.7 (27.1)	81.1 (27.3)
2	83.9 (28.8)	72.9 (22.7)
1	84.0 (28.9)	78.2 (25.7)
3	81.9 (27.7)	79.8 (26.6)
1	81.7 (27.6)	75.8 (24.3)
1	83.3 (28.5)	74.7 (23.7)
2	86.3 (30.2)	76.4 (24.7)
1	85.4 (29.7)	71.9 (22.2)
3	82.0 (27.8)	75.8 (24.3)
1	90.0 (32.2)	79.1 (26.2)
2	85.4 (29.7)	85.5 (29.7)
3	86.3 (30.2)	85.4 (29.7)
1	81.3 (27.4)	77.2 (25.1)
2	80.4 (26.9)	83.8 (28.5)
3	79.5 (26.4)	75.6 (24.2)
2	78.0 (25.6)	77.3 (25.2)

<i>w/cm</i> Batch	Concrete Temperature, °F (°C)	Ambient Temperature, °F (°C)
2	78.6 (25.9)	74.6 (23.7)
3	74.0 (23.3)	73.1 (22.8)

From the data recorded it can be assumed that GCC mixes have some heat generation, which can contribute to a typically higher mixing temperature compared to ambient temperatures. However, as previously mentioned in Section 2.5.2, the solution was heated prior to mixing in order to create a viscous solution. In a plant setting, it is important to be aware of the possibility of high heat generation as a result of mixing. Due to the viscous nature of the fresh GCC, the bulk of the heat generation during mixing is due to friction. The geopolymerization reaction is only mildly exothermic.

3.6.2 Slump Flow

Previous slump testing of GCC has shown it to be a fairly difficult material to test using the Standard Test Method for Slump of Hydraulic-Cement Concrete (ASTM 2014). GCC material becomes thick and viscous when mixed and does not hold shape as PCC does when mixed. The standard method of measuring slump for PCC does not properly represent the workability of GCC. As a result, numerous researchers have alternatively selected the Standard Test Method for Slump Flow of Self-Consolidating Concrete (ASTM C1611) as a means of measuring the consistency of the fresh concrete (ASTM 2014). The test consists of two assessments - the first being a visual stability index and a measurement of the circular spread of the concrete. Test procedure B was used in the testing of the concrete. The steps as outlined by ASTM 1611 and performed for this study are as described below (ASTM 2014).

A 4'x8' (1.2m x 2.4m), half inch thick plexiglass sheet was used as the consistent flat surface. Following the mixing of the concrete, the mold was dampened and placed in an inverted position on the plexiglass sheet, as shown in Figure: 3.1. The mixed concrete was then scooped into the mold, topped off, and leveled by striking the surface. The mold was then steadily raised vertically and the concrete allowed to flow out of the bottom completely. Following the complete flow, the largest diameter was measured and recorded and a second diameter, perpendicular to the first, was also measured and recorded (a typical flow pattern is shown in Figure: 3.2). These two measurements were averaged to determine the slump flow of the concrete. Table: 3.7 details the readings over a minute and a half interval and Figure: 3.3 shows the plotted results for the readings. The reading at a minute and a half was the final reading. However, the readings at the 30-second intervals were used to determine the velocity of the spread and whether or not the additional water content had a significant contribution to the GCC consistency.



Figure: 3.1 Slump flow test setup using Procedure B of ASTM C1611.



Figure: 3.2 Slump flow test sample once allowed to flow completely per ASTM C1611.

Table: 3.7 Average reading of slump flow, in. (mm), over a minute and a half interval.

Mix Label	Time elapsed at reading (seconds)		
	0:30	1:00	1:30
1	22.75 (577.85)	23.50 (603.25)	24.38 (619.25)
1	22.05 (560.07)	22.25 (565.15)	23.75 (603.25)
1	22.00 (558.80)	24.25 (615.95)	24.38 (619.25)
2	18.25 (463.55)	20.75 (527.05)	21.75 (522.45)
2	21.00 (533.40)	23.00 (584.20)	24.00 (609.62)
2	19.75 (501.65)	21.25 (539.75)	21.75 (552.45)
3	23.25 (590.55)	25.50 (647.70)	26.25 (666.75)
3	22.25 (565.15)	24.00 (609.60)	25.25 (641.35)
3	24.50 (622.30)	26.75 (679.45)	27.25 (692.15)

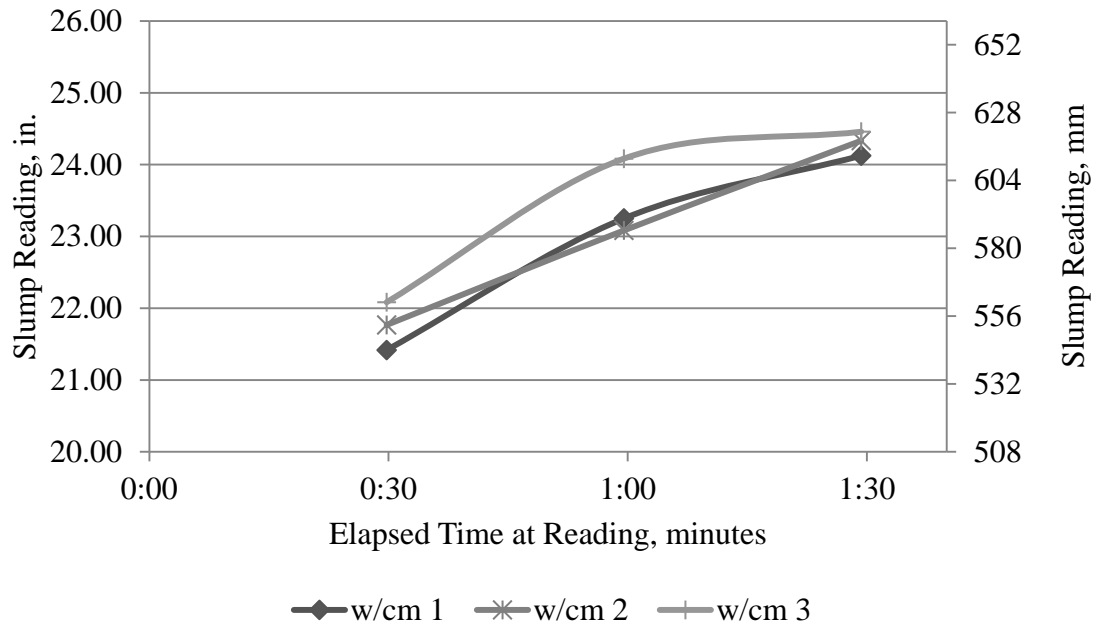


Figure: 3.3 Graph depicting average slump flow over 1:30 of reading.

The results indicated some consistency between similar batches at a small degree. As expected, the highest water content had the highest slump flow values; however, the change between the slump flow of *w/cm 1* and *w/cm 2* was not as expected and showed values much closer to each other. Figure: 3.4 further illustrates the average slump flow reading and speed of flow of each mix. On average *w/cm 3* was a more workable mix and had a greater flow than the other two mixes.

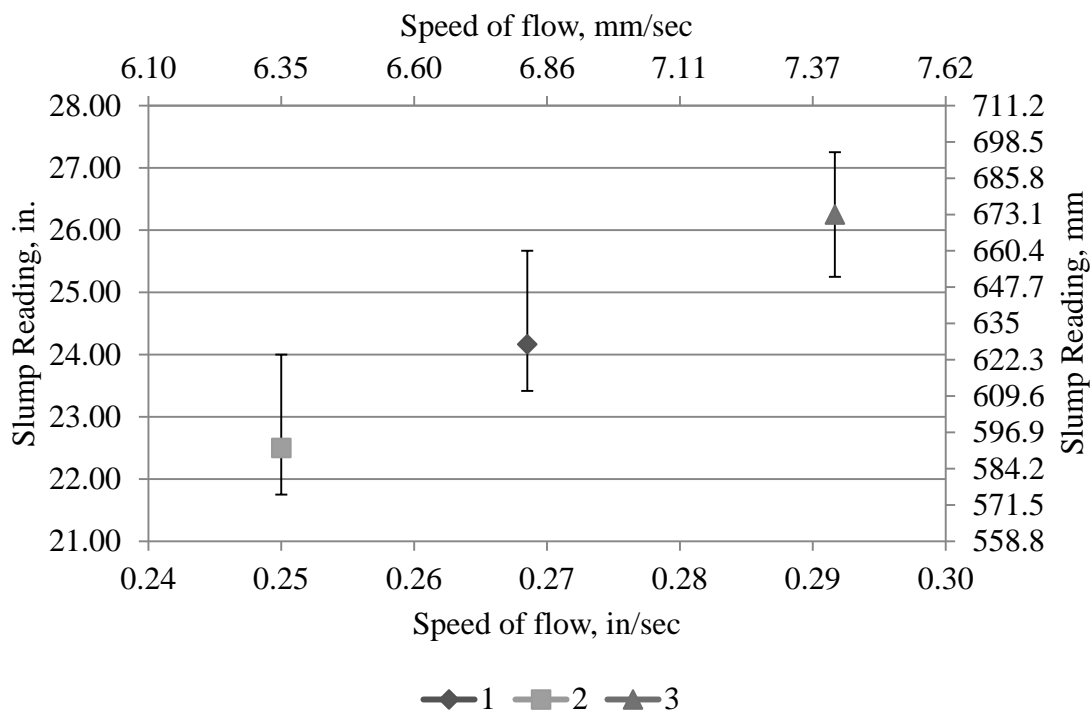


Figure: 3.4 Graph depicting average slump flow reading and slump flow speed for each w/cm value.

The applicability of the slump flow testing on geopolymer cement concrete can be further analyzed by examining the use of the test procedure in construction. The University of Texas Center for Transportation Research has published the document, “Inspection Manual for Self-Consolidating Concrete in Precast Members,” which outlines acceptance criteria for self-consolidating concrete (Koehler, 2007). Table: 3.8 summarizes the acceptance criteria and indicates most acceptable of the consistencies is that of the *w/cm* 3. This is also confirmed by the observation that this mixture design was more workable than its counterparts. Accordingly, it is assumed that a higher water content would create a concrete more appropriate for beam constructions or others which provide challenges to consolidation.

Table: 3.8 Acceptance criteria of self consolidating concrete workability as produced by the University of Texas Center for Transportation Research (Koehler, 2007).

Slump Flow Range, in.	Acceptance details
21-24	Appropriate for members with light or no reinforcement, short lateral flow distances, or high placement energy (e.g. panels, barriers, coping)
24-27	Ideal for most applications
27-30	Appropriate for members with highly congested reinforcement, long lateral flow distances, or low placement energy (e.g. U-beams, I-beams, and other beams)

The use of GCC in various types of construction can be analyzed from these common construction standards. Based on the average values, the less workable mix (*w/cm* 1) has an average value slightly above 24 indicating its acceptance in most applications. While mix 2 (*w/cm* 2) has an average reading less than 24, it would indicate that it can be used in the category for light or no reinforcement, essentially, nonstructural components. However, the 20% increase in water content (*w/cm* 3) would allow for more heavily reinforced structural components. This slight increase in water content is a positive aspect for the applicable uses of GCC.

3.6.3 Air Content

The air content of concrete is a crucial design parameter used to determine the durability and is used as a guide for the functionality of the concrete. The American Concrete Institute is one of the governing design organizations setting parameters for the ranges of acceptable air contents of concrete in construction settings.

Two test procedures were used to measure the fresh concrete air content, the “Standard Test for Air Content of Freshly Mixed Concrete by the Pressure Method” (ASTM 2014) and the “Standard Test Method for Air Content of Freshly Mixed Concrete by the Volumetric Method” (ASTM 2014). Table: 3.9 includes the final readings for the tests.

Table: 3.9 GCC fresh concrete air content values measured with procedures from ASTM C173 and ASTM C231.

Batch Label	Volumetric ASTM C173	Pressure ASTM C231
1	1.25%	2.80%
1	*	3.00%
1	1.00%	*
2	1.75%	2.80%
2	*	2.80%
3	1.25%	2.40%
3	1.50%	4.00%

*Test was unsuccessful.

The measured values using both the volumetric (ASTM C173) and pressure (ASTM C231) methods varied only slightly. The range was from a 1% air content to a 4% air content. Taking into consideration the varying water contents, as previously discussed in Section 3.1, the discrepancies in air content would likely be minimal. Furthermore, the consistency of fresh GCC is an influencing property for the material as it tends to be stickier and flows less than its PCC counterpart.

CHAPTER 4: MECHANICAL PROPERTIES OF HARDENED CONCRETE

In this chapter, the results of mechanical properties tests conducted on concretes batched as outlined in previous chapters are described. This data was used in analysis of the sensitivity of these properties to mixture design and curing conditions was performed on the geopolymer mixes which is presented in Chapter 6. The primary purpose of these experiments and analyses is to establish appropriate tolerances for production parameters that can be controlled or should be monitored at precasting facilities if they prepare GCC. Because repeatability, quality and economy are key factors to the success of construction materials producers, it is important to understand the acceptable limits of production parameters. The case study presented previously in Chapter 2 indicated that the parameters requiring control are water content, curing temperature, and curing duration.

The following sections include a brief literature review on the mechanical property characterization of GCC.

4.1 Literature Review

Various literature exists regarding the most common mechanical properties of GCC's. Typically compressive strengths, modulus of rupture, and modulus of elasticity are some of the most common parameters that are used for characterizing concrete properties for strength-based design. In the case of GCC, the variability of these properties is dependent on the mixture design and curing conditions, as it is with PCC. Some findings are presented in the following sections on the effects of age, curing

duration, curing temperature, and mixture designs on the mechanical properties of concrete.

4.1.1 Hardjito et al. (2004)

Hardjito et al. (2004) investigated how compressive strength changes as a result of concrete age, curing duration, curing temperature, addition of superplasticizer, rest period before heat curing, and water content in the mixture designs. The first part of their study focuses on the age and curing duration of the GCC. Their test set up focused on samples with varying curing temperatures from 86°F (30°C) to 194°F (90°C) and their primary mixture design characteristics are as follows:

- Class F fly ash
- Sodium silicate to sodium hydroxide ratio of 2.5
- Sodium hydroxide molarity of 8M (water content tests changed molarity to 14M)
- Activator liquids to fly ash ratio of 0.35
- Aggregates at 77% by mass of mix

Cylinder test specimens (4" x 8", 101.6mm x 203.2 mm) were produced by the following mixing procedure:

1. Dry mixing fly ash and aggregates – 3 minutes
2. Addition of alkaline solution and superplasticizer – 3 to 5 minutes
3. Casting cylinders (4" x 8" , 101.6mm x 203.2 mm), 5 samples per variable
4. Room temperature setting for 30 to 60 minutes
5. Specified temperature curing for specified time
6. Specimen removal from molds six hours after complete curing

7. Sample testing at specified ages

Hardjito et al. (2004) found that there is little change in compressive strength as the concrete ages. They have also found that a longer curing duration produces higher compressive strengths but the increases become less significant after 48 hours. The compressive strength trends as found by the researchers are shown in Figure: 4.1 and Figure: 4.2 (Hardjito et al. 2004).

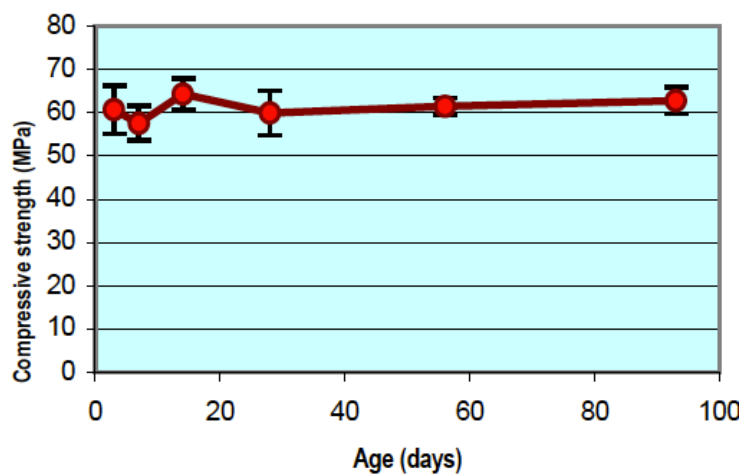


Figure: 4.1 Experimental data showing the change in compressive strength as samples aged as shown by Hardjito et al. (2004).

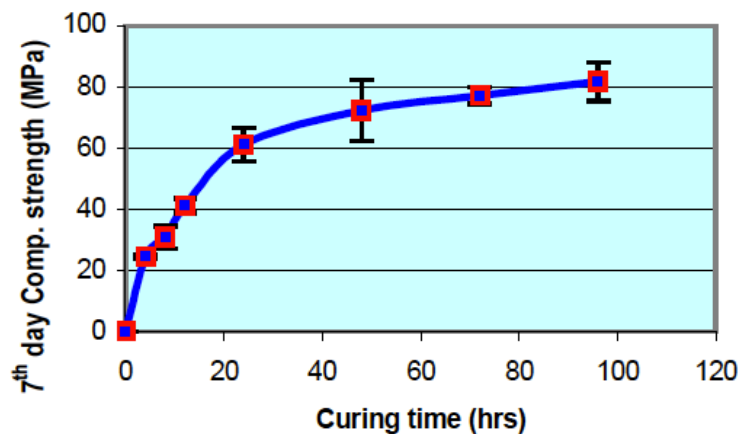


Figure: 4.2 Experimental data showing the change in compressive strength with varying curing duration as noted by Hardjito et al. (2004).

The addition of a naphthalene-based superplasticizer (1.0-3.5%) improved the workability of the mixture, but was linked to a decrease the compressive strength after two percent, 2%. It is also important to note that in their study of the addition of a superplastizer, the authors found that no large difference in compressive strength exists when samples are allowed to rest for an hour versus no rest before heat curing.

Furthermore, the authors found that a lower water content produced a higher compressive strength, but more water produced a better workability. Similarly, higher curing temperatures resulted in an increased concrete compressive strength. However, after 167°F (75°C) no significant changes were noted. The experimental results are shown in Figure: 4.3 and indicate minimal variations in the compressive strength among the highest water/solids ratio and a consistent increase as the water:solids ratio increased. The difference in increased compressive strength between curing temperatures is not as significant between 167°F (75°C) and 194°F (90°C) as it was between 86°F (30°C) and 113°F (45°C).

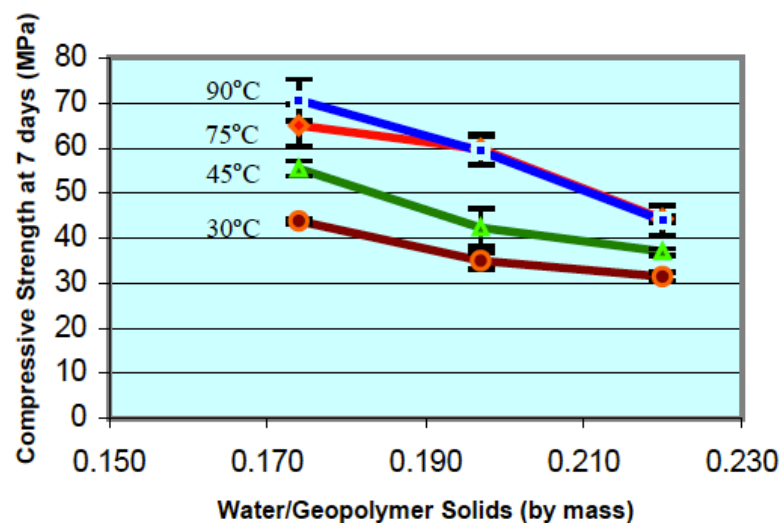


Figure: 4.3 Experimental data showing the change in compressive strength with varying water:solids ratio as noted by Hardjito et al. (2004).

4.1.2 Khale and Chaudhary (2007)

Khale and Chaudhary (2007) have explored the chemistry and mechanics of geopolymers and the geopolymerization process. Their study published in 2007, provided a broad analysis of geopolymer source materials including fly ash. They provide a summary of numerous existing studies on using fly ash, metakaolin, kaolinite, and numerous other sources. The relevant data to this study includes the studies, which used fly ash as a source material with no other additives. In this presentation, there are a few significant conclusions including the effects of the curing temperature, curing duration, liquid to solids ratios, and the age of concrete on the concrete's mechanical properties. The consensus regarding the curing temperature based on data presented by the authors is that higher temperatures produce higher compressive strengths however a few investigators have found that after 140°F (60°C) to 167°F (75°C) the increases become less significant. The next component of the curing, the duration of curing is also investigated in this paper. Numerous studies are referenced which vary the curing duration from 24 to 48 hours of cure time. References are made to the significance of higher curing duration in conjunction with longer curing duration with the authors' studies indicating that geopolymerization reactions are significantly affected by higher heats and longer times, indicating limits to the chemical processes. The effect of liquid to solids ratio is also a significant portion of this study where the authors indicate that the "strength decreases as the ratio of water-to-geopolymer solid increases." The water in geopolymer mixes is referenced to have a different effect to that of water in OPC concrete which requires water for its hydration. A second significant difference to Portland cement concrete is the age of the concrete where the maximum compressive

strength is gained. The authors indicate that GCC can gain 70% of its strength in the first three to four hours of its' curing, this is a significant difference to the properties of OPC concrete. A second portion of this study, which is important to note, involves the engineering properties of the GCC. Again, numerous studies are referenced which have shown, among other things, that GCC's have similar stress-strain behaviors to OPC concrete.

4.1.3 Hardjito and Rangan (2005)

Hardjito and Rangan (2005) have performed an extensive study of GCC using class F fly ash. The study presents the preliminary mixture design steps for their concrete. Things to note from the mixture design and process used in this study are the following:

- Sodium silicate to sodium hydroxide ratios from 0.4 to 2.5
- Sodium hydroxide molarity's of 8M to 16M
- Activator solution to fly ash (by mass) ratio of 0.3 and 0.4
- Aggregate ratios of 75% to 80% of total mass
- Oven and steam curing

Hardjito and Rangan (2005) provide results and analysis of numerous factors. The curing temperatures analyzed were 86°F (30°C), 113°F (45°C), 140°F (60°C), 167°F (75°C), and 194°F (90°C). Their study found that the higher temperatures increased the compressive strength and higher temperatures consistently also increased the compressive strength regardless of the curing duration. The curing duration in this study varied from 6 to 96 hours. Increases in compressive strength occurred at rapid rates up until 24 hours curing indicating that any gains leveled off. The third factor of importance in this study involves the water to solids ratio (the water to solids ratio takes into the

composition of the activating solution chemicals as referenced in section 3.2, Equation 4.1). The authors present data on ratios of 0.174, 0.197, and 0.220 showing that with each increase in the water the compressive strength decreased. Following the mixing ratios and curing procedures, the authors also studied the effect of age after curing on the samples, finding that over time the compressive strength of the samples did not vary (Hardjito and Rangan 2005).

Other mechanical properties investigated by the authors include the modulus of elasticity, which they found to be lower than the values calculated by the indexing equations published by the Australian Standard AS3600 and the American Concrete Institute Committee 363. They attribute this difference to the properties of the aggregates used in the mixes. Furthermore, the stress-strain relationship of three of their GCC mixes was also studied. Their study reports strains of 0.0024 in./in. to 0.0026 in./in. at peak stresses, which is similar to those, produced in studies on OPC concrete (Hardjito and Rangan 2005).

4.1.4 Vora and Dave (2013)

Vora and Dave (2013) performed a comprehensive study analyzing the effects of various mixture design factors on the compressive strength of GCC. The study focuses on mixture designs using one-hundred percent fly ash of Class F. Samples were mixed by preparing the alkaline solution a day in advance of concrete mixing. Concrete mixing occurred by mixing the fly ash with the aggregates and adding in the alkaline solution and water with a total mixing time under ten minutes. Casting of prismatic specimens followed the mixing with appropriate consolidation techniques; however, specific specimen sizes are not described.

The test set up consisted of analyzing the effects of the following parameters on compressive strength:

- Ratio of alkaline liquid to fly ash
- Concentration of sodium hydroxide solution
- Ratio of sodium silicate to sodium hydroxide
- Curing time
- Curing temperature
- Dosage of superplasticizer
- Rest period (The time from the end of casting to before heat cure.)
- Additional water content

The primary mixture design characteristics considered were the following:

- Class F fly ash
- Sodium silicate to sodium hydroxide ratios of 2.0 and 2.5
- Sodium hydroxide molarity of 8M, 10M, 12M, and 14M
- Activator liquids to fly ash ratios of 0.40 and 0.35

Vora and Dave (2013) found the following when analyzing the effects of the aforementioned mixture designs on the compressive strength:

- Ratio of alkaline liquid to fly ash
 - The ratio of alkaline liquids to fly ash from 0.35 to 0.40 does not significantly impact the compressive strength. Testing was performed at three days.
- Concentration of sodium hydroxide

- Four concentrations of sodium hydroxide, 8M, 10M, 12M, and 14M were compared resulting in significantly higher compressive strengths at the highest concentrations compared to that of the lowest.
- Ratio of sodium silicate to sodium hydroxide
 - A lower sodium silicate to sodium hydroxide ratio of 2.0 versus 2.5 was found to increase the compressive strength. Testing was performed at three days.
- Curing time
 - Two curing times of 24 hours and 48 hours were compared and an increase in compressive strength was observed in the 48 hour samples. Testing was performed at three days.
- Curing temperature
 - Three curing temperatures of 140°F (60°C), 167°F (75°C), and 194°F (90°C) and 24 hour curing time were compared and an increase in compressive strength was noted. However, the increase from 167°F (75°C) to 194°F (90°C) was less significant than that of 140°F (60°C) to 167°F (75°C). Testing was performed at seven days.
- Dosage of superplasticizer
 - The addition of commercially available Naphthalene Sulphonate based superplasticizer at two, three, and four percent by mass of fly ash was compared. The increasing percentage of superplasticizer was found to improve the workability of the concrete while decreasing the compressive strength.

- Rest period
 - A rest period of zero and one day was compared and an increase in compressive strength was observed in the one day rest period samples. Testing was performed at three days.
- Additional water content
 - Three comparisons of added water were performed, a base mix and additions of fifty percent and one-hundred percent. Or increases in ratio of added water to fly ash, by mass of ten, fifteen, and twenty percent. Increases in workability were noted with the increase in added water. However, a decrease in compressive strength by thirty-three percent was observed in the mix with the most water compared to that with the least.

4.1.5 Tempest et al. (2016)

Tempest et al. (2016) detail a study focused on the evaluation of the stress-strain relationship of flexural GCC members. The study focuses on the formulations of design equations commonly used for reinforced concrete. Primarily the determination of the α and β_1 factors of the equivalent stress-block is a focus of the study, which results in a modification to the ACI 318-14 (2014) section 8.5 modulus of elasticity equation. Six beam-column specimens were created using the same base mixture design as that discussed in Section 2.5. The resulting equation is shown below:

$$E_c = 43,000 \times \sqrt{f'_c} \text{ (psi)} \quad \text{Equation 4.1a}$$

$$E_c = 3,575 \times \sqrt{f'_c} \text{ (MPa)} \quad \text{Equation 4.1b}$$

4.2 Specimen Preparation

Specimens for this thesis were prepared according to the previously mentioned mixture designs, described in Chapter 3. Concrete cylinders of 4"x8" (100mmx200mm) were used to test for compressive strength and modulus of elasticity. Small beams of 20"Lx6"Wx6"H (508x152x152mm) were used to test for the modulus of rupture. Specimens were cast within a half hour of the concrete mixing. A vibration table was used to consolidate concrete cylinders and an immersion vibrator was used for the small beams. The samples were then set out in a room at approximately 70°F (21°C) for 24 hours prior to curing in an oven at their designated temperatures. Once cured, the samples were tested for compressive strength immediately after being removed from the oven, 14 days after removal, and 28 days after removal. The modulus of rupture was tested at 28 days after high temperature curing.

4.3 Parameters of Analysis

The purpose of this study is to determine which field controllable factors of the GCC mixing and preparation process should have limited tolerances during production in order to maintain quality. The goal is to determine the level of importance of each factor (based on the magnitude of its impact to strength and durability) and to determine a priority ranking based on what can be reasonably achieved in a plant setting. The three parameters which were analyzed were the w/cm , the curing temperature, and the curing duration of the concrete. It is important to determine which of these parameters contribute the most to the mechanical properties of GCC. As well, a combination of these parameters may exist and the level of importance may vary given any variations in the other parameters.

4.3.1 Water To Cementitious Materials Ratio (w/cm)

The w/cm is generally accepted as a critical determinant in the properties of GCC, as previously noted. Although the presence of water is not necessary for chemical reactions to occur in GCC, it has been noted that the initial presence and later loss of the water molecules creates pockets of air which affect the mechanical properties as with PCC. However, the amount of water is critical for the workability of the concrete. Therefore in this study, the degree of detrimental effects on the mechanical properties by increasing the water content for better workability is measured. The mixture design with w/cm 1 is a stiff mix, w/cm 2 is a 10% increase in water content and allows for some workability, and w/cm 3 is a 20% increase in water content which creates a much more workable material.

4.3.2 Curing Temperature

The curing temperature of GCC has largely been observed to play a role in the mechanical properties of the concrete, primarily in the compressive strength. An increase in curing temperature generally has a positive effect on the properties but the cost of energy to create a higher temperature is an economic burden as well as a cause for decreasing the sustainability benefits of the finished GCC product. In this study, the focus is to actualize the gains in mechanical properties given the increase in curing temperature. An 18°F (10°C) range from 140°F (60°C) to 176°F (80°C) was analyzed to determine this relationship.

4.3.3 Curing Duration

The curing duration of GCC is also a factor of great importance in the mechanical properties with previous research indicating an increase in compressive strength when

allowed to cure for a longer period of time. In this study the role of the curing duration was analyzed such that properties were measured given 12 hour intervals of curing (i.e 12, 24, 36, 48 hours).

4.4 Mechanical Properties Affected

As with previous studies on GCC's, the focus of the mechanical properties is on the compressive strength, modulus of rupture, and modulus of elasticity. These properties are those, which are used in design manuals and codes for structural components.

4.4.1 Compressive Strength

Cylinder samples were tested according to ASTM C39 (2015), "Standard Test Method for Compressive Strength of Cylindrical Concrete Specimens," with the following procedures. Four by eight inch (100mmx200mm) cylindrical cylinders were tested in a Universal Testing Machine (UTM). The samples were set in between rubber caps to properly distribute the loading; Figure: 4.4 shows the standard testing setup for the samples. The test procedure was produced on a representative set of all the batches. Appendix B provides the ultimate loads for all samples tested. Table: 4.1 through Table: 4.9 show the distribution of average compressive strengths per batch. The axial compressive strength was computed using Equation 4.2.



Figure: 4.4 Standard testing setup for compressive strength testing per ASTM C39.

$$\sigma = \frac{P}{A} \quad \text{Equation 4.2}$$

Where:

- P is the applied load
- A is the cross-sectional area

Table: 4.1 Average compressive strength of batch 1.60.

1.60	0 - day		14 - days		28 - days	
	psi	MPa	psi	MPa	psi	MPa
12 hour	1,506	10	2,378	16	2,715	19
24 hour	2,715	19	3,426	24	3,554	25
36 hour	2,601	18	3,016	21	3,298	23
48 hour	3,136	22	3,414	24	3,751	26

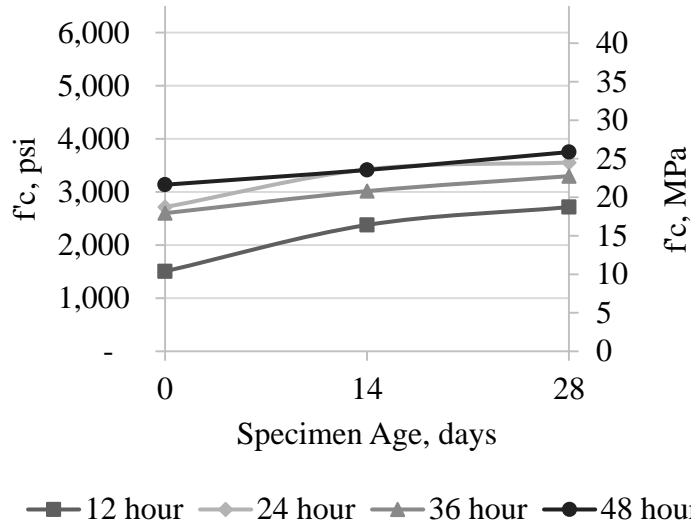


Figure: 4.5 Strength development with specimen age of batch 1.60, Mix 1 cured at 140°F (60°C).

Table: 4.2 Average compressive strength of batch 2.60.

2.60	0 - day		14 - days		28 - days	
	psi	MPa	psi	MPa	psi	MPa
12 hour	1,120	8	1,679	12	2,148	15
24 hour	2,004	14	2,558	18	2,631	18
36 hour	2,278	16	2,713	19	2,892	20
48 hour	2,769	19	3,148	22	3,358	23

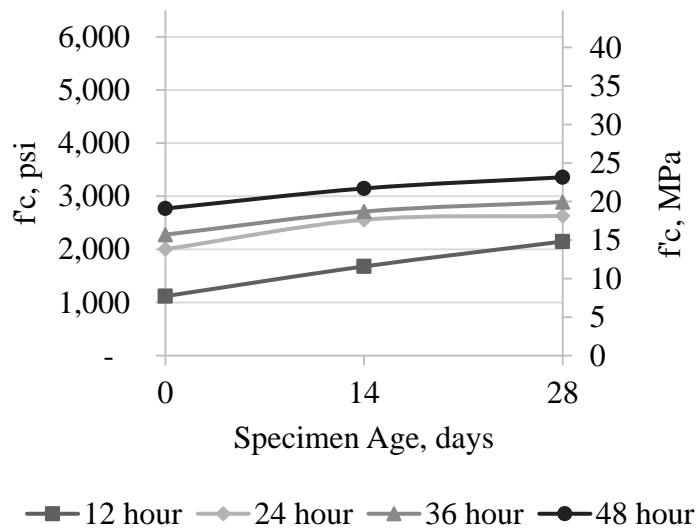


Figure: 4.6 Strength development with specimen age of batch 2.60, Mix 2 cured at 140°F (60°C).

Table: 4.3 Average compressive strength of batch 3.60

3.60	0 - day		14 - days		28 - days	
	psi	MPa	psi	MPa	psi	MPa
12 hour	532	4	957	7	1,048	7
24 hour	1,335	9	1,806	12	1,954	13
36 hour	1,969	14	2,278	16	2,511	17
48 hour	2,305	16	2,736	19	2,859	20

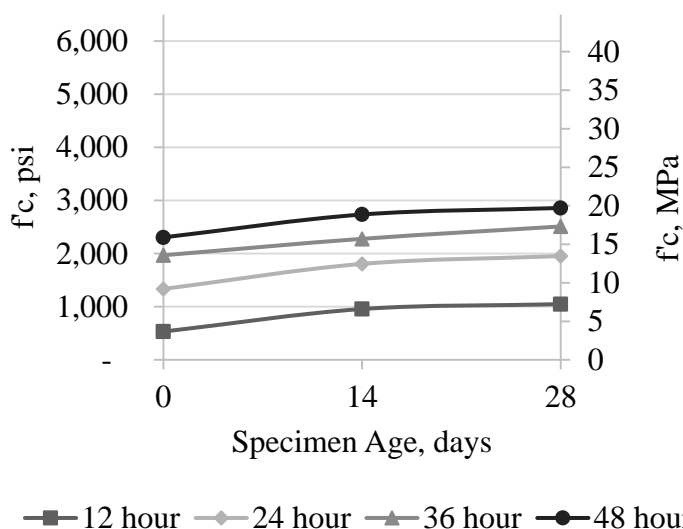


Figure: 4.7 Strength development with specimen age of batch 3.60, Mix 3 cured at 140°F (60°C).

Table: 4.4 Average compressive strength of batch 1.70.

1.70	0 - day		14 - days		28 - days	
	psi	MPa	psi	MPa	psi	MPa
12 hour	2,387	16	3,000	21	3,250	22
24 hour	4,074	28	4,660	32	4,763	33
36 hour	4,541	31	5,561	38	5,517	38
48 hour	5,168	36	5,938	41	6,008	41

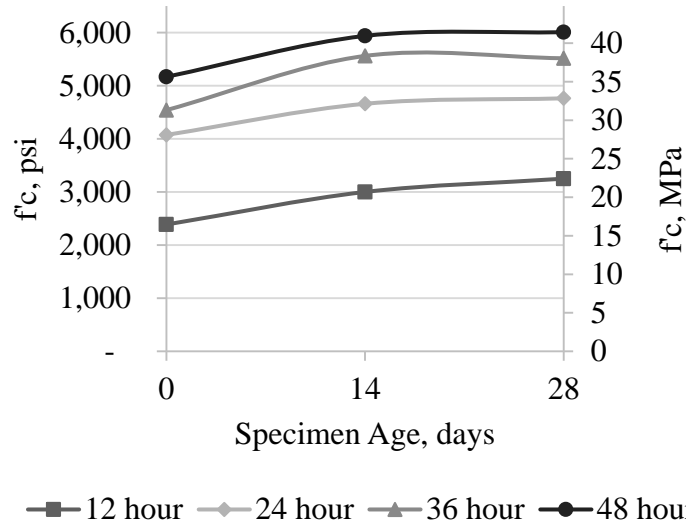


Figure: 4.8 Strength development with specimen age of batch 1.70, Mix 1 cured at 158°F (70°C).

Table: 4.5 Average compressive strength of batch 2.70.

2.70	0 - day		14 - days		28 - days	
	psi	MPa	psi	MPa	psi	MPa
12 hour	2,083	14	2,821	19	2,965	20
24 hour	3,195	22	3,955	27	3,904	27
36 hour	4,005	28	4,711	32	5,038	35
48 hour	4,748	33	4,935	34	5,231	36

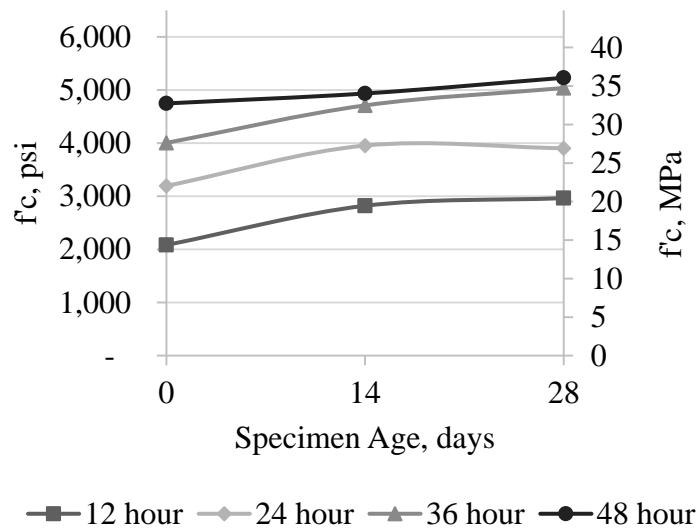


Figure: 4.9 Strength development with specimen age of batch 2.70, Mix 2 cured at 158°F (70°C).

Table: 4.6 Average compressive strength of batch 3.70.

3.70	0 - day		14 - days		28 - days	
	psi	MPa	psi	MPa	psi	MPa
12 hour	2,189	15	2,816	19	2,950	20
24 hour	3,129	22	3,947	27	4,149	29
36 hour	3,402	23	3,725	26	3,973	27
48 hour	3,800	26	4,065	28	4,443	31

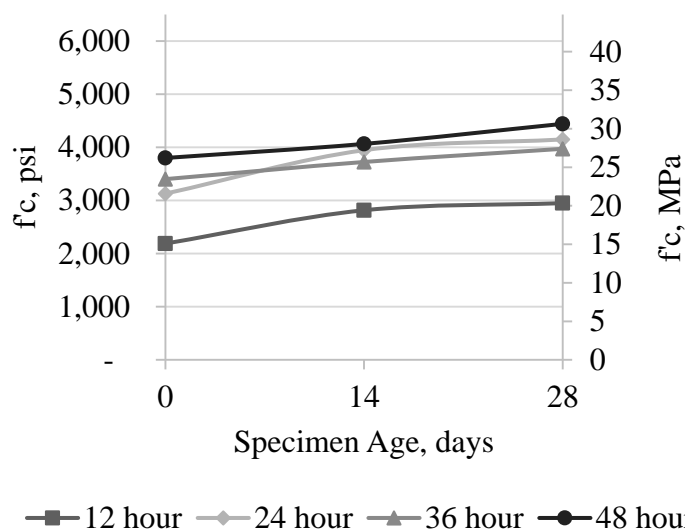


Figure: 4.10 Strength development with specimen age of batch 3.70, Mix 3 cured at 158°F (70°C).

Table: 4.7 Average compressive strength of batch 1.80.

1.80	0 - day		14 - days		28 - days	
	psi	MPa	psi	MPa	psi	MPa
12 hour	3,418	24	3,983	27	5,153	36
24 hour	4,611	32	4,867	34	5,143	35
36 hour	5,210	36	5,730	40	5,843	40
48 hour	5,618	39	5,675	39	5,772	40

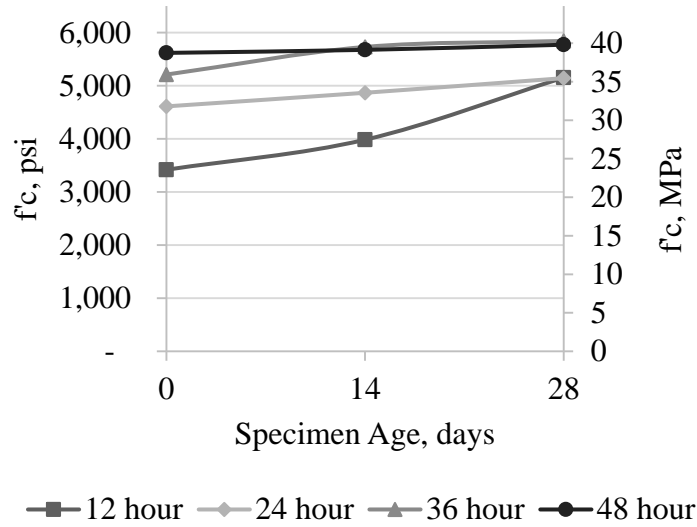


Figure: 4.11 Strength development with specimen age of batch 1.80, Mix 1 cured at 176°F (80°C).

Table: 4.8 Average compressive strength of batch 2.80.

2.80	0 - day		14 - days		28 - days	
	psi	MPa	psi	MPa	psi	MPa
12 hour	2,937	20	3,529	24	3,481	24
24 hour	3,898	27	4,307	30	4,347	30
36 hour	4,234	29	4,923	34	4,622	32
48 hour	5,213	36	4,953	34	5,407	37

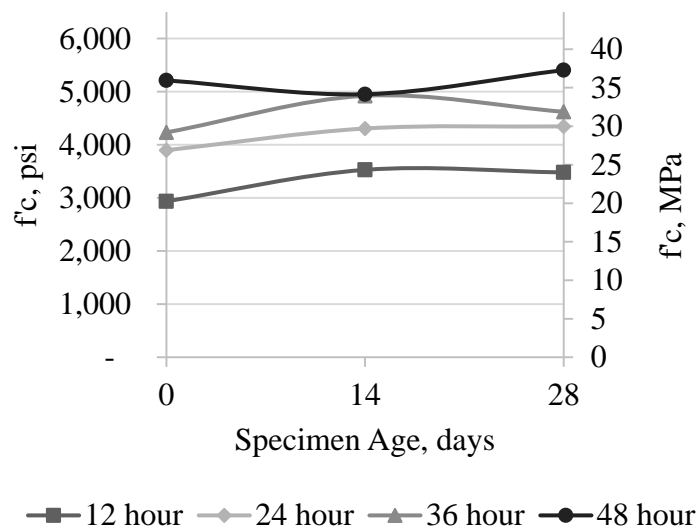


Figure: 4.12 Strength development with specimen age of batch 2.80, Mix 2 cured at 176°F (80°C).

Table: 4.9 Average compressive strength of batch 3.80.

3.80	0 - day		14 - days		28 - days	
	psi	MPa	psi	MPa	psi	MPa
12 hour	3,171	22	3,567	25	3,691	25
24 hour	4,047	28	4,230	29	4,397	30
36 hour	3,827	26	4,359	30	5,485	38
48 hour	4,669	32	4,401	30	4,446	31

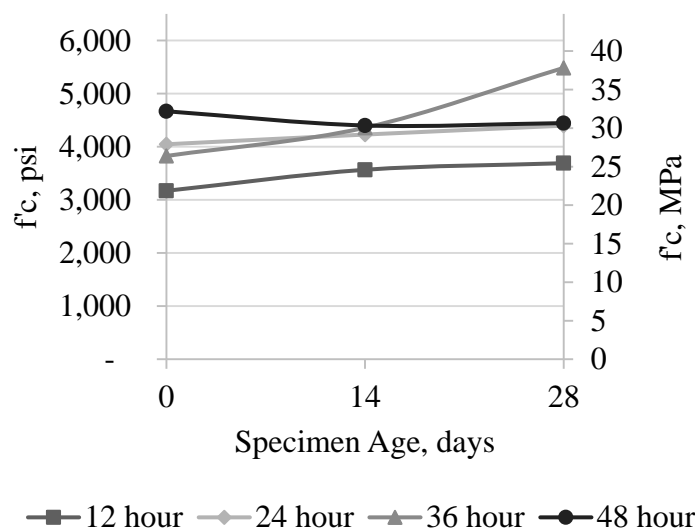


Figure: 4.13 Strength development with specimen age of batch 3.80, Mix 3 cured at 176°F (80°C).

4.4.2 Modulus of Rupture

Small beam samples were tested according to ASTM C78 (2010), “Standard Test Method for Flexural Strength of Concrete (Using Simple Beam with Third-Point Loading),” with the following procedures. The small beams of size 20”Lx6”Wx6”H (508mmx152mmx152mm) were tested in third-point loading. The test again used the Universal Testing Machine (UTM) to load the samples. The samples were placed on two supports at one-inch from the edges and loaded by placing two point loads at six inches from each edge on the opposing face. The loads were applied at a rate of 125-175 pounds (56.7 kg – 79.4 kg) per minute until failure. Upon failure the samples were removed to

ensure the failure occurred within the middle third of the sample. Figure: 4.14 shows the testing setup of a sample following rupture. The modulus of rupture (MOR) was then calculated using Equation 4.3 and is shown in Table: 4.10.



Figure: 4.14 Testing setup for modulus of rupture per ASTM C78.

$$R = \frac{PL}{bd^2} \tag{Equation 4.3}$$

Table: 4.10 Average modulus of rupture results, psi (MPa).

Curing duration and Batch						
	1.60		2.60		3.60	
24 hour	515 (3.551)	*	510 (3.516)	776 (5.350)	*	398 (2.744)
48 hour	787 (5.426)	644 (4.440)	635 (4.378)	514 (3.544)	492 (3.392)	503 (3.468)
	1.70		2.70		3.70	
24 hour	612 (4.220)	594 (4.095)	915 (6.309)	649 (4.475)	723 (4.985)	849 (5.854)
48 hour	1087 (7.495)	1017 (7.012)	677.5 (4.675)	996 (6.867)	551 (3.799)	528 (3.640)
	1.80		2.80		3.80	
48 hour	*	*	789 (5.440)	920 (6.343)	761 (5.245)	*

Samples tested all failed within the middle third.

*Samples were not tested.

The results of the modulus of rupture are compared to the ACI 318-14 (2014)

Equation 9-10, which is shown below as Equation 4.4a and 4.4b.

$$f_r = 7.5 \times \lambda \times \sqrt{f'_c} \text{ (psi)} \quad \text{Equation 4.4a}$$

$$f_r = 70.6 \times \lambda \times \sqrt{f'_c} \text{ (Mpa)} \quad \text{Equation 4.4b}$$

Where:

f_r is the Modulus of Rupture
 λ is equal to 1 for normalweight concrete
 f'_c is the design compressive strength

Table: 4.12 provides a comparison of the calculated and measured values. Figure: 4.15 illustrates the comparison of the values. Measured values of modulus of rupture of GCC were higher than those calculated using the compressive strength indicating a conservative calculation with the equation provide by ACI 318-14 (2014).

Table: 4.11 Average modulus of rupture results, psi (MPa).

Batch	f'c		ACI, f _r		Measured	
	psi	MPa	psi	MPa	psi	MPa
1.60.24	3554	24.50	447	3.08	515	3.55
1.60.48	3751	25.86	459	3.16	715	4.93
2.60.24	2631	18.14	385	2.65	643	4.43
2.60.48	3358	23.15	435	3.00	575	3.96
3.60.24	1954	13.47	332	2.29	398	2.74
3.60.48	2859	19.71	401	2.76	497	3.43
1.70.24	4763	32.84	518	3.57	603	4.16
1.70.48	6008	41.42	581	4.01	1052	7.25
2.70.24	3904	26.92	469	3.23	782	5.39
2.70.48	5231	36.07	542	3.74	837	5.77
3.70.24	4149	28.61	483	3.33	786	5.42
3.70.48	4443	30.63	500	3.45	540	3.72
2.80.48	5407	37.28	551	3.8	855	5.9
3.80.48	4446	30.65	500	3.45	761	5.25

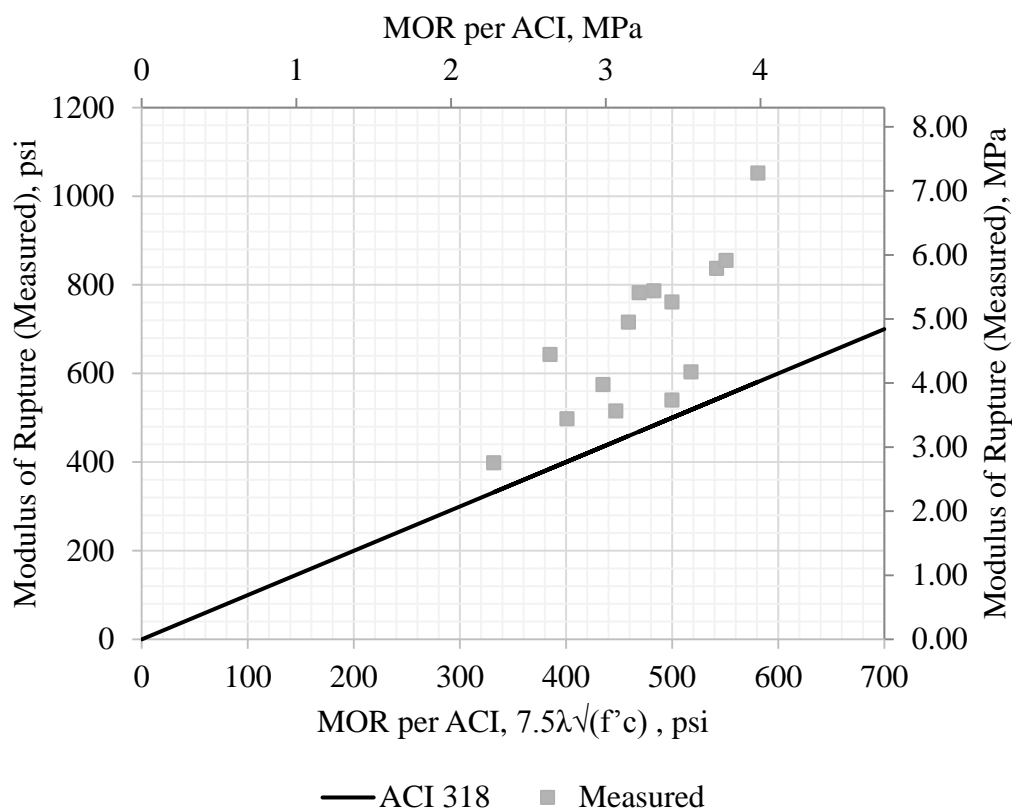


Figure: 4.15 Graph illustrating the comparison between measured modulus of rupture values and those calculated from ACI 318-14 (2014).

4.4.3 Modulus of Elasticity

Cylinder samples were tested according to ASTM C49 with the following procedures. A laser extensometer was used to measure and track the distance between two locations on the surfaces of the concrete cylinders as they were loaded. This test was performed simultaneously with the compressive strength tests. The longitudinal strain was recorded at intervals of one thousand pounds and used to calculate the strain in the samples. The stress and the strain at approximately 40% of the compressive strength of the cylinder were then used to calculate the modulus of elasticity. The recorded values were also plotted and linear trend line was fitted to the data associated with up to forty percent of the compressive strength to estimate the slope, which was taken as another

measurement of the modulus of elasticity value. A further comparison was made by estimating the modulus of elasticity according to the index equation provided in section 8.5 of ACI 318-14 (2014) and a modification proposed by Tempest et al. (2016).

4.4.3.1 Calculations

The following is a summary of calculations performed for the modulus of elasticity.

$$\sigma = \frac{P}{A} \quad \text{Equation 4.5}$$

$$\varepsilon = \frac{\Delta L}{L} \quad \text{Equation 4.6}$$

Where:

- P is the applied load
- A is the cross-sectional area
- ΔL is the difference in the distance between the two points
- L is the original distance

$$E = \frac{\sigma}{\varepsilon} \quad \text{Equation 4.7}$$

4.4.3.2 Design Equations

ACI 318 (ACI 2014) proposes the following equation for the modulus of elasticity of concrete:

$$E_c = 33 \times w_c^{1.5} \times \sqrt{f'_c} \text{ (psi)} \quad \text{Equation 4.8a}$$

$$E_c = 0.043 \times w_c^{1.5} \times \sqrt{f'_c} \text{ (MPa)} \quad \text{Equation 4.8b}$$

Tempest et al. (2016) proposed the following modification for calculating the modulus of elasticity of GCC:

$$E_c = 43,000 \times \sqrt{f'_c} \text{ (psi)} \quad \text{Equation 4.9a}$$

$$E_c = 3,575 \times \sqrt{f'_c} \text{ (MPa)} \quad \text{Equation 4.9b}$$

4.4.3.3 Modulus of Elasticity Results

Table: 4.12 details a summary of selected modulus of elasticity (MOE) values as recorded by successful readings of the laser extensometer with a comparison to the equations presented by ACI 318 (ACI 2014) and Tempest et al. (2016). Figure: 4.16 illustrates the method of determining the slope of the calculated strain values used to compare MOE values with those recommended. Figure: 4.17 illustrates the comparison of calculated values by ACI 318 (ACI 2014) and Tempest et al. (2016) compared to the measured values. Typically, the measured values fell closer to the equation proposed by Tempest et al. (2016) as is illustrated by Figure: 4.17.

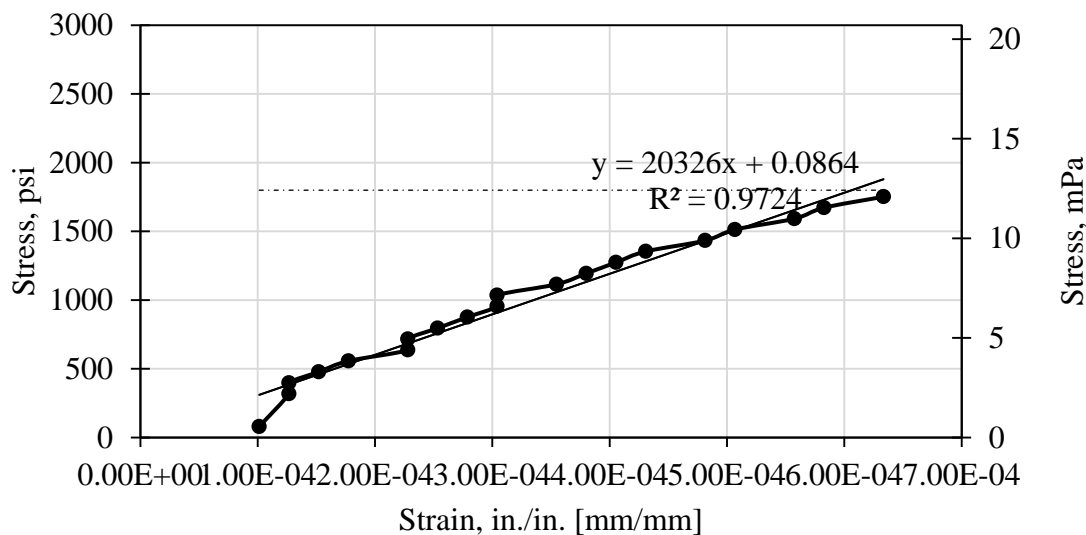


Figure: 4.16 Graph illustrating method of determining MOE of measured data for direct comparison to alternate methods.

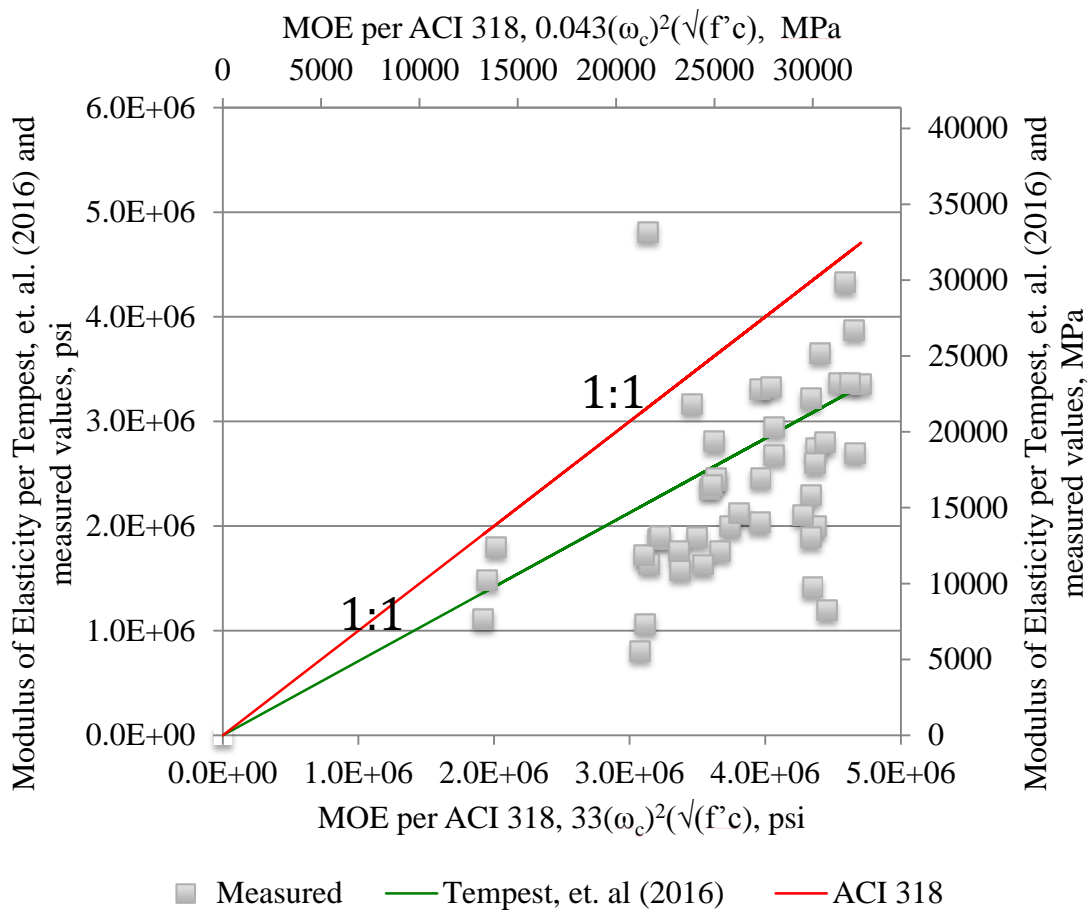


Figure: 4.17 Graph illustrating the comparison between measured modulus of elasticity values and those calculated from Tempest et al. (2016), and ACI 318-14 (2014).

Table: 4.12 Sample 28 day modulus of elasticity measurements and comparison with ACI 318-14 (2014) and Tempest et al. (2016)

Sample ID	f_c		$0.4 \times f_c$		ACI 318-14 (2014)		Tempest et al. (2016)		Measured MOE	
	psi	MPa	psi	MPa	psi	MPa	psi	MPa	psi	MPa
3.80.C.24.28.1	4,499	31.0	1,800	12.4	4,066,388	28,036.8	2,884,207	19,885.9	2,947,969	20,325.5
2.80.C.24.28.3	4,274	29.5	1,710	11.8	3,963,402	27,326.7	2,811,161	19,382.3	3,306,881	22,800.2
2.80.C.24.28.2	4,266	29.4	1,706	11.8	3,959,691	27,301.1	2,808,529	19,364.1	2,034,913	14,030.2
2.80.C.24.28.1	4,500	31.0	1,800	12.4	4,066,840	28,039.9	2,884,528	19,888.1	2,683,514	18,502.2
1.80.C.24.28.3	5,201	35.9	2,080	14.3	4,372,142	30,144.9	3,101,072	21,381.1	2,743,179	18,913.6
1.80.C.24.28.2	5,117	35.3	2,047	14.1	4,336,692	29,900.5	3,075,928	21,207.8	2,298,937	15,850.6
1.80.C.24.28.1	5,112	35.2	2,045	14.1	4,334,572	29,885.8	3,074,425	21,197.4	3,221,629	22,212.4
1.80.B.48.28.3	6,029	41.6	2,412	16.6	4,707,317	32,455.8	3,338,805	23,020.3	3,358,548	23,156.4
1.80.B.48.28.1	5,613	38.7	2,245	15.5	4,542,013	31,316.1	3,221,558	22,211.9	3,368,062	23,222.0
1.80.C.12.28.3	5,201	35.9	2,080	14.3	4,372,142	30,144.9	3,101,072	21,381.1	1,996,165	13,763.1
1.80.C.12.28.2	5,145	35.5	2,058	14.2	4,348,540	29,982.1	3,084,332	21,265.7	1,415,573	9,760.0
1.80.C.12.28.1	5,112	35.2	2,045	14.1	4,334,572	29,885.8	3,074,425	21,197.4	1,890,450	13,034.2
2.80.C.12.28.3	3,599	24.8	1,440	9.9	3,636,987	25,076.2	2,579,642	17,786.0	2,442,753	16,842.2
2.80.C.12.28.2	3,514	24.2	1,406	9.7	3,593,782	24,778.3	2,548,997	17,574.7	2,356,706	16,248.9
2.80.C.12.28.1	3,329	23.0	1,332	9.2	3,497,903	24,117.2	2,480,992	17,105.8	1,890,400	13,033.9
3.80.C.12.28.3	3,657	25.2	1,463	10.1	3,666,176	25,277.4	2,600,345	17,928.8	1,764,111	12,163.1
3.80.C.12.28.2	3,810	26.3	1,524	10.5	3,742,082	25,800.8	2,654,183	18,300.0	1,997,782	13,774.2
3.80.C.12.28.1	3,605	24.9	1,442	9.9	3,640,017	25,097.0	2,581,791	17,800.8	2,460,950	16,967.7
1.80.B.36.28.3	5,730	39.5	2,292	15.8	4,589,107	31,640.8	3,254,961	22,442.2	4,329,911	29,853.7
1.80.B.36.28.2	5,908	40.7	2,363	16.3	4,659,841	32,128.5	3,305,131	22,788.1	2,696,319	18,590.5
1.80.B.36.28.1	5,891	40.6	2,356	16.2	4,653,132	32,082.2	3,300,373	22,755.3	3,873,762	26,708.7
3.70.C.24.28.3	3,949	27.2	1,580	10.9	3,809,732	26,267.2	2,702,166	18,630.8	2,122,000	14,630.7

Table: 4.12 (Continued.)

3.70.C.24.28.1	4,277	29.5	1,711	11.8	3,964,792	27,336.3	2,812,147	19,389.1	2,461,220	16,969.5
3.70.C.12.28.2	3,098	21.4	1,239	8.5	3,374,361	23,265.4	2,393,366	16,501.7	1,580,006	10,893.8
3.70.C.12.28.1	2,801	19.3	1,120	7.7	3,208,539	22,122.1	2,275,752	15,690.8	1,876,578	12,938.6
2.60.C.24.28.3	2,576	17.8	1,030	7.1	3,076,974	21,215.0	2,182,435	15,047.4	806,935	5,563.6
2.60.C.24.28.2	2,691	18.6	1,076	7.4	3,144,906	21,683.4	2,230,619	15,379.6	1,640,846	11,313.2
2.60.C.24.28.1	2,626	18.1	1,050	7.2	3,106,692	21,419.9	2,203,514	15,192.7	1,719,893	11,858.2
1.60.C.24.28.3	3,536	24.4	1,414	9.7	3,605,014	24,855.7	2,556,964	17,629.7	2,395,994	16,519.8
1.60.C.24.28.1	3,576	24.7	1,430	9.9	3,625,347	24,995.9	2,571,386	17,729.1	2,809,913	19,373.7
3.60.C.12.28.3	1,104	7.6	442	3.0	2,014,352	13,888.5	1,428,739	9,850.8	1,799,346	12,406.1
3.60.C.12.28.2	1,005	6.9	402	2.8	1,921,914	13,251.1	1,363,175	9,398.8	1,115,881	7,693.7
3.60.C.12.28.1	1,035	7.1	414	2.9	1,950,388	13,447.5	1,383,371	9,538.0	1,483,023	10,225.1
1.60.C.12.28.3	2,670	18.4	1,068	7.4	3,132,611	21,598.6	2,221,898	15,319.5	4,812,258	33,179.4
1.60.C.12.28.2	2,833	19.5	1,133	7.8	3,226,815	22,248.1	2,288,715	15,780.1	1,905,252	13,136.3
1.60.C.12.28.1	2,642	18.2	1,057	7.3	3,116,142	21,485.1	2,210,217	15,238.9	1,068,180	7,364.8
1.70.B.48.28.1	5,819	40.1	2,328	16.1	4,624,609	31,885.6	3,280,142	22,615.8	3,367,774	23,220.0
2.70.B.48.28.2	5,274	36.4	2,110	14.5	4,402,718	30,355.7	3,122,759	21,530.7	3,657,724	25,219.1
2.70.B.48.28.1	5,191	35.8	2,076	14.3	4,367,937	30,115.9	3,098,090	21,360.6	2,599,541	17,923.2
1.70.C.24.28.1	4,986	34.4	1,994	13.7	4,280,820	29,515.2	3,036,299	20,934.6	2,109,747	14,546.2
1.70.B.36.28.2	5,359	36.9	2,144	14.8	4,438,055	30,599.3	3,147,823	21,703.5	2,799,155	19,299.5
1.70.B.36.28.1	5,403	37.3	2,161	14.9	4,456,237	30,724.7	3,160,719	21,792.4	1,197,087	8,253.6
1.70.C.12.28.3	3,413	23.5	1,365	9.4	3,541,759	24,419.6	2,512,098	17,320.3	1,631,943	11,251.9
1.70.C.12.28.2	3,079	21.2	1,232	8.5	3,363,998	23,194.0	2,386,016	16,451.0	1,758,692	12,125.8
1.70.C.12.28.1	3,259	22.5	1,304	9.0	3,460,932	23,862.3	2,454,769	16,925.0	3,169,606	21,853.7
3.70.B.48.28.2	4,446	30.7	1,778	12.3	4,042,365	27,871.1	2,867,168	19,768.4	3,332,319	22,975.5

CHAPTER 5: SENSITIVITY ANALYSIS

5.1 Statistical Analysis Methodology

The purpose of the sensitivity analysis presented here is to determine the level of influence of a production variable on the resulting mechanical properties. The production variables w/cm , temperature during high temperature curing, and high temperature curing duration are each known to impact the compressive strength and elastic properties of GCC. This analysis determines the level of influence by changing each variable or a combination of variables and measuring the outcome.

Multiple experiments were performed by varying the independent variables and measuring the outcome on the dependent variable (compressive strength). The study uses the compressive strength as the dependent variable and the w/cm , curing temperature, and curing duration as the three separate independent variables. The age of the sample is also taken into account as a separate variable. This portion of the analysis seeks to determine whether the level of importance of a variable increases or decreases as the concrete ages and the microstructure continues to develop.

The primary method of analysis for the data involved a multiple regression analysis. In the analysis, two multiple regression models are used. In the multiple regression, it is assumed that the compressive strength is the dependent or y-variable. The production variables become the independent X_n -variables. The following is the breakdown of the parameters:

Y : compressive strength

X_1 : w/cm

X_2 : curing temperature

X_3 : curing duration

β_x : Variable representing the additional affect of adding a specific factor

As there are three independent variables, interactions between the variables were also considered. It was previously known that each of the production variables can potentially affect the compressive strength. But the goal of this multiple regression analysis and model is to determine how more than one variable can affect the compressive strength. The analysis seeks 1) to identify the magnitude of the effect that each production variable has on the compressive strength outcome and, 2) to determine whether the effects of the production variables are fully independent to each other, or are dependent on the value of the other production variables. The goal becomes then to achieve the types of if-then scenarios for combinations or adjustments of variables.

The multi variable model can take on a few different forms, four primary models are shown below.

A first-order linear model

$$Y = \beta_0 + \beta_1 X_1 + \beta_2 X_2 + \beta_3 X_3 \quad \text{Equation 6.1}$$

A second-order no-interaction model

$$Y = \beta_0 + \beta_1 X_1 + \beta_2 X_2 + \beta_3 X_3 + \beta_4 X_1^2 + \beta_5 X_2^2 + \beta_6 X_3^2 \quad \text{Equation 6.2}$$

A first-order predictors and interactions model

$$Y = \beta_0 + \beta_1 X_1 + \beta_2 X_2 + \beta_3 X_3 + \beta_4 X_1 X_2 + \beta_5 X_2 X_3 + \beta_6 X_1 X_3 \quad \text{Equation 6.3}$$

A second-order model (full quadratic model)

$$Y = \beta_0 + \beta_1 X_1 + \beta_2 X_2 + \beta_3 X_3 + \beta_4 X_1^2 + \beta_5 X_2^2 + \beta_6 X_3^2 + \beta_7 X_1 X_2 + \beta_8 X_2 X_3 + \beta_9 X_1 X_3 \quad \text{Equation 6.4}$$

These models represent the possibilities of equations created to fit a data set with three different independent variables. The equations range from the first order linear model that places a multiplication factor on each independent variable to sum to the dependent variable reaction. The more complicated second-order model, also known as a full quadratic model, begins to allow for more complex relationships between the independent variables. It depicts a relationship between any of the two independent variables as influencing the dependent variable. A simple example is the relationship between the curing temperature and the curing duration, as previously noted in Section 4.1, a higher curing temperature paired with a high curing duration can result in a higher compressive strength.

The appropriateness of the model that is created is then measured by the *coefficient of determination* typically defined as a measure of model accuracy based on the experimental data. The coefficient of determination is best known as the “ R^2 ” of a model equation and the closer the value is to one, the better the model fits the data. The relationship is given in Equation 6.5. The R^2 value indicates what percentage of data points fall into the proposed model for the experimental data.

$$R^2 = 1 - \frac{\Sigma non\ fit\ values^2}{\Sigma total\ values^2} \quad \text{Equation 6.5}$$

In the case of this data, a statistical processor, Minitab, was used to create the regression models for this study (Minitab Inc.). The input to the processor were the production variables and the compressive strength results of over three hundred samples (see Section 3.2 for a breakdown of samples) to build the best fitting model. The processor builds each variable into the equation as shown in Figure: 5.1. It then performs a stepwise process to add in the pieces of the multiple regression model following the

same form of the primary models. Following each addition of a variable the R^2 value is checked for the fitting of the model. Once the processor completes the additions of parameters it finalizes the model. As shown in Figure: 5.1, the processor took seven steps to create a final model with a final R^2 value of 88.39%.

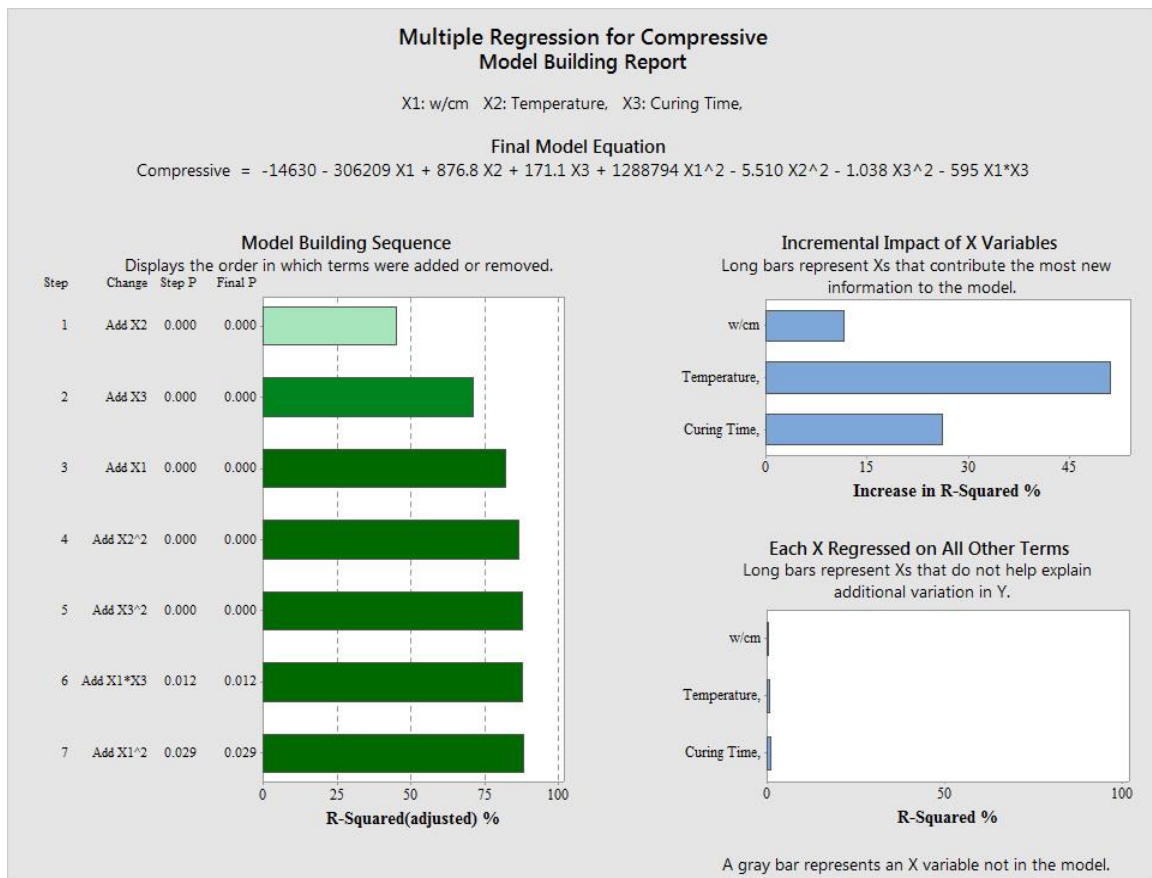


Figure: 5.1 Multiple regression model building by the Minitab statistical processor.

Data from over three hundred samples was used in the model building. Two general models were created to determine the relationships among all data points, a linear model and a full quadratic model. The data is further broken down based on the age of the samples, translating to roughly one hundred samples at zero, fourteen, and twenty-eight days of testing. The purpose of further separating the data was to determine if the same production parameters would continue to have the same effects on the compressive

strength over time. The models at each stage are full quadratic models. At this stage the linear models were not considered as they did not provide an accurate enough model.

The following is a list of the analyses that were performed to provide the sensitivity analysis:

1. Multiple regression analysis of all data
 - a. Interaction plots of parameters
 - b. Main effects plots of parameters
 - c. Compressive strength optimization analysis
2. Multiple regression analysis of 0-day specimen age data
 - a. Compressive strength optimization analysis
3. Multiple regression analysis of 14-day specimen age data
 - a. Compressive strength optimization analysis
4. Multiple regression analysis of 28-day specimen age data
 - a. Compressive strength optimization analysis

5.1.1 Multiple Regression Analysis of All Data

The multiple regression analysis of all the data considers the production variables, w/cm , curing temperature, and curing duration, and their impact to the compressive strength. The modeling results from the Minitab statistical processor are shown in Table: 5.1. The first analysis is a single interaction model where the parameters are individually taken into account creating first-order linear model. The second model builds on the possibility of interactions between parameters creating a full quadratic model; this is indicated by the polynomial and squaring of variables in the equation.

Table: 5.1 Multiple regression models and optimization results of analysis of all data.

Model Equation	R^2 , %, of model	Incremental increase in R^2 , %
Linear Model $Y = 296 - 53188X_1 + 107.41X_2 + 47.78X_3$	82.36%	X_1 , 10.9666 X_2 , 47.1551 X_3 , 25.6197
Quadratic Model $Y = -14630 - 306209X_1 + 876.8X_2 + 1711X_3 + 1288794X_1^2 - 5.510X_2^2 - 1.038X_3^2 - 595X_1*X_3$	88.39%	X_1 , 11.5560 X_2 , 50.9746 X_3 , 26.0861

Both models show that the curing temperature has the largest impact on the compressive strength followed by the curing duration and w/cm . The impact defined by the model is the progressive adjustment of the model and the increasing of the R^2 value. Thus, the conditions that resulted in the greatest compressive strength were related to the highest curing temperature, the longest curing duration, and the lowest w/cm . The equations consistently show that the higher compressive strengths depend on the maximized highest curing temperature, maximized curing duration, and minimized water content.

The quadratic model fits the data more closely. As the model changes from a first-order linear model to a quadratic model an increase from $R^2 = 82.36\%$ to $R^2 = 88.39\%$ is observed. This indicates that the relationship between the production parameters and the compressive strength is not linear, and also has some dependence on combinations of variables. The model building as previously shown in Figure: 5.1 shows the stepwise building of the full quadratic model, a similar process occurred for the first-order linear model. The model shows interactions between the w/cm and the curing duration as a part of the equation (the $-595X_1*X_2$ portion). This demonstrates that the w/cm in conjunction with the curing duration have an effect on the compressive strength. The third column in Table: 5.1, “Incremental increase in R^2 , %” shows the individual production variables’

impacts to the final model. It shows which independent variable led to a higher R^2 value for the model. The higher contribution to R^2 is associated with greater influence over compressive strength development. In both models, the curing temperature has the greatest influence to the R^2 value of the equation followed by the curing duration and the w/cm , respectively. This pattern was found in both the linear and non-linear models and indicates the importance of the curing temperature on the compressive strength. Based on the models, a lower w/cm is ideal. However, it is possible to overcome the benefit of a lower w/cm with a higher curing temperature and even a lower curing temperature with a higher curing duration.

The linear model is graphed in Figure: 5.2 and the quadratic model in Figure: 5.3. The test data is shown with the linear and quadratic models equations in Figure: 5.4 through Figure: 5.6. The overall trend shows the lowest w/cm as having the highest compressive strengths throughout. However, observation of the results shows that a range of strength between approximately 3500 psi (24 MPa) to 4000 psi (27.6 MPa) could be achieved using any of the w/cm by varying the curing duration and curing temperature. Greater curing duration consistently increases the compressive strength and the quadratic models show the more significant impact of increasing from a 24 hour curing duration to a 48 hour curing duration. As the curing duration is increased the values of the compressive strength increase and the apparent impact of the w/cm increase as well.

Of the 158°F (70°C) curing temperature series, the lowest curing duration of 12 hours for each w/cm is very similar to the 140°F and 48 hour curing samples. These trends are distinctly visible in Figures 4-6 and show the concurrent relationships between the production variables of GCC as they may impact the compressive strength. These

production variables show that there is a degree of flexibility in mixture designs if the target compressive strength is a plus or minus 500 psi (3.45 MPa), for most cases. Essentially, the relationships show that if too much water is added to the mix it can, potentially, be accommodated by increasing the curing temperature and curing duration to achieve the desired compressive strength.

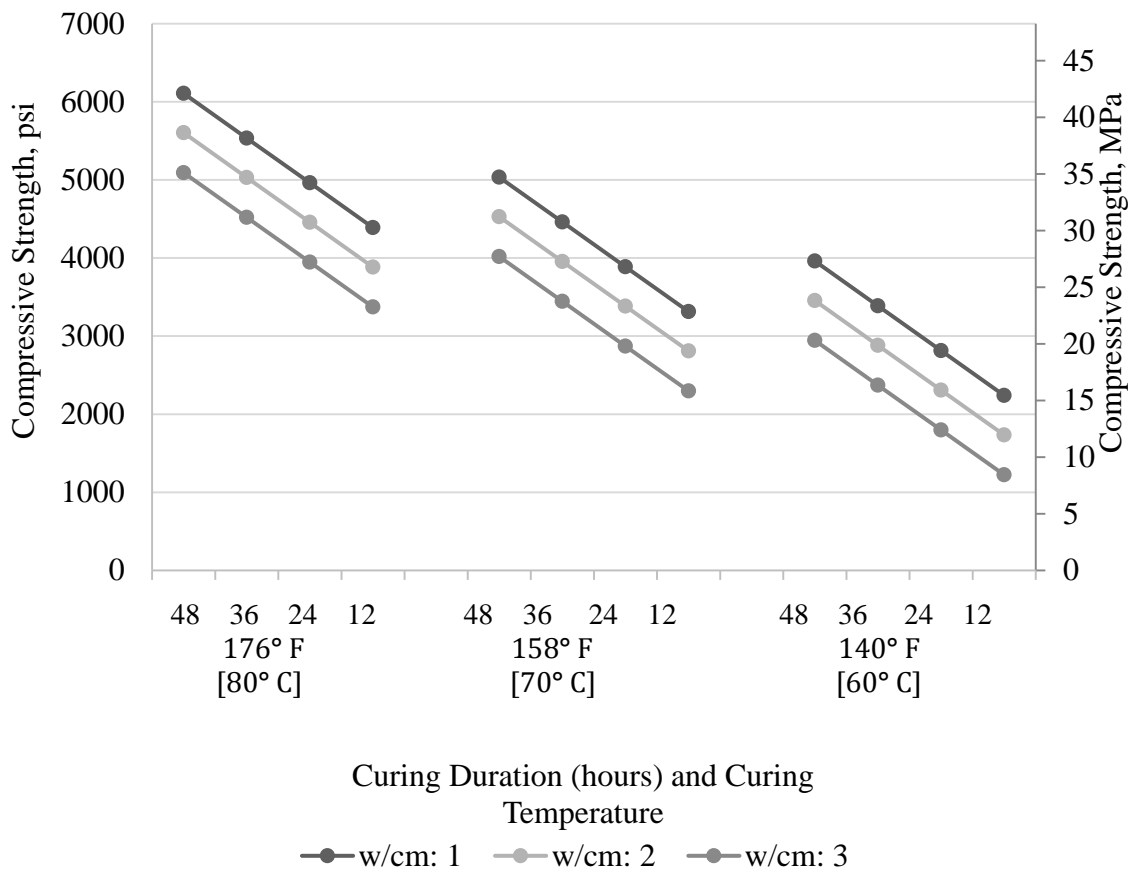


Figure: 5.2 First-order linear equation model showing values for curing durations of 48, 36, 24, and 12 hours.

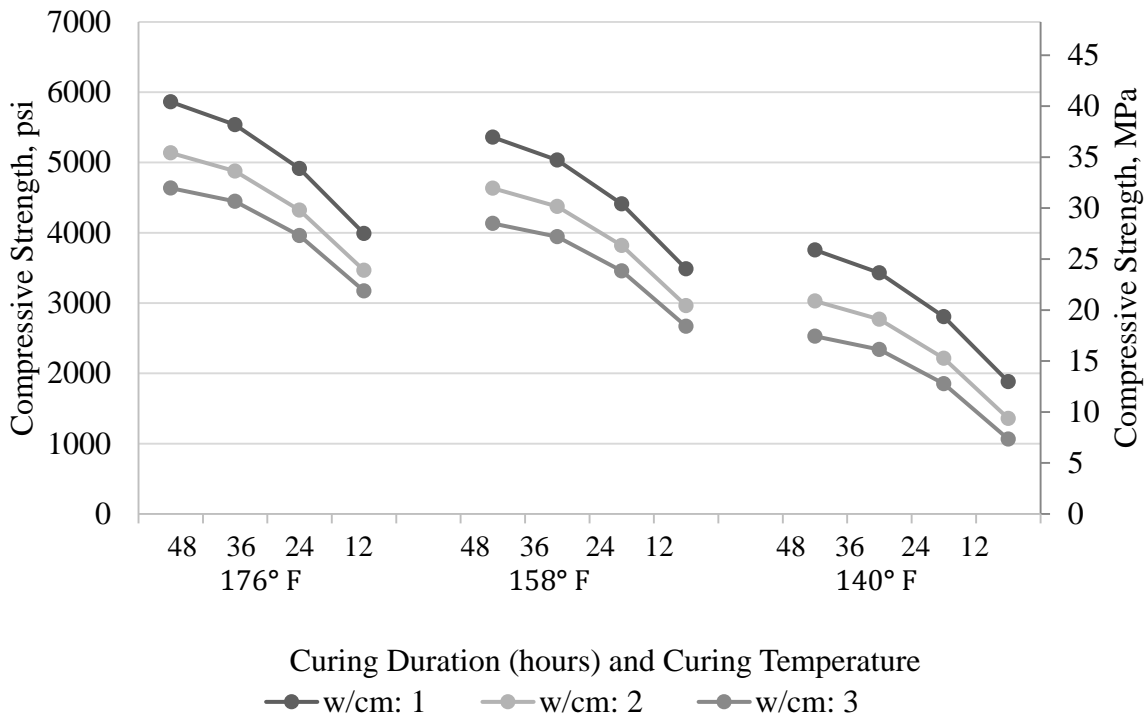


Figure: 5.3 Full quadratic model equation showing the trend for curing durations of 48, 36, 24, and 12 hours at the three curing temperatures.

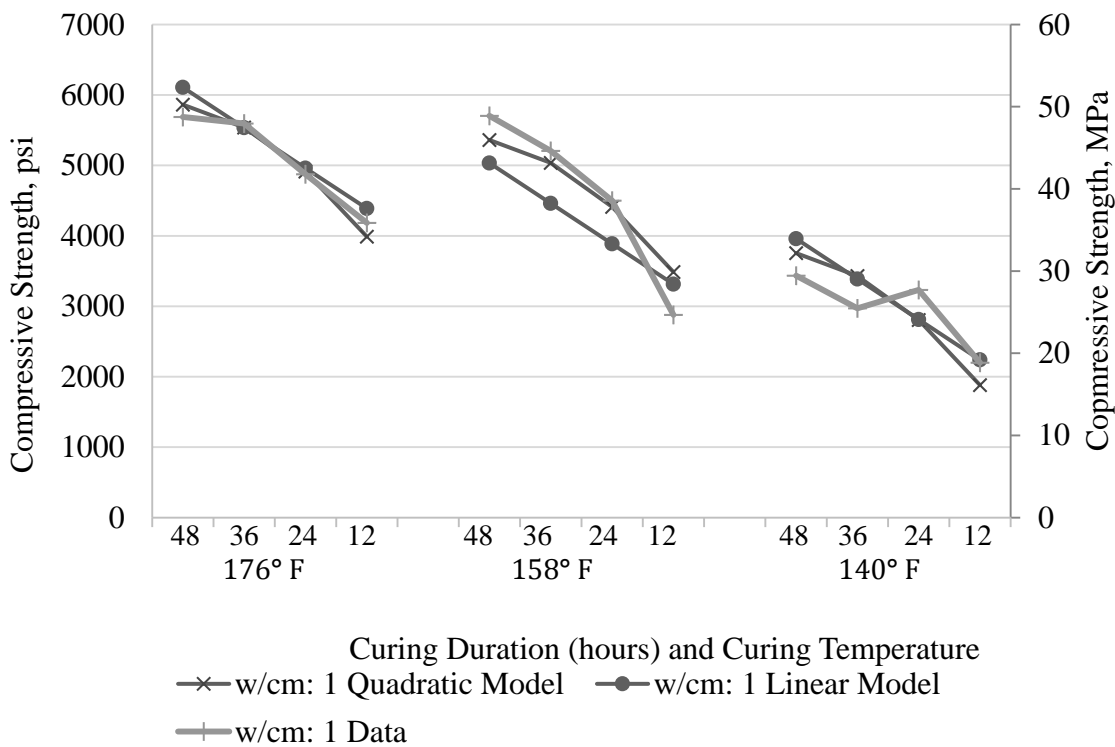


Figure: 5.4 Quadratic model and linear model with experimental data w/cm 1 shown.

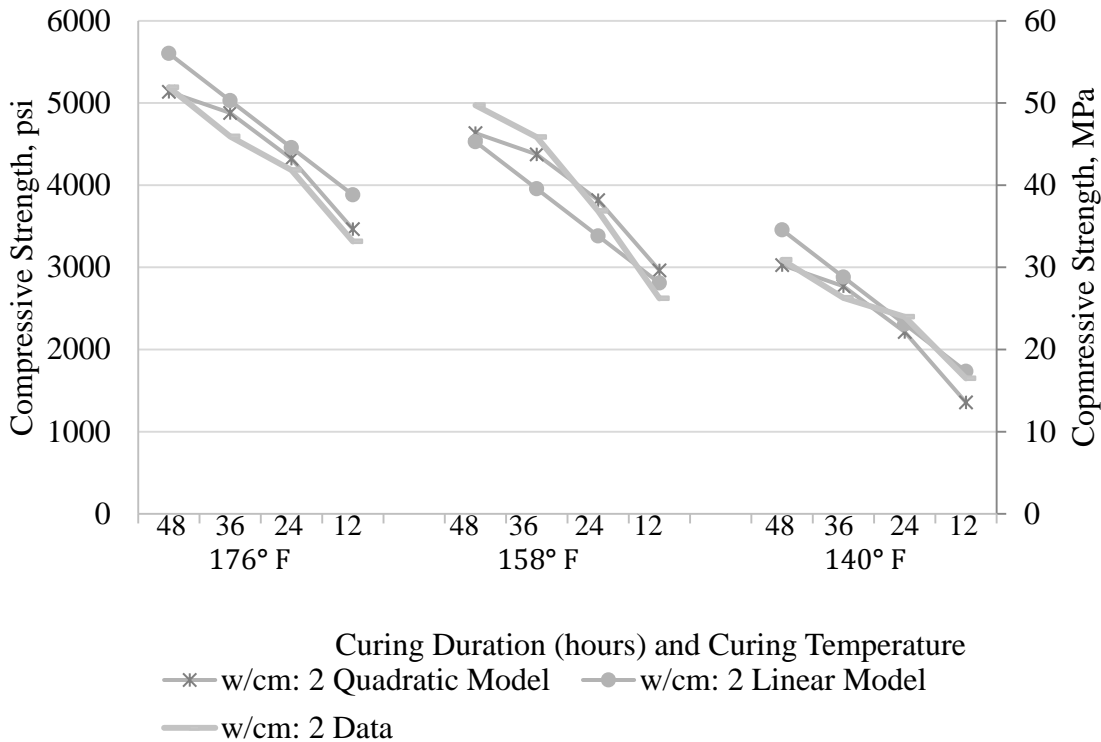


Figure: 5.5 Quadratic model and linear model with experimental data *w/cm* 2 shown.

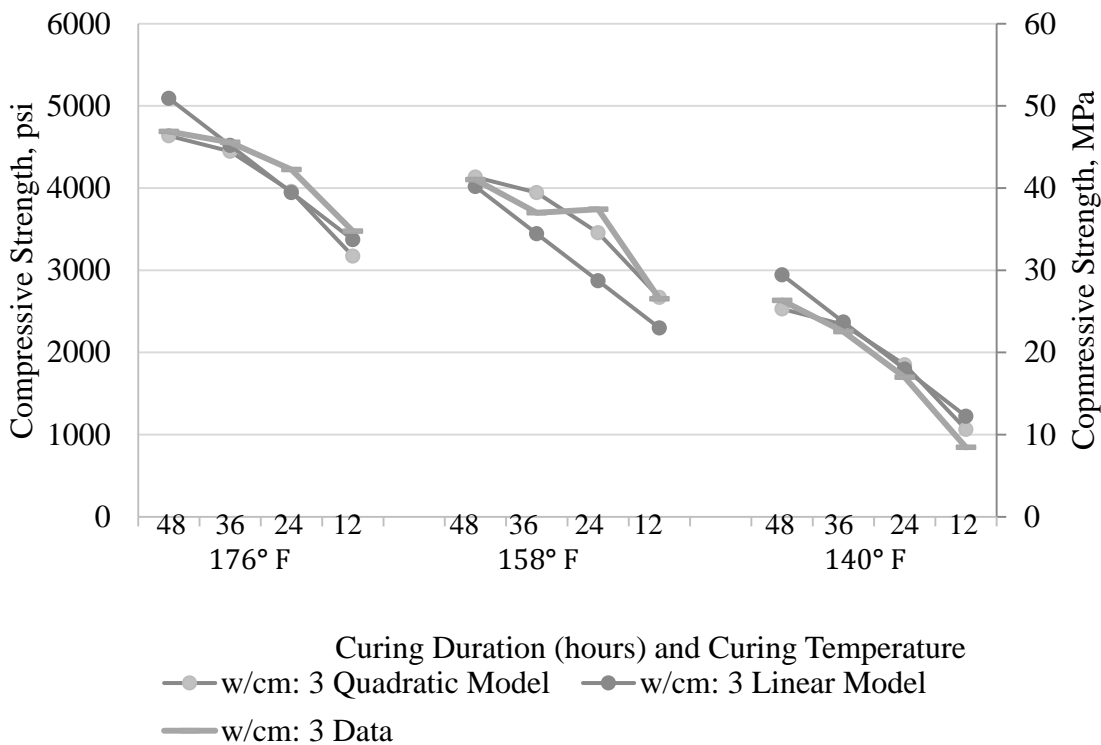


Figure: 5.6 Quadratic model and linear model with experimental data *w/cm* 3 shown.

5.1.2 Multiple Regression Analysis of Data by Concrete Age

The regression analysis has also been broken down by specimen age in order to determine how the variable interactions evolve over time. In prestressed, precast concrete applications, a high early strength is required to resist loads applied during the manufacturing and transporting processes. Other applications such as ground slabs, may only require a design strength the standard 28-day age. Because of this, the analysis for GCC is also divided into sampling at the 0-day, 14-day, and 28-day ages. Table: 5.2 shows the quadratic model equations at each stage in concrete age. In Figure: 5.7, Figure: 5.8, and Figure: 5.9 the full quadratic models for samples tested at three concrete ages are shown. In these models the same overall trend as with the general model is evident; however, some patterns alter as the concrete ages.

Table: 5.2 Multiple regression models analyzed by concrete age.

Samples	Model Equation	R^2 , %, of model	Incremental increase in R^2 , %
0 day curing	$Y = -12214 - 268508X_1 + 709.0X_2 + 191.5X_3 + 1174310X_1^2 - 4.271X_2^2 - 0.921X_3^2 - 796X_1 * X_3$	95.97%	X ₁ , 8.90562 X ₂ , 55.1171 X ₃ , 34.0691
14 day curing	$Y = -33893 - 28954X_1 + 1009.4X_2 + 213.0X_3 - 6.479X_2^2 - 1.251X_3^2 - 901X_1 * X_3$	93.95%	X ₁ , 13.6137 X ₂ , 54.2761 X ₃ , 25.9390
28 day curing	$Y = -7208 - 448686X_1 + 927X_2 + 99.3X_3 + 1862514X_1^2 - 5.887X_2^2 - 0.947X_3^2$	91.98%	X ₁ , 14.6107 X ₂ , 53.3016 X ₃ , 22.2221

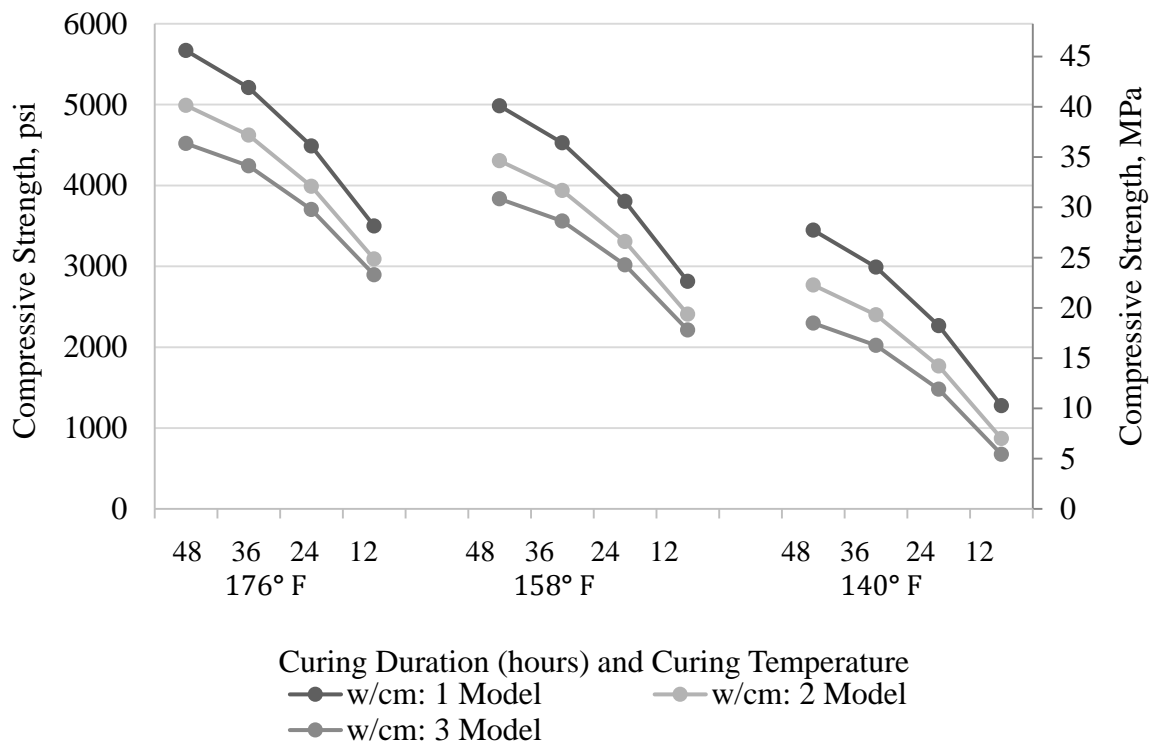


Figure: 5.7 Full quadratic models for samples tested directly following curing.

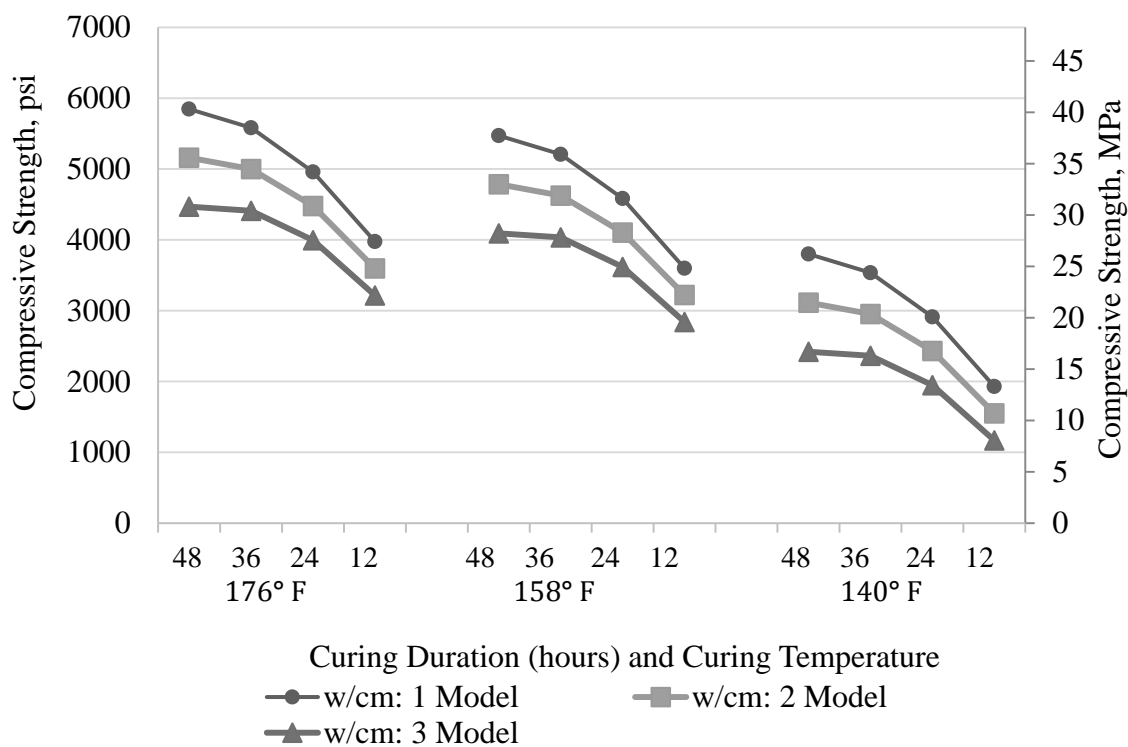


Figure: 5.8 Full quadratic models for samples tested at 14 days following curing.

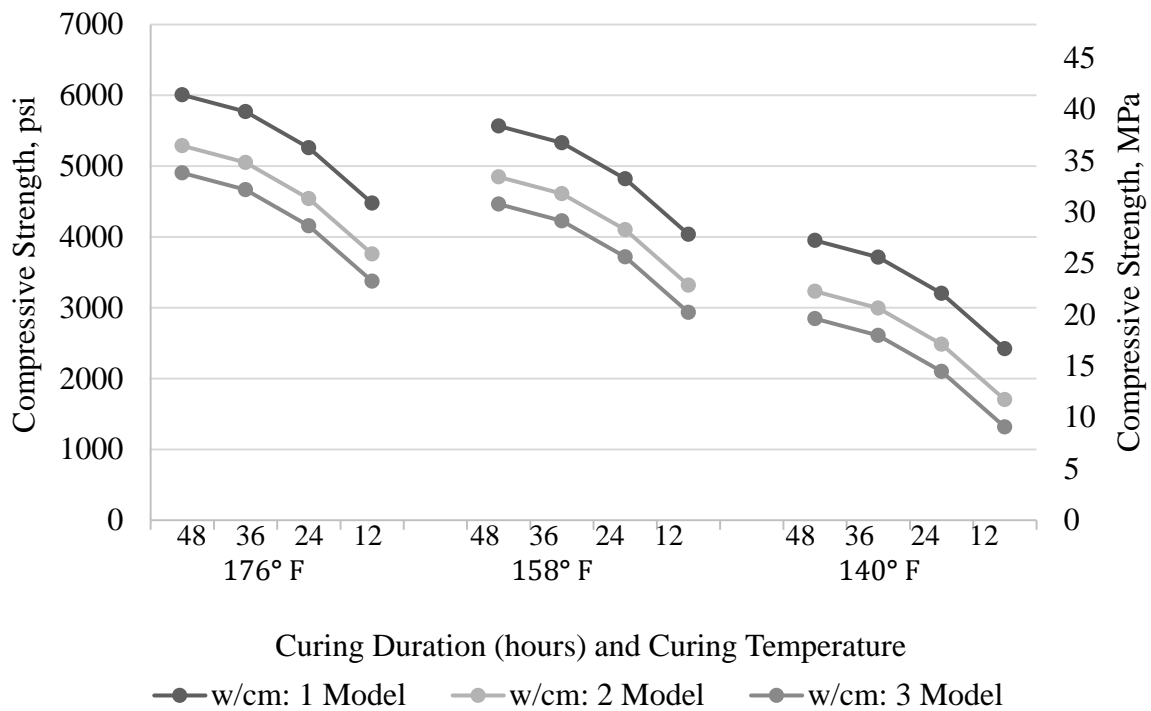


Figure: 5.9 Full quadratic models for samples tested at 28 days following curing.

At the initial testing, directly following heat curing, most of the samples have attained approximately 85% of their 28-day strength. At 14 days of aging in ambient conditions, the concrete is at approximately 93% of its 28-day strength. As the concrete ages the R^2 value of the models decrease which is also indicated by the changes in variables influencing the compressive strength. From the initial testing to the 28-day testing the change in “Incremental increase in R^2 , %” values indicate an increase in influence by the w/cm and a decrease by the curing temperature and curing duration over time. This trend is further illustrated in Figure: 5.10.

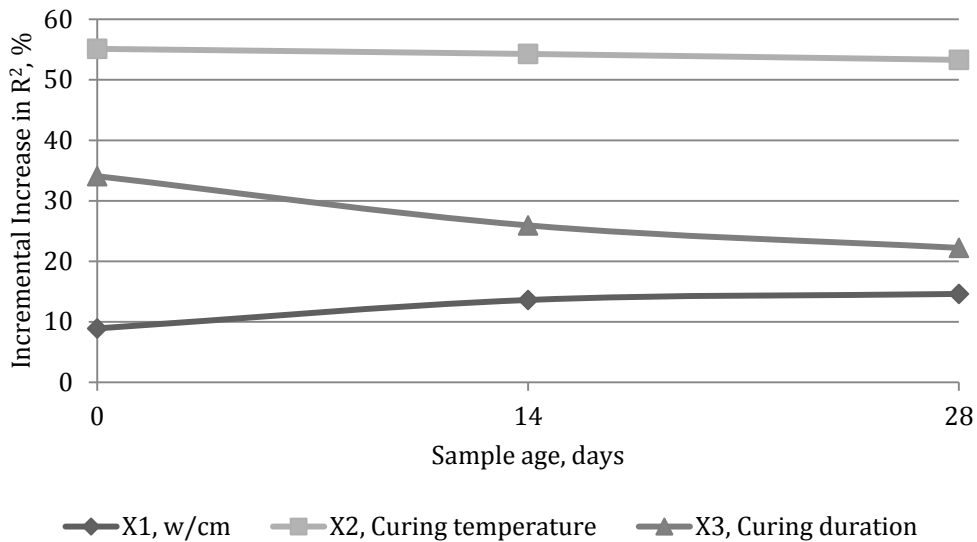


Figure: 5.10 Trend in “Incremental increase in R², %” of each parameter.

Figure: 5.11 through Figure: 5.19 are a combination of the quadratic models and the experimental data. The purpose of these figures is to further create a visual representation of the accuracy of the models as previously discussed.

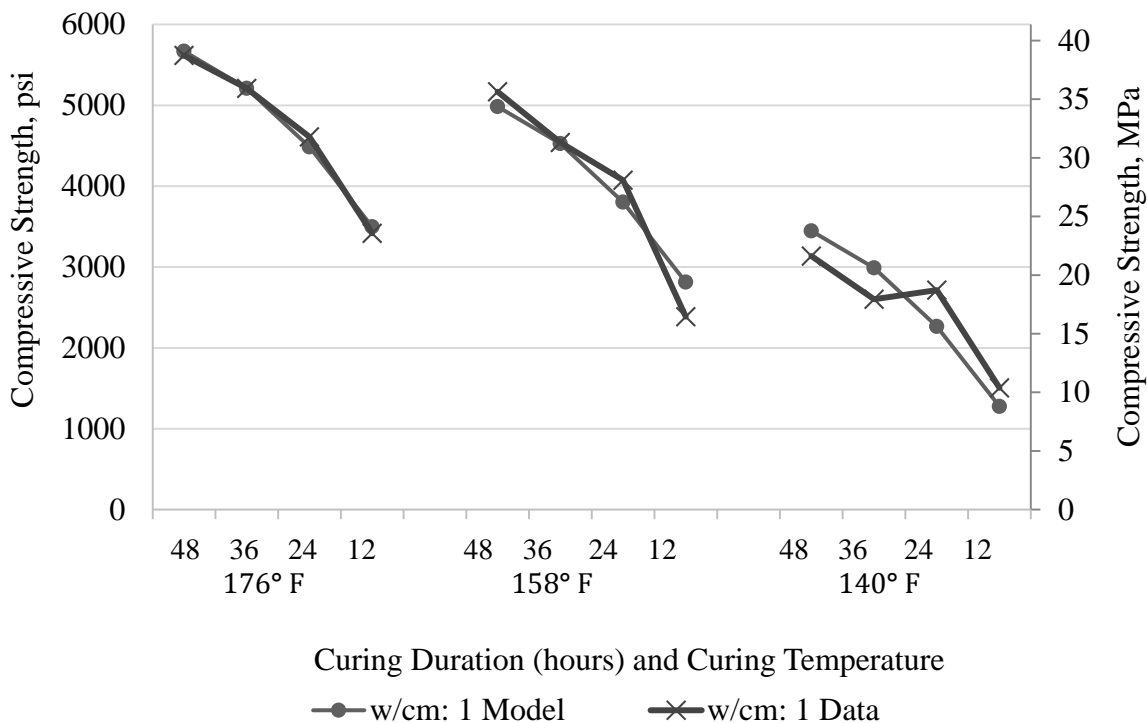


Figure: 5.11 Full quadratic model equation showing the model and experimental data for the three curing temperatures for w/cm 1; concrete age is zero days.

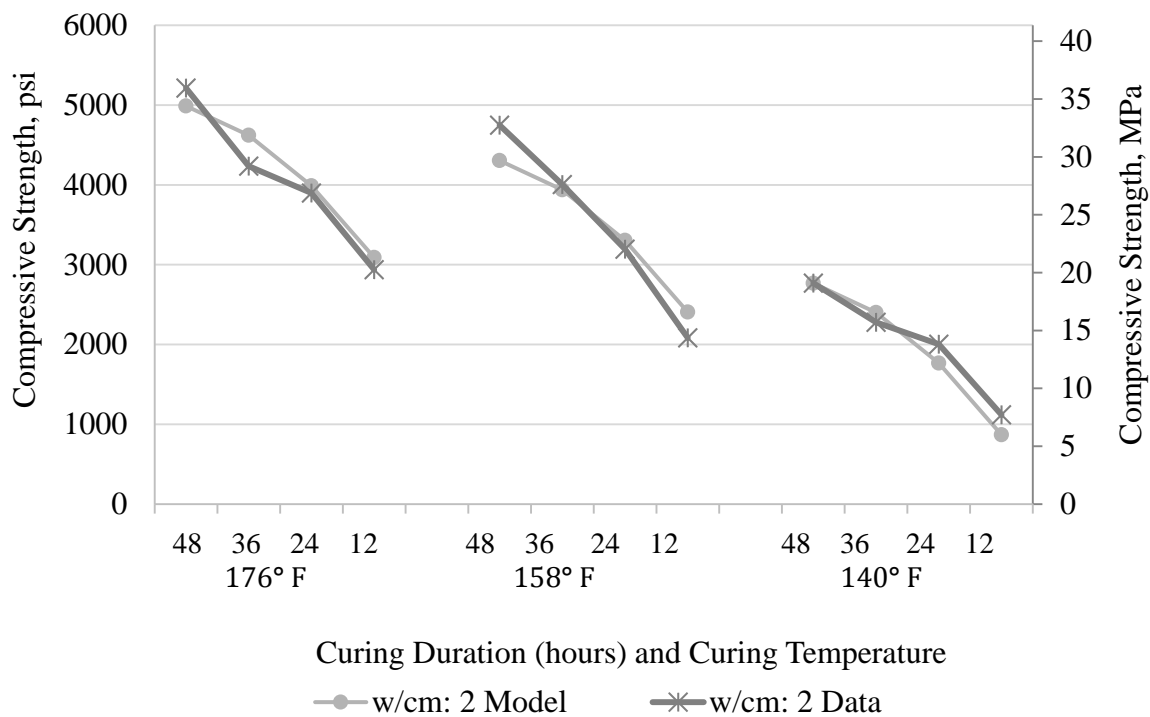


Figure: 5.12 Full quadratic model equation showing the model and experimental data for the three curing temperatures for w/cm 2; concrete age is zero days.

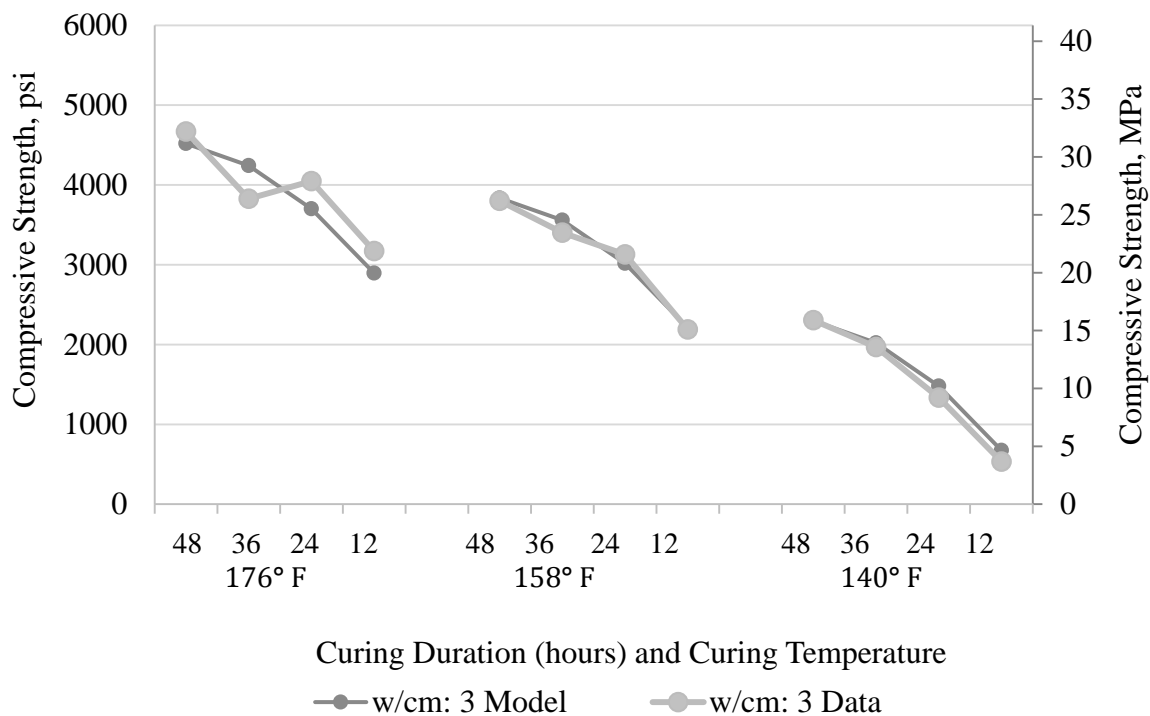


Figure: 5.13 Full quadratic model equation showing the model and experimental data for the three curing temperatures for w/cm 3; concrete age is zero days.

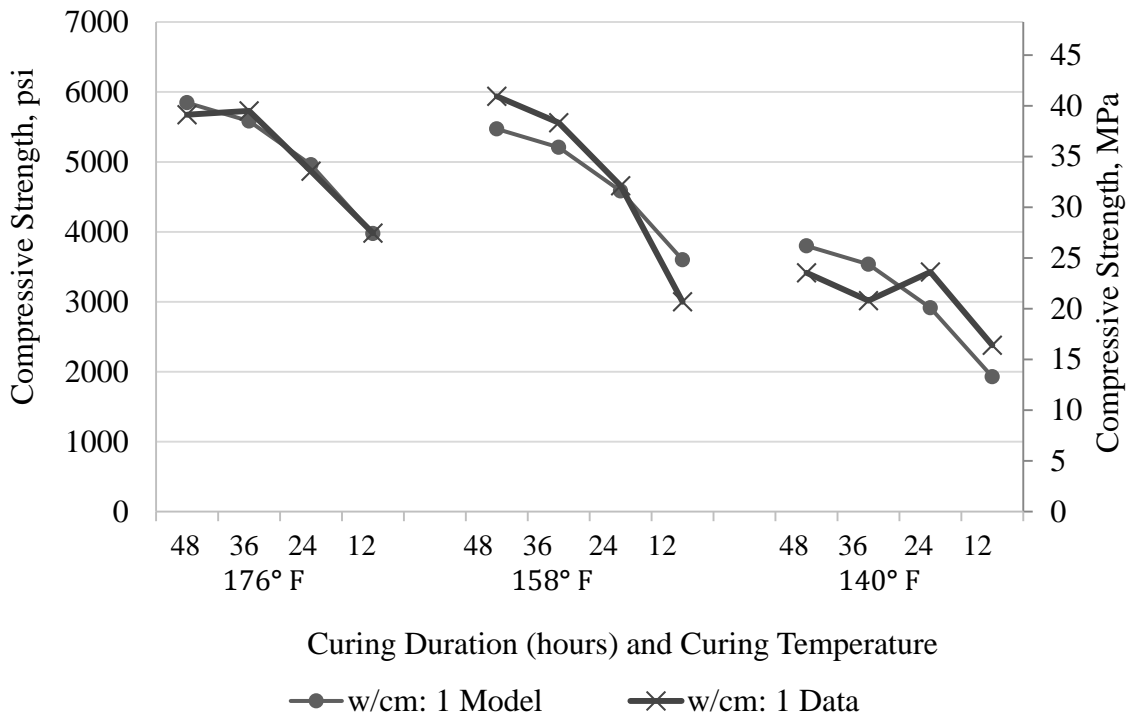


Figure: 5.14 Full quadratic model equation showing the model and experimental data for the three curing temperatures for *w/cm* 1; concrete age is fourteen days.

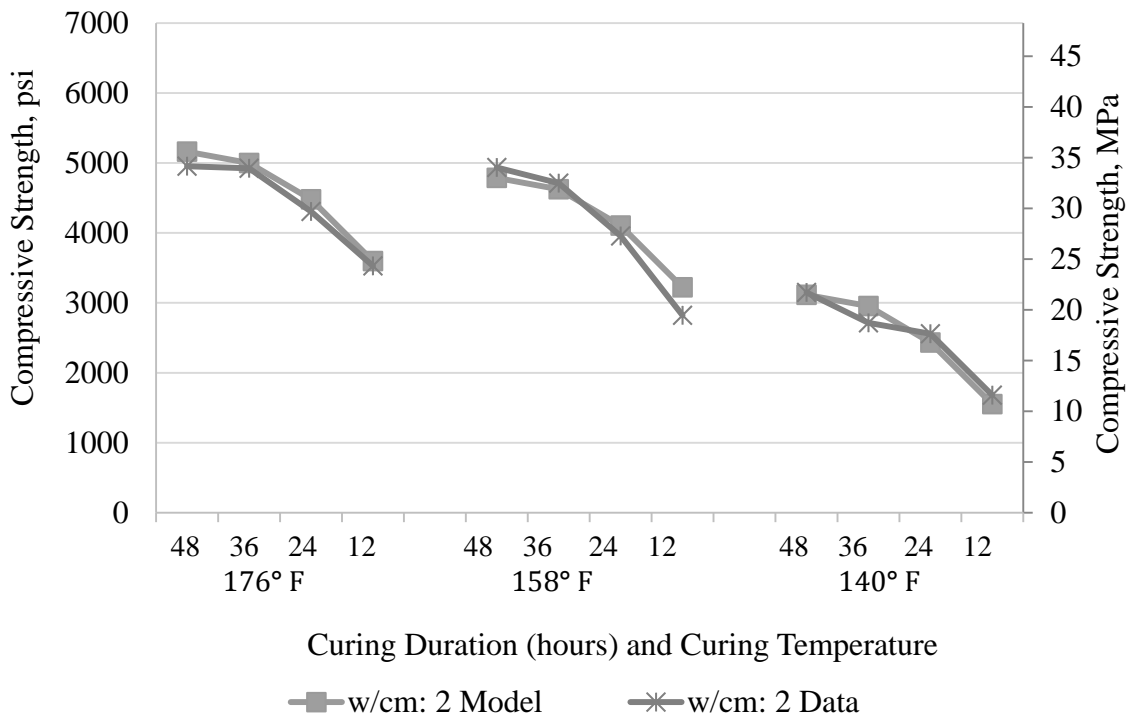


Figure: 5.15 Full quadratic model equation showing the model and experimental data for the three curing temperatures for *w/cm* 2; concrete age is fourteen days.

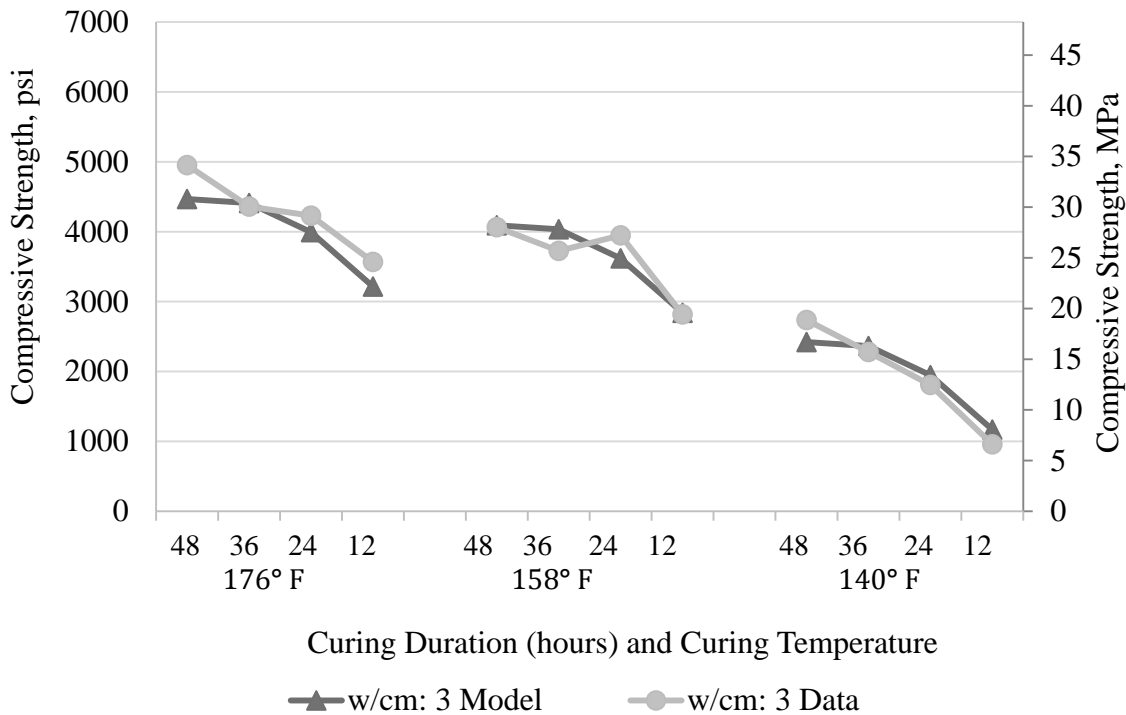


Figure: 5.16 Full quadratic model equation showing the model and experimental data for the three curing temperatures for w/cm 3; concrete age is fourteen days.

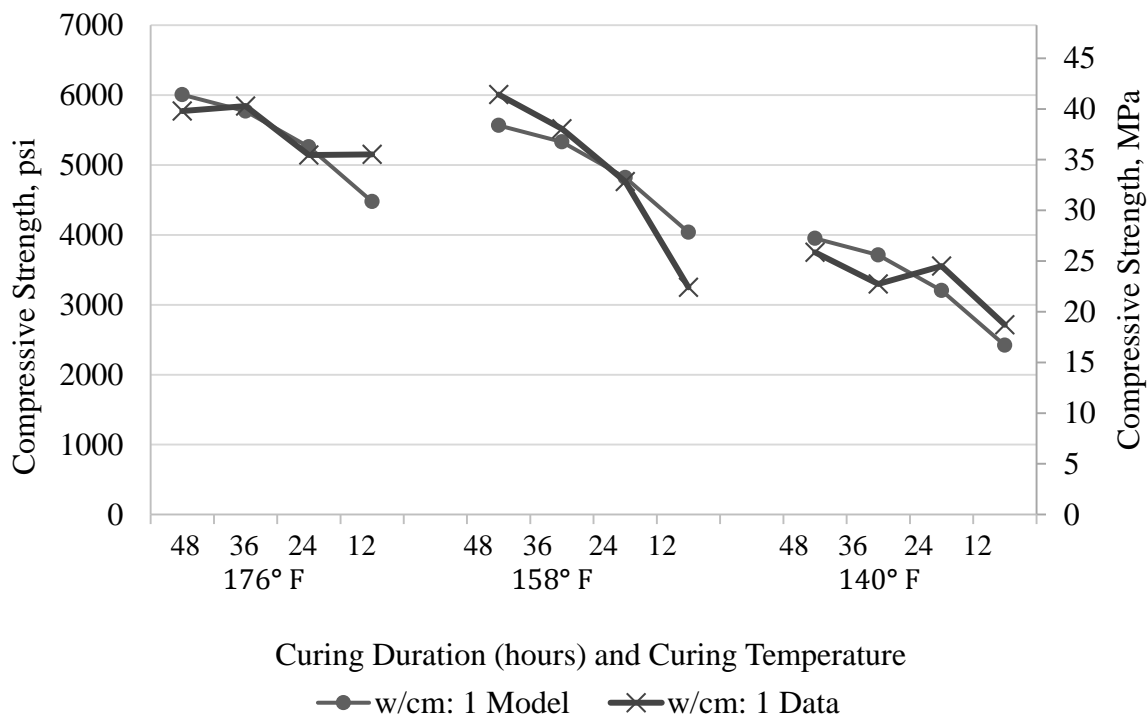


Figure: 5.17 Full quadratic model equation showing the model and experimental data for the three curing temperatures for w/cm 1; concrete age is twenty-eight days.

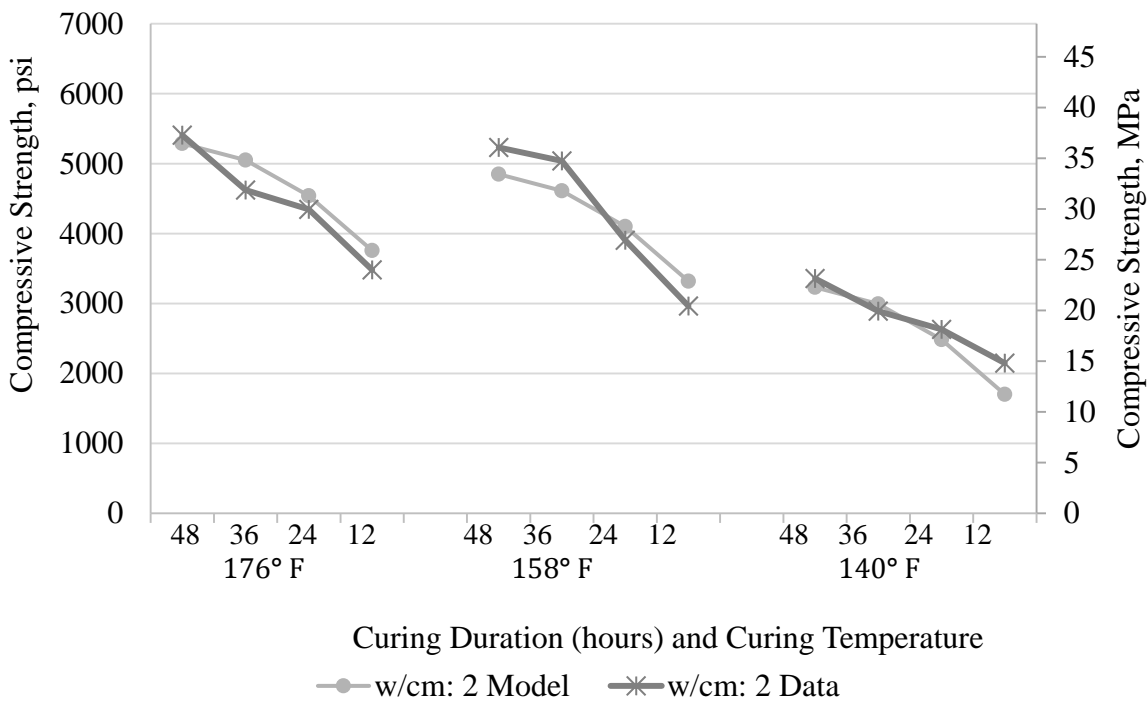


Figure: 5.18 Full quadratic model equation showing the model and experimental data for the three curing temperatures for w/cm 2; concrete age is twenty-eight days.

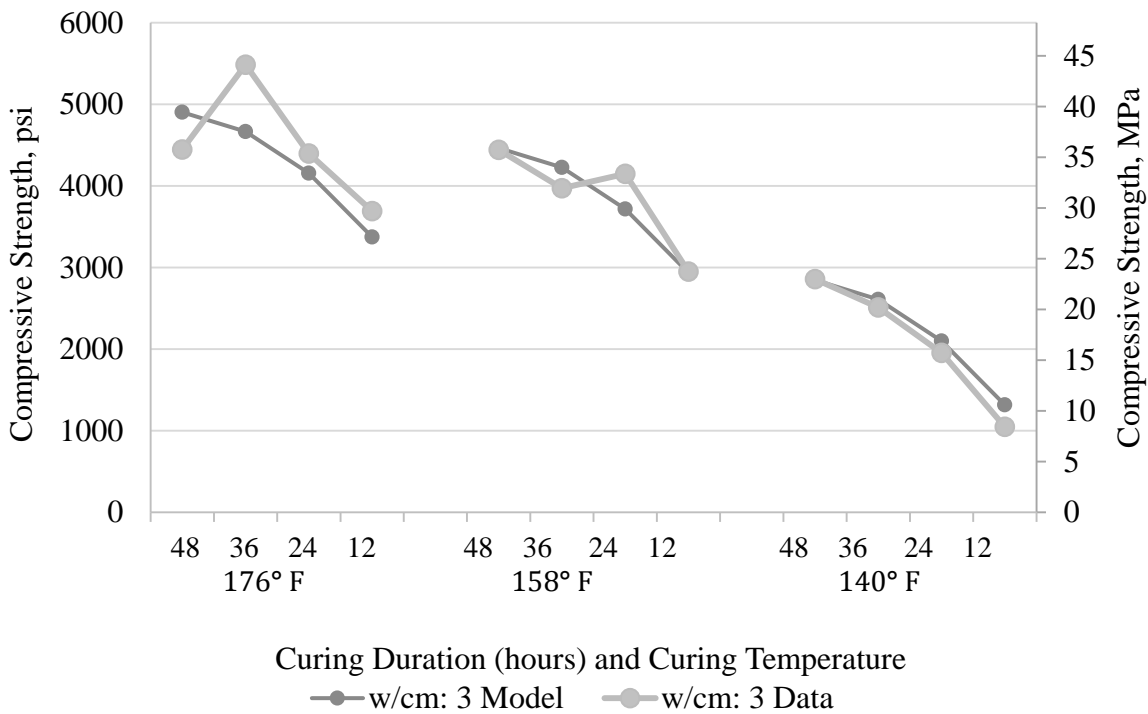
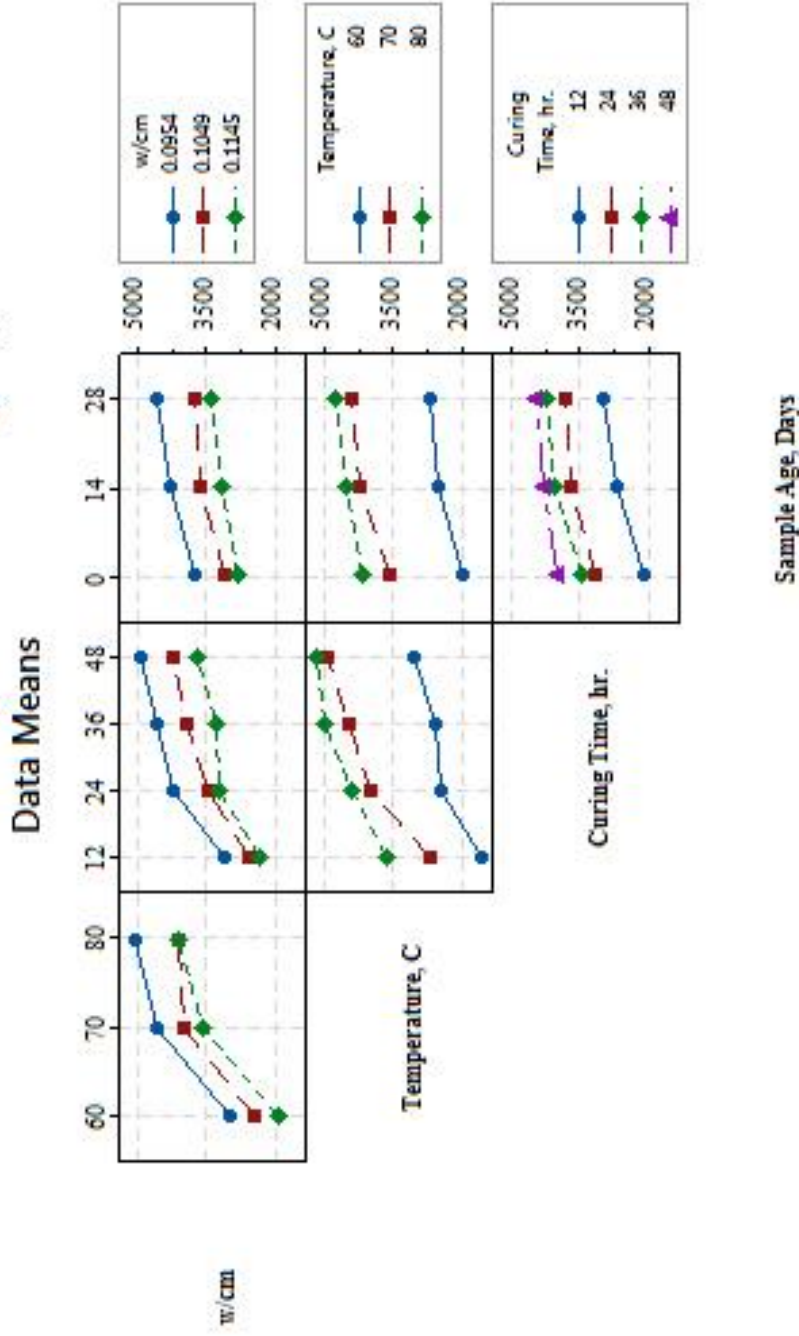


Figure: 5.19 Full quadratic model equation showing the model and experimental data for the three curing temperatures for w/cm 3; concrete age is twenty-eight days.

5.1.3 Interaction plots

Interaction plots are another tool used in the multiple regression modeling that interpret the mean data of a combination of variables to determine the level of influence by the dependent variables. The primary pattern to look for in an interaction plot is a deviation of lines from being parallel. When lines are not parallel, an interaction can be assumed and further analyzed. Figure: 5.20 shows the interactions between the four parameters on the compressive strength when considering all of the compressive strength data. It is important to note that few interactions can be extrapolated from the plots, the most important being minimizing the water content and maximizing both the curing temperature and curing duration. These plots are discussed more in depth in Section 5.2.

Interaction Plot for Compressive Strength, psi



Worksheet: All data

Figure: 5.20 Interaction plot of compressive strength as affected by w/c ratio, curing temperature, curing duration, and sample age.

5.1.4 Main Effects Plots

A third tool used to analyze the multiple regression model effectiveness is a main effects plot. The main effects plot shown in Figure: 5.21 is a representation of the means for the data separated by the four parameters of analysis. The primary conclusions to take from these plots are the slope changes between the evaluated parameters. The following is a summary of conclusions found in the main effects plots:

- Compressive strength drops at a faster rate when changing from w/cm 1 to w/cm 2 compared to the rate of change between w/cm 2 to w/cm 3.
- A curing temperature of 158°F (70°C) has a much greater effect on compressive strength over the 140°F (60°C) indicated by a greater increase in compressive strength between samples cured at 140°F (60°C) compared to those cured at 158°F (70°C).
- Increase in compressive strength is linear between 24 to 48 hours
- The greatest increases in compressive strength occurs prior to 14 days

Further analysis of the main effects by the specimen age results in the following conclusions: Figure: 5.22, Figure: 5.23, and Figure: 5.24 show the main effects plots for 0-day, 14-day, and 28-day aged samples.

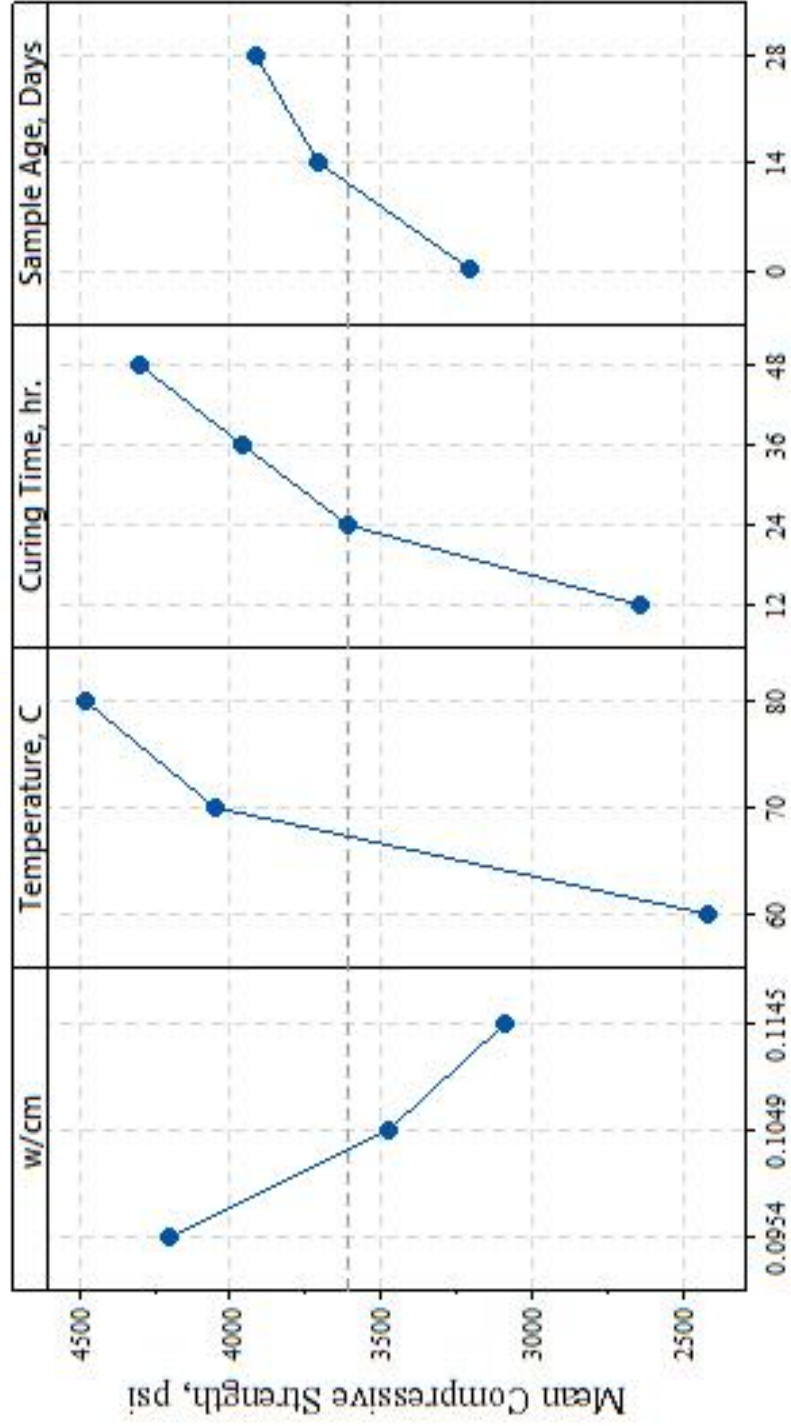
- An increase in water content decreases compressive strength more significantly at a specimen age of 0-days indicating that the relationship between the water content and the compressive strength at an older age is not as significant.
- The curing temperature affects compressive strength less after 14-days.

- The impact of the curing duration decreases with age indicated by a decreased rate of change between samples cured for 36 to 48 hours than the change between samples cured from 12 to 24 hours.

These plots are discussed more in depth in Section 5.2.

Main Effects Plot for Compressive Strength, psi

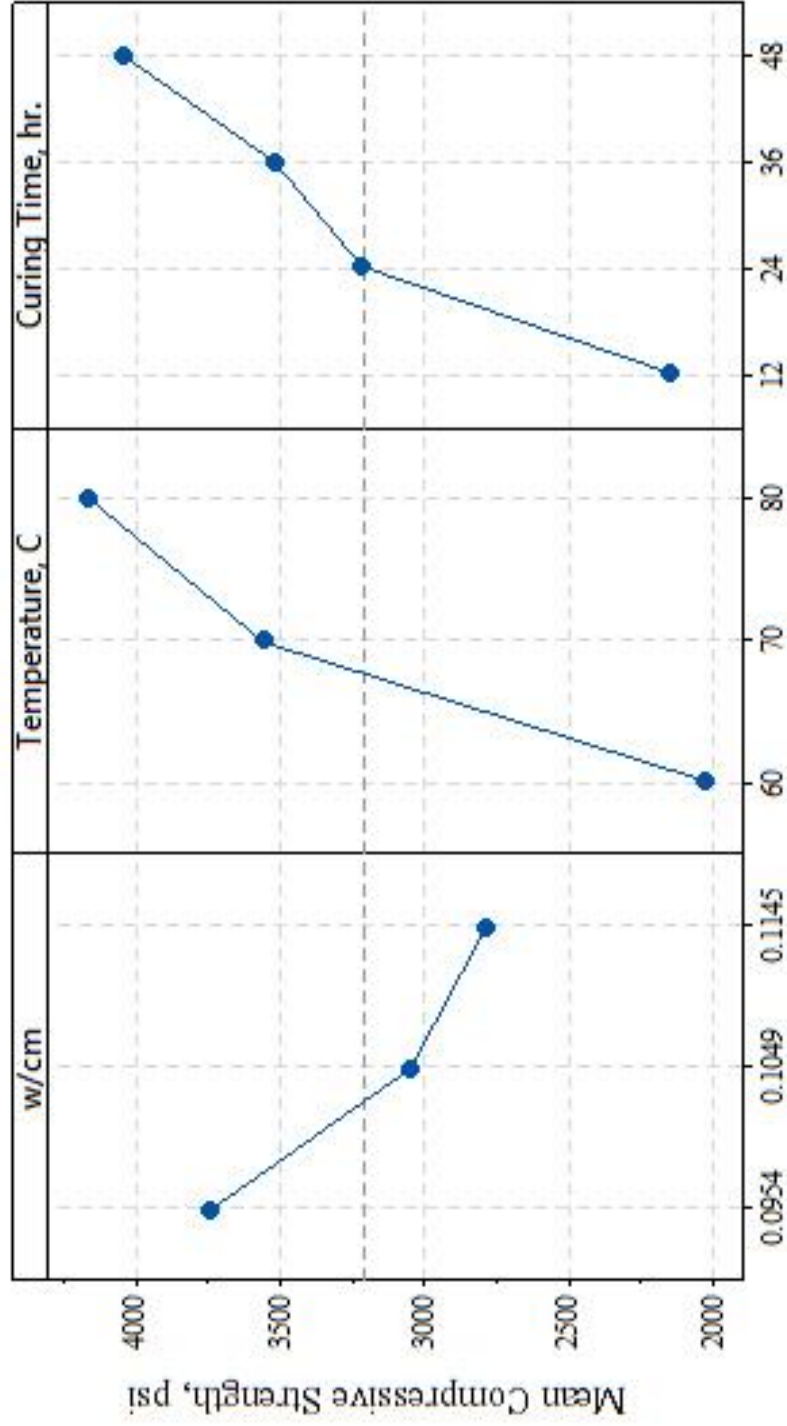
Data Means



Worksheet: All data

Figure: 5.21 Main effects plot for compressive strength of all data collected.

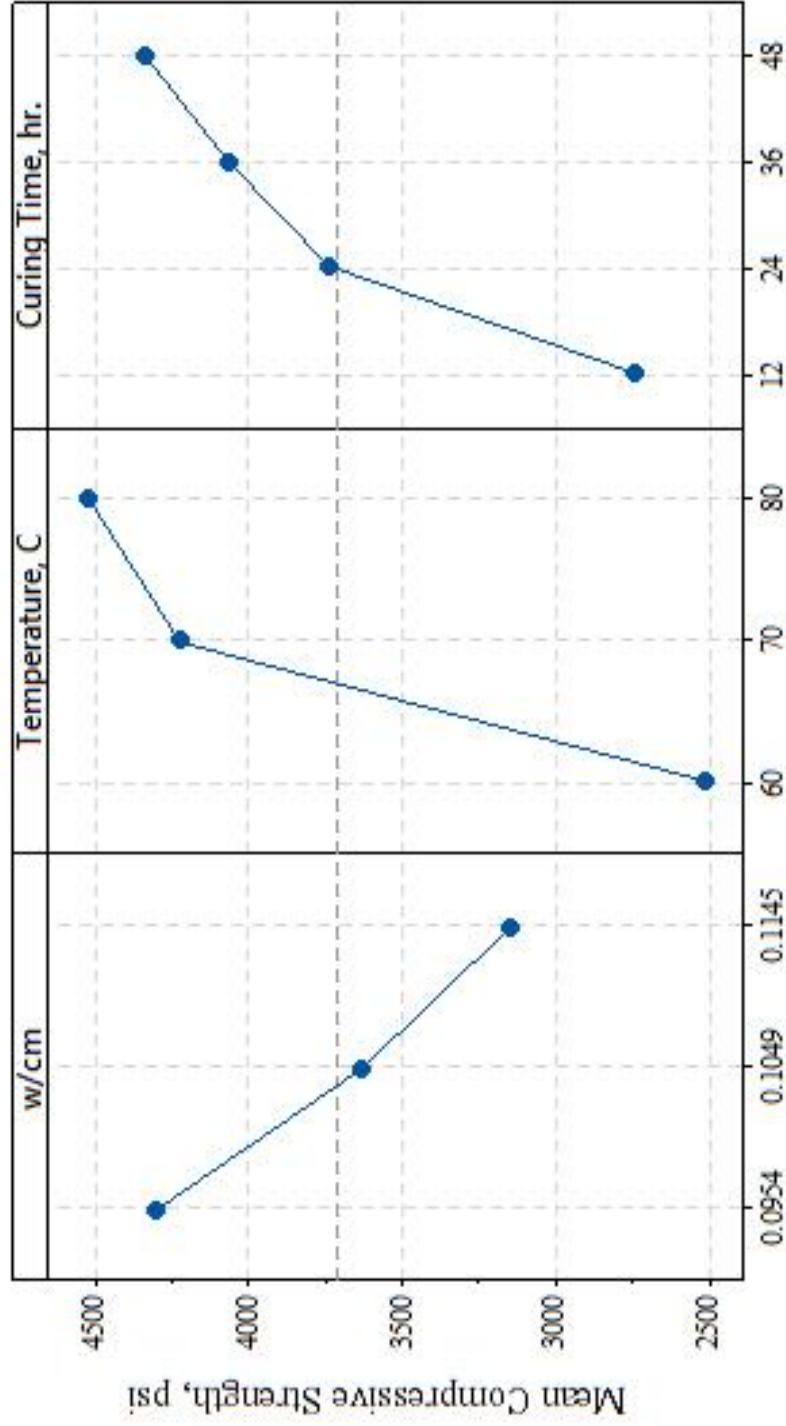
Main Effects Plot for Compressive Strength, psi
Data Means



Worksheet: 0-day

Figure: 5.22 Main effects plot for compressive strength of 0-day aged samples.

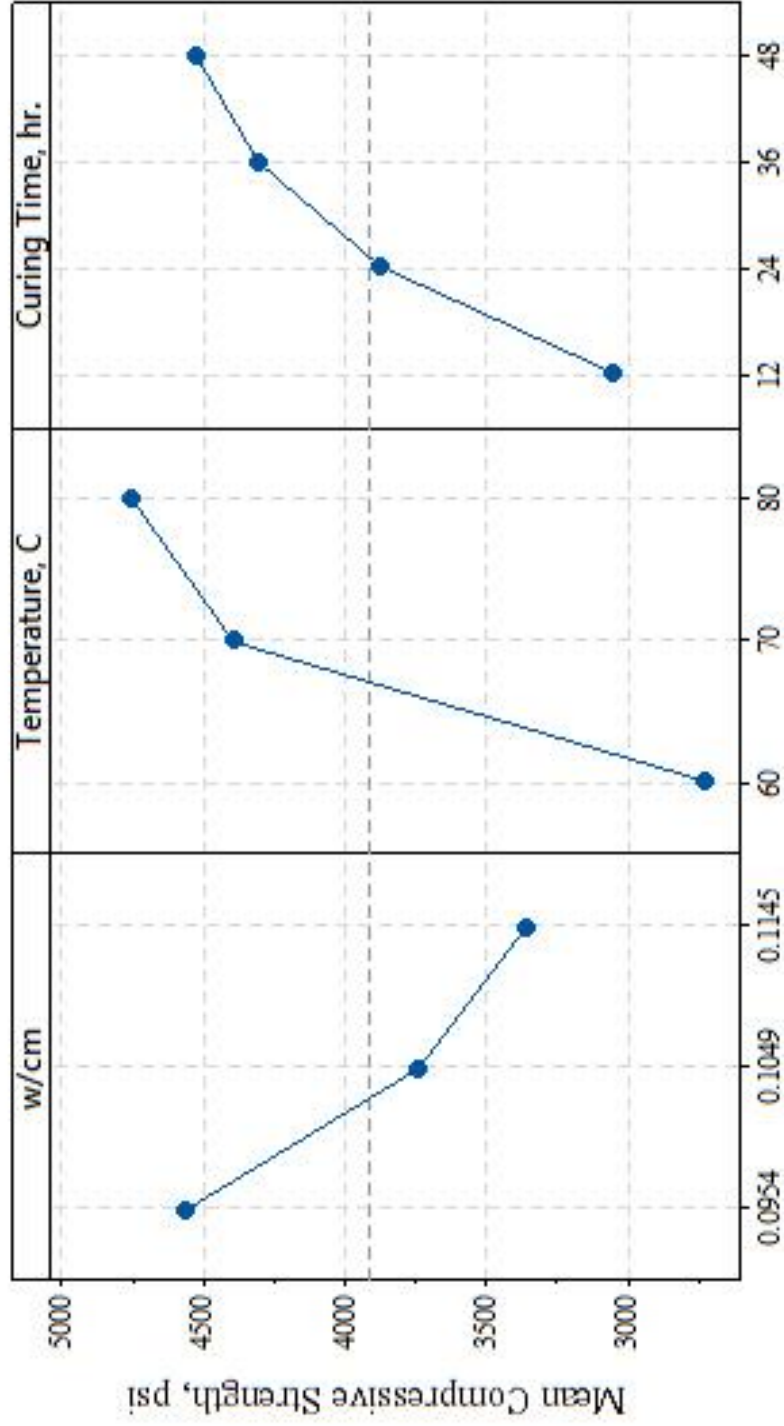
Main Effects Plot for Compressive Strength, psi
Data Means



Worksheet: 14-day

Figure: 5.23 Main effects plot for compressive strength of 14-day aged samples.

Main Effects Plot for Compressive Strength, psi Data Means



Worksheet: 28-day

Figure: 5.24 Main effects plot for compressive strength of 28-day aged samples.

5.1.5 Optimization Analysis

Another analysis performed with the data is an optimization analysis on each set of data and used to determine the highest compressive strength combinations based on the model by Minitab, Inc. In this analysis the model seeks to maximize compressive strength given any possible array of combinations of the three parameters. The results of the optimization analyses for each group of samples based on age are shown in Table: 5.3, Table: 5.4, Table: 5.5, and Table: 5.6. The tables show the w/cm , curing temperature, and curing duration combination that results in the highest compressive strengths based on the models created in the regression analysis. The “Composite Desirability” column assesses the effectiveness of the combinations towards achieving the goal of a maximized compressive strength. A value closer to one is ideal in the “Composite Desirability” column as it indicates the optimal combinations. Table: 5.7 illustrates the optimization of samples tested at 28-days with the compressive strength goal set at 4000 psi (27.6 MPa). The goal of 4000 psi (27.6 MPa) was set because it is a common compressive strength used in structural designs.

Table: 5.3 Optimization analysis of samples tested at 0-days with compressive strength goal maximized.

Solution	w/cm	Temperature		Curing Duration		Compressive Strength		Composite Desirability
		C	F	Hours	psi	MPa		
1	0.095	80.0	176.0	48.0	5671	39.1	0.99	
2	0.095	80.0	175.9	48.0	5669	39.1	0.99	
3	0.107	77.9	172.2	46.8	4754	32.8	0.82	
4	0.114	80.0	176.0	48.0	4542	31.3	0.78	
5	0.095	73.4	164.1	29.5	4493	31.0	0.77	
6	0.095	80.0	176.0	17.4	3980	27.4	0.67	
7	0.113	69.0	156.1	45.9	3734	25.8	0.63	
8	0.105	69.5	157.1	29.4	3574	24.6	0.60	
9	0.114	79.8	175.6	17.9	3321	22.9	0.55	

Table: 5.4 Optimization analysis of samples tested at 14-days with compressive strength goal maximized.

Solution	w/cm	Temperature		Curing Duration		Compressive Strength		Composite Desirability
		C	F	Hours	psi	MPa		
1	0.095	78.0	172.4	48.0	5873	40.5	0.94	
2	0.095	79.6	175.3	48.0	5853	40.4	0.94	
3	0.967	76.0	168.8	47.8	5756	39.7	0.92	
4	0.095	72.2	162.0	25.8	4894	33.7	0.76	
5	0.113	79.5	175.1	47.5	4574	31.5	0.69	
6	0.095	79.4	174.9	17.8	4509	31.1	0.68	
7	0.111	70.5	159.0	46.7	4371	30.1	0.66	
8	0.105	69.6	157.3	29.8	4369	30.1	0.65	
9	0.113	79.2	174.5	18.4	3739	25.8	0.53	

Table: 5.5 Optimization analysis of samples tested at 28-days with compressive strength goal maximized.

Solution	w/cm	Temperature		Curing Duration		Compressive Strength		Composite Desirability
		C	F	Hours	psi	MPa		
1	0.095	78.8	173.8	48.0	6036	41.6	0.98	
2	0.095	77.4	171.4	48.0	6026	41.6	0.98	
3	0.095	66.3	151.3	45.6	5093	35.1	0.80	
4	0.114	79.8	175.6	48.0	4936	34.0	0.77	
5	0.095	70.1	158.2	21.7	4719	32.5	0.72	
6	0.102	76.2	169.2	23.2	4670	32.2	0.71	
7	0.114	69.3	156.8	46.7	4415	30.4	0.66	
8	0.105	69.5	157.1	29.4	4350	30.0	0.65	
9	0.114	79.6	175.3	17.8	3826	26.4	0.55	

Table: 5.6 Optimization analysis of all samples tested with compressive strength goal maximized.

Solution	w/cm	Temperature		Curing Duration		Compressive Strength		Composite Desirability
		C	F	Hours	psi	MPa		
1	0.095	79.6	175.3	48.0	5863	40.4	0.95	
2	0.054	78.6	173.5	48.0	5858	40.4	0.95	
3	0.096	77.4	171.2	47.3	5732	39.5	0.92	
4	0.114	79.9	175.9	48.0	4659	32.1	0.74	
5	0.095	79.9	175.8	16.5	4371	30.1	0.69	
6	0.095	69.6	157.3	22.9	4295	29.6	0.67	
7	0.105	69.5	157.2	29.5	4074	28.1	0.64	
8	0.113	68.7	155.6	46.0	4019	27.7	0.63	
9	0.102	76.6	169.8	12.1	3553	24.5	0.55	

Table: 5.7 Optimization analysis of samples tested at 28-days with compressive strength goal set at 4000 psi (27.6 MPa).

Solution	w/cm	Temperature		Curing Duration		Compressive Strength		Composite Desirability
		C	F	Hours		psi	MPa	
1	0.095	60.1	140.2	48.0		3995	27.5	1.00
2	0.114	65.9	150.6	47.2		3959	27.3	0.99
3	0.114	79.6	175.3	17.8		3826	26.4	0.94
4	0.095	64.7	148.5	16.5		3673	25.3	0.89
5	0.097	80.0	176.0	12.0		4336	29.9	0.84
6	0.105	69.5	157.1	29.4		4350	30.0	0.84
7	0.114	69.0	156.2	20.7		3455	23.8	0.82
8	0.115	80.0	176.0	46.7		4912	33.9	0.57
9	0.095	80.0	176.0	42.6		5954	41.1	0.09

5.2 Sensitivity Analysis Conclusion

In the sensitivity analysis, the production variables water content, curing temperature, and curing duration are separated. The sample age is also considered as an independent variable. Four major statistical analyses were performed to assess the data and examine the effects of the production variables and age of the concrete. In the study, the data analyzed all of the data as a lumped group results in a linear and quadratic model with R^2 values of 82% and 88%, respectively. In the second portion of the study, data was grouped by age of samples, producing three quadratic models at age zero, 14-day, and 28-day following heat curing; these produce R^2 values of 96%, 94%, 92%. Supplementary plots and analyses were performed. These included interaction plots, main effects plots, and an optimization analysis. The interaction plots can be used to identify direct causes and effects on the compressive strength in two-way interactions. In the main effects plots the production variables are broken down visually to analyze each production variables affect on compressive strength. Lastly, the optimization analysis provides a look at the model created by MiniTab and attempts to provide the specific values for the production parameters that would maximize the compressive strength.

For this analysis, the goal is to answer the following questions and find the limits of the indicated relationships between production variables. These conclusions and observed trends are as a result of a limited range for the production variables

1. How does the w/cm affect the compressive strength of the concrete?

- The trend indicates that as w/cm increases, the compressive strength decreases, similar to PCC.

- With time, the significance of the w/cm is increased. A trend that is evident in the increasing value of R^2 for the w/cm variable in Figure: 5.2.
- The greatest rate of change in compressive strength consistently occurred from w/cm 2 to w/cm 1 indicating that the lower w/cm 1 is desirable. However, it is possible to achieve up to 80% of w/cm 1's maximum compressive strength when identical curing conditions are maintained and only the w/cm changes.

For example, assuming the maximum potential of w/cm 1 is 6000 psi (41 MPa) at 28-days then with the same curing conditions a strength of about 5200 psi (36 MPa) with w/cm 2 can be achieved and 4800 psi (38.1 MPa) with w/cm 3. Controlling the water content in this scenario can increase the compressive strength by about 125% above w/cm 1.

2. How does the curing temperature affect the compressive strength of the concrete?
 - The curing temperature is more significant when curing at 158°F (70°C) or higher.
 - The rate of change in compressive strength between samples cured between 140°F (60°C) and 158°F (70°C) was much greater than the change between 158°F (70°C) and 176°F (80°C). (This trend is observed from the main effects plots shown in Section 5.1.4.)
 - The trend in the data is that regardless of the mixture design a 158°F (70°C) minimum curing temperature is desirable to achieve a more precise range of strengths for the mixture designs. Curing at temperatures lower than 158°F (70°C) produce too much variability in the strengths.

3. How does the curing duration affect the compressive strength of the concrete?
 - A significant increase in compressive strength is noted when increasing the curing duration from 12 hours to 24 hours. The same trend does not apply to any curing above 24 hours. The same trend does not apply to any curing above 24 hours.
 - The main effects plots of Section 5.1.4 illustrate that the greatest change in compressive strength occurs before the 24 hour curing duration. However, a more significant change over time is from the 36 hour to 48 hour curing duration where at age zero there is a greatest difference in strength from the final 28-day strength. This indicates that a higher percentage of the total strength can be attained earlier on by curing for 48 hours.
4. How does the aging process affect the compressive strength of the concrete?
 - Initially, a higher rate of change in compressive strengths is observed between the 0-day and 14-day testing. After the 14-day mark, the concrete has reached approximately 93% of its 28-day strength, indicating that any chemical reactions occurring in the GCC slow down at this point.
5. In the event that too much water is added to the matrix, can adjusting the curing temperature and/or curing duration still achieve a desired strength?
 - It is possible to accommodate a higher w/cm but it can result in a difference of up to 1000 psi (6.89 MPa).
 - Within the range of production variables used in this study, each w/cm had the potential to achieve a compressive strength of approximately 5,000 psi (34.47 MPa). For many structural applications this is an adequate strength.

CHAPTER 6: FREEZE THAW DURABILITY

6.1 Freeze-Thaw Study Methodology

The freeze thaw durability study performed for this thesis introduces an aspect of GCC research which has not yet been thoroughly reported in the literature. One of the most important characteristics of concrete mixtures relates to the materials' ability to endure harsh or extreme conditions. Concrete may be placed in environments with heavy chemical attack, intense physical attack, or in environments where the microstructure is susceptible to deterioration and physical failure. For these reasons, designers must specify concrete with adequate resistance to deleterious aspects of the service environment. This study, therefore, seeks to contribute to the body of knowledge regarding durability of GCC in order to eventually properly design for extreme conditions.

The study focused on two types of samples cured at 158°F (70°C) and 176°F (80°C), these were found to have the superior mechanical properties as described in Chapters 5 and 6. In this study, twenty-four samples were tested using an environmental chamber to rapidly cycle the samples between freezing and thawing, as per the methods described in ASTM C666, Standard Test Method for Resistance of Concrete to Rapid Freezing and Thawing (ASTM International, 2008).

The freeze thaw durability is evaluated by the capability of water to enter the concrete matrix and expand creating pressure on the walls of voids without causing

damage. With enough force, the expansion of water causes increases in pore pressure that can damage the matrix at sufficiently high levels. The characterization of freeze thaw resistance is then approached by determining the number of freezing cycles that can be endured prior to the onset of substantial damage. Resistance to freezing damage is provided by the network of entrained air voids within the matrix. In addition to the volume of air in a concrete mixture design required for freeze protection, the size of the individual pores created by air is also important. In order for freezing damage to occur, water must enter voids in the concrete matrix and remain there through freezing temperatures. (Mindness et al. 2002) indicate that smaller pores in a concrete matrix will freeze at lower temperatures as low as -4°F (-20°F) for pores of 3.5 nanometers in diameter.

The study of concrete freeze thaw resistance focuses on how entrained air protects concrete from freezing damage. ASTM C666 makes use of ASTM C215, Standard Test Method for Fundamental Transverse, Longitudinal, and Torsional Resonant Frequencies of Concrete Specimens, by measuring the resonant frequency of the concrete. In this test method, a wave is passed through the concrete and is used to measure the dynamic modulus of the concrete, which decreases due to freezing damage (ASTM 2008). The parameter which characterizes freezing damage is the relative dynamic modulus. This measure is a ratio of the final to original resonant frequency measure calculated per ASTM C666.

6.2 Literature Review

The following sections include a brief literature review on concrete durability, freeze-thaw mechanisms in concrete, and an overview of durability studies performed on GCC.

6.2.1 FHWA (2006) and Kosmatka and Wilson (2011)

The following is a summary of the freeze thaw mechanisms of PCC which lay the groundwork for the mechanisms of geopolymer cement concrete. Certain properties, such as compressive strength, tensile strength, and other mechanical properties are parameters that are determined by selecting proper mixture design and curing routine and are directly measurable. Durability properties refer to how much and for how long a concrete can endure in its environment. As such, they are more difficult to measure or to accurately predict at the beginning-of-service, since they are very dependent on the exact features of the service environment. The Portland Cement Association (PCA) (Kosmatka and Wilson 2011) defines durability as “the ability to last a long time without significant deterioration.” PCA defines a number of durability properties of concrete primarily caused by chemical or climate situations (Kosmatka and Wilson 2011). The following list is presented by PCA as a durability aspect or exposure reaction of concrete.

- Alkali-Aggregate Reaction
- Chemical Resistance
- Corrosion of Reinforcement
- Freeze Thaw Resistance
- Miscellaneous

Concrete is a conglomerate of cement, water, fine and coarse aggregates, and air which makes it a non-homogenous material at a small/microscopic scale. In the concrete matrix there will, by default, exist capillaries, pores, and voids. The presence of water as a liquid will be subject to movement among these capillaries and as the water moves between voids it is likely to create friction along the paste walls. Currently, the Federal Highway Administration (FHWA) (2006) details three primary theories for the freezing and thawing mechanisms, detailed below.

- Critical Saturation
 - This theory states that the voids in the concrete matrix have a saturation point of 91.7%. The saturation point refers to when the maximum amount of solution has entered a substance and no more mixing can occur. If any voids in the concrete matrix happened to reach a higher saturation point then the freezing water will create pressures on the void walls. The pressure is due to the expansion of water, which expands by 9% in volume when it freezes. Fundamentally, the voids are filling with water and the freezing water can push at the void walls making it liable to crack the mortar matrix of the concrete.
- Hydraulic Pressure
 - The hydraulic pressure theory is in addition to the occurrence of freezing situations in the void network of the concrete. This theory refers to the idea that if a void already has a frozen volume of water and then by its expansion it will push out any extra unfrozen water. The pushing by this water will then cause cracks in the paste surrounding the void.

- Ice Accretion and Osmotic Pressure
 - This theory seeks to further account for the composite characteristic of concrete. OPC concrete has numerous chemical interactions that change over time. The theory focuses primarily on thermodynamics and osmosis theories as an explanation for the movement of solutions within the concrete matrix. In simple terms, the theory follows that as a solution is interacting with the alkalis in the concrete, the solution will seek to reach equilibrium, namely, the high to low phenomena of movement between molecules. Through this theory the movement of water between pores will be controlled by where a lower concentration is present and as water freezes the molecular attractions will change as equilibrium is sought.

These theories of the freezing damage mechanism all focus on one crucial property of the concrete matrix, the air content or allowance in a given mixture design. The presence of air is crucial to the concrete matrix because it allows for voids or pores to fill with expanding water and the spacing of these voids can allow for the proper movement of water without compromising the concrete integrity.

Work performed as a part of the Strategic Highway Research Program (SHRP) under FHWA (2006) included testing various mixture designs to determine the influence of water content and air content on the freeze thaw resistance of a concrete. The focus of this study was to determine how the addition of air-entraining admixtures would affect the freeze thaw durability of concrete. Research found that while there were no significant signs of the w/cm ratios affecting the mixes, the spacing and distribution of the void and capillary network played an important role. The spacing and distribution refers

to the location and size of the voids in the matrix, which are related to an empirical evaluation of how far water must travel in the paste to move from one void to another.

The metric used to identify the durability of a concrete is the durability factor. The durability factor is a term used to categorize the expected soundness of the concrete over a long period of time as a result of a set number of freezing and thawing cycles. The factor is influenced by the air content, distribution, and size of voids in the matrix. The air content contributes to the quantity of voids per volume of concrete in a matrix. The distribution outlines where the voids are located and the relative location to one another; if too many voids are closer together, the concrete is more susceptible to large quantities of water collection in the void space. The size of the voids is in direct relation to the air content and distribution as many small voids could be the same as a few large voids. In this way, the production of durable concrete requires that the quantity, size, and spacing of voids such that water intrusion and movement in the matrix is minimized. These characteristics are measured by testing concrete samples in an intense cycling. In the study, a higher value of space created a lower durability factor; the samples varied from a spacing factor of 0.0104 in. (0.264 mm) to 0.0398 in. (1.011 mm) with a durability factor of 3.4% to 94.8%, respectively (FHWA 2006). It is noted that a spacing factor less than 0.00787 in. (0.20 mm) is generally preferred of freezing and thawing and imitating a long period of time with the cycles (FHWA 2006).

A higher durability factor is ideal, as it represents a longer concrete life span in harsh environmental conditions. Figure: 7.1 shows an example of the results found by SHRP where for their testing procedures a durability factor greater than eighty was determined to be *good* (FHWA 2006). The figure shows the resulting relative dynamic

modulus after completing freeze-thaw cycles for three samples (one control) and the measured air content (A) and durability factor (DF) for each sample. The air content is a measured fresh concrete property and the durability factor is the metric used to determine the freeze-thaw resistance of a concrete. The relative dynamic modulus is measure of how much deterioration has occurred comparatively to the original state of the concrete; in effect, the existing dynamic modulus to the original dynamic modulus. The durability factor is a rate measure of the status of the relative dynamic modulus at the cycle iteration relative to the final expected number of iterations.

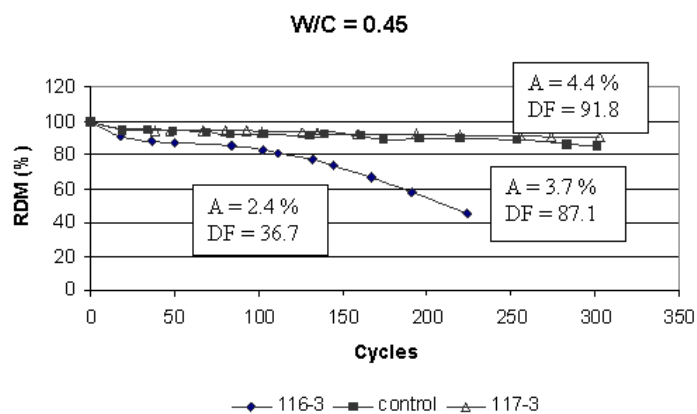


Figure: 6.1 Relative dynamic modulus to freeze thaw cycles of samples with varying air content as reported by SHRP. (FHWA 2006)

PCA details five important parameters in their “Design and Control of Concrete Mixtures” publication. They recommend the following characteristics of a concrete in order to have good freeze thaw durability:

- Good quality aggregates
- Low water cement ratio with a maximum of 0.45
- Minimum cement content of 564 pounds per cubic yard (334.6 Kg/m³)
- Good finishing and curing techniques

- Compressive strength of at least 4,000 psi (27.6 MPa) when freezing and thawing is expected

Among other characteristics for good freeze thaw durability are those also referenced by the FHWA which cites criteria established by Cordon and Merrill (1963). Figure: 6.2 shows what was established for durability parameters as good durability when the durability factor is above eighty and poor durability below twenty.

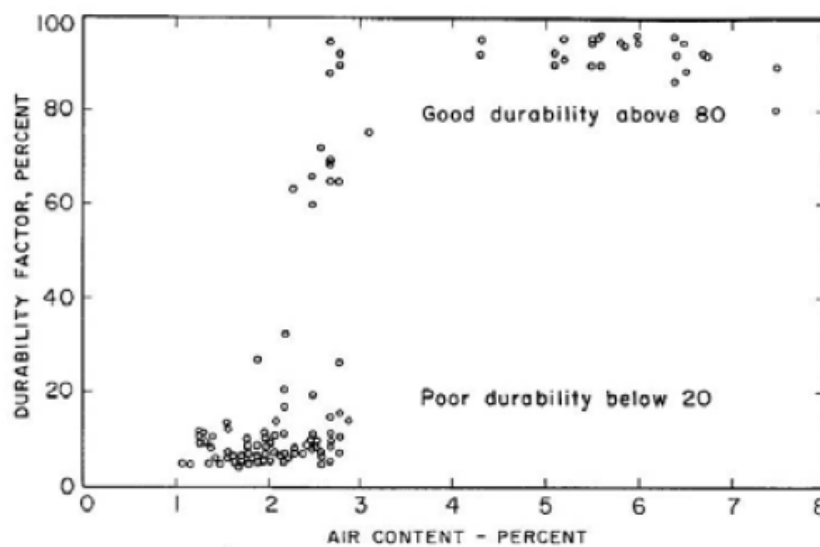


Figure: 6.2 Freeze-thaw durability factor parameters against total air content (Cordon and Merrill 1963).

These measures, relative dynamic modulus and the durability factor are the fundamental measurements necessary to categorize concrete as suitable or unsuitable for freezing and thawing environments.

6.2.2 Mindness et al. (2002)

In addition to the guidelines previously noted, Mindness et al. (2002) have outlined the following guidelines for freeze-thaw durability:

- Spacing factor, L – less than 0.008 in. (0.2 mm)

- Specific surface area, a – greater than $600 \text{ in}^2/\text{in}^3$ ($25 \text{ mm}^2/\text{mm}^3$)
- Bubble frequency, n – between $8\text{-}16 \text{ in}^{-1}$ ($0.3 \text{ - } 0.6 \text{ mm}^{-1}$)

6.3 Freeze Thaw Testing

Testing standard ASTM C666, “Standard Test Method for Resistance of Concrete to Rapid Freezing and Thawing,” was used to test the samples in conjunction with ASTM C215 (2008), “Standard Test Method for Fundamental Transverse, Longitudinal, and Torsional Resonant Frequencies of Concrete Specimens.”

6.4 Specimen and Material Preparation

Specimens used for freeze thaw durability testing were prepared along with the previously indicated samples. Two types of molds were used to prepare a total of twelve samples at a time, six of the molds were steel and the other six were made from 2x4's and plywood. The samples are of dimensions 3"x3"x12" (76.2mmx76.2mmx304.8mm). Two samples per batch combinations were cast with the combinations including the three w/cm , two curing durations (24 hour and 48 hour), and three curing temperatures (140°F (60°C), 158°F (70°C), and 176°F (80°C)). Upon completion of mixing the samples were cast and allowed to vibrate on a mixing table until visibly settled. Once cast, the samples were cured according to their designated batch conditions as referenced in Section 3.5. After curing, the selected freeze thaw samples were aged for approximately five months. This time period is longer than typical lab specimens are tested; however, the ASTM Standard allows for some discretion at specifying the parameters. In the case of GCC, very little additional curing or development of the microstructure occurs after the elevated temperature phase. Samples were saturated by submerging in lime water for approximately four weeks prior to the start of testing. The testing trays for the samples

were made from stainless steel boxes of dimensions $3\frac{1}{4}'' \times 3\frac{1}{4}'' \times 3\frac{1}{4}'' \times 12\frac{1}{4}''$ (82.5mmx82.5mmx82.55mmx311.15mm). The dimensions were set to meet the ASTM tolerance of at least $\frac{1}{32}''$ (0.793 mm) and at most $\frac{1}{8}''$ (3.175 mm) of water surrounding any one side of the sample.

6.5 Chamber Temperature Calibration

Testing was performed on two samples of each combination previously indicated in Section 4.2. The series of samples cured at 140°F (60°C) were used as preliminary calibration samples in anticipation of any complications. The use of the samples facilitated the testing of 158°F (70°C) and 176°F (80°C) samples which were more adequate for freeze thaw testing given their mechanical strengths as outlined in Section 5.4. These samples exhibited the most positive potential for the durability testing.

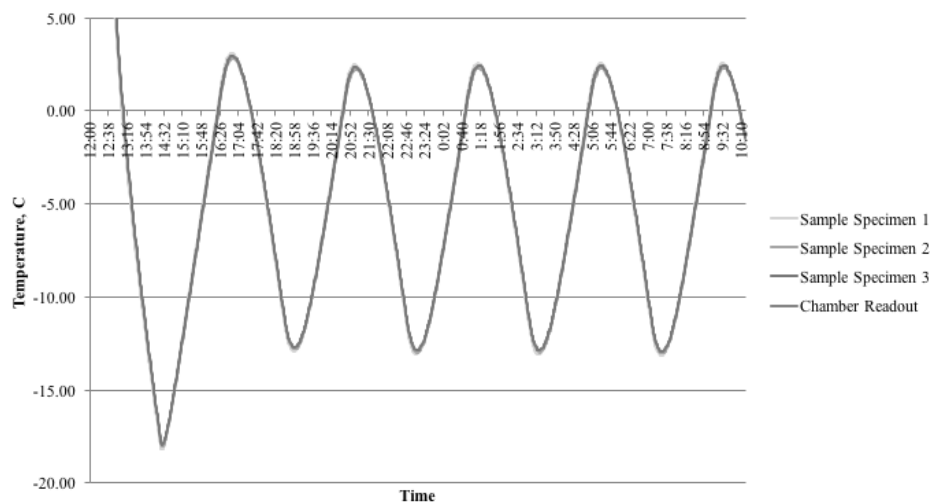


Figure: 6.3 Temperature output of environmental chamber calibration.

An environmental chamber (CSZ Zplus16) was used to test the specimens. Specimens were cycled from -9.4°F (-23°C) to 44.6°F (7°C), the cycle was based on a calibration of the chamber with concrete samples embedded with temperature sensors which ensured that the specimen cores cycles from -0.4°F (-18°C) to 39.2°F (4°C) and remained at these temperatures for the required time, see Figure: 6.3. The temperature

requirements are discussed in Section 7.6. A set of three freeze thaw specimens were prepared with thermocouples embedded in the concrete. These samples were then tested multiple times at nine locations in the chamber; the chamber has three shelves and samples were rotated between each side and center of the three shelves. During the calibration the temperatures were monitored and recorded at the location of the thermocouples in the freeze thaw calibration samples. The recorded temperatures were then compared to the temperatures recorded by the chamber as it was cycling through its programmed setting and the ambient temperature in the chamber recorded by the chamber thermocouple. In total, readings were taken over the course of approximately one month or 150 cycles. As the freeze thaw calibration samples were rotated in the chamber, an additional set of concrete mass was placed in the chamber to mimic the amount of space that would be taken up during testing by all samples.

6.6 Testing Procedure

Procedure A of ASTM C666 (2008), “Standard Test Method for Resistance of Concrete to Rapid Freezing and Thawing,” was selected for testing of samples. The procedure prescribes a number of requirements during testing and of the cycling between freezing and thawing temperatures. Samples are placed in a water bath to be surrounded by between 1/32 and 1/8 inches (0.793 mm and 3.175mm, respectively) of water on any surface of the prism. This procedure requires beam specimens of width and depth between three and five inches (76.2 mm and 127 mm, respectively) and length between eleven and sixteen inches (279.4 mm and 406.4 mm, respectively). Once the samples are placed in their water bath container, they must also be elevated in the container such that the water requirement is also met; in this case, two one-eighth inch (3.175 mm) brass

rods were placed in the bottom of the water bath container to provide the required elevation.

The testing requirements for the freezing and thawing cycling are specific in how long it must take to meet a certain temperature in the sample. Per the standard, sample cores must achieve the freezing and thawing temperatures to assure uniform freezing or thawing. The Standard requires the cycling of temperatures between 40°F (4°C) and 0°F (-17°C) for freezing and vice versa for thawing with a tolerance of 3°F (-16°C) at the center of the specimen. A *cycle* in this manner is a change in temperature from 40°F (4°C) to 0°F (-17°C) and back to 40°F (4°C) where the change in temperature of 40°F (4°C) to 0°F (-17°C) is the freezing portion and the 0°F (-17°C) to 40°F (4°C) is the thawing portion. A complete *cycle* is required to occur between two and five hours where the thawing portion of the cycle must make up at least one-quarter of the cycle time. Furthermore, the transition period between lowering the temperature and raising the temperature has to stay under ten minutes. The testing of samples began by conditioning samples to fully saturated moisture levels so that samples are not absorbing water from the water bath during freezing or thawing. The samples are also conditioned to a target thaw temperature. Samples are placed at the beginning of the thawing cycle and cycled through no more than thirty-six cycles at a time. At the end of the cycling, samples are removed from the testing chamber at the target thaw temperature and tested for fundamental transverse frequency. At this time, the weight and dimensions of the samples are also recorded. Once the series of measurements are completed, the samples are returned to the testing chamber and cycling begins once again. Per the Standard, testing

continues until three-hundred cycles are completed or the measured relative dynamic modulus reaches sixty percent of the initial relative dynamic modulus.

The testing of the fundamental transverse frequency was completed per ASTM C215 (2008), “Standard Test Method for Fundamental Transverse, Longitudinal, and Torsional Resonant Frequencies of Concrete Specimens.” The test excites the concrete medium and measures the fundamental transverse frequency. In this study, the test set up used is shown in Figure: 6.4, and is a slight modification to the ASTM. For comparison, Figure: 6.5 details the setup per ASTM C215 (2008). The modification consisted of using a flat ½ inch (12.7 mm) neoprene sheet instead of two independent supports at the nodal points. The dynamic testing kit used for the study used a PCB Pizotronics top mounted accelerometer, labeled in Figure: 6.4. Due to the sensitivity of the accelerometer, a light Velcro strap was used to hold the pickup in place during testing. The sample was also placed directly on a ½ inch (12.7 mm) neoprene sheet. The neoprene was selected for its firmness and ability to restrict any wave transfer between the base and the sample.

Once a sample was ready for testing, the pickup was placed on the sample at the approximate 1/8 of the length location. The sample was then struck with a metal PCB Piezotronics impact hammer at the center of the specimen (shown with an arrow). At this time, the sample was struck numerous times until a stable consistent readout was produced. The readout of the program created for the dynamic testing kit is shown in Figure: 6.6, the resonant frequency was determined by a fast fourier transformation (FFT) of the acceleration versus time data. This testing was conducted and the data recorded for each sample at the end of the 33 freeze thaw cycles until 300 cycles or the resonant frequency fell below sixty percent of the starting value.

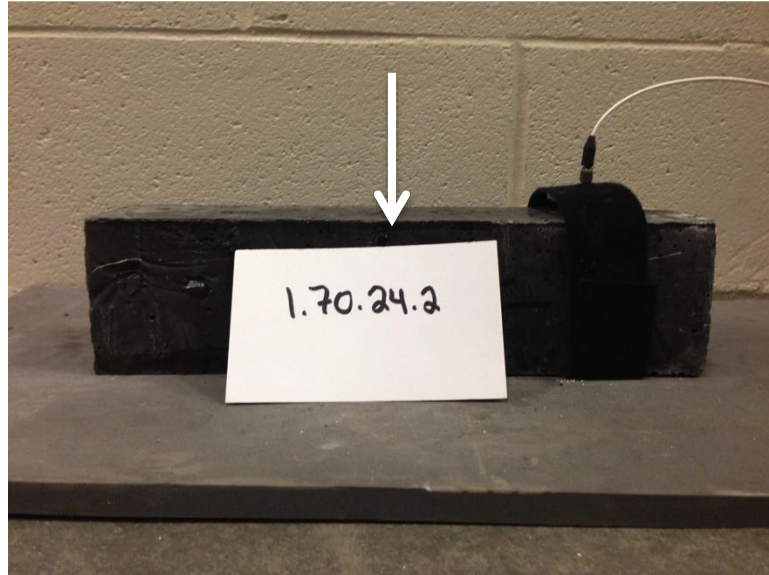


Figure: 6.4 Resonant frequency testing set up of sample.

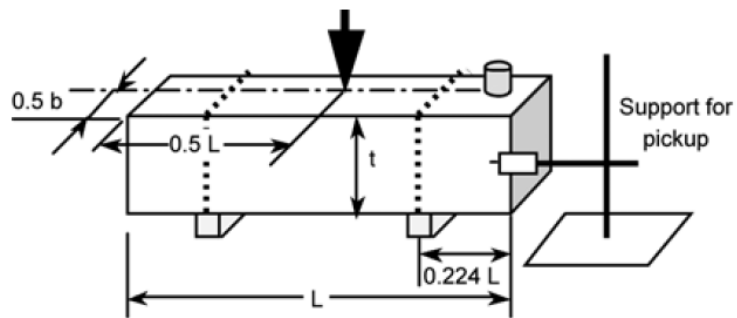


Figure: 6.5 Set up for transverse frequency testing.

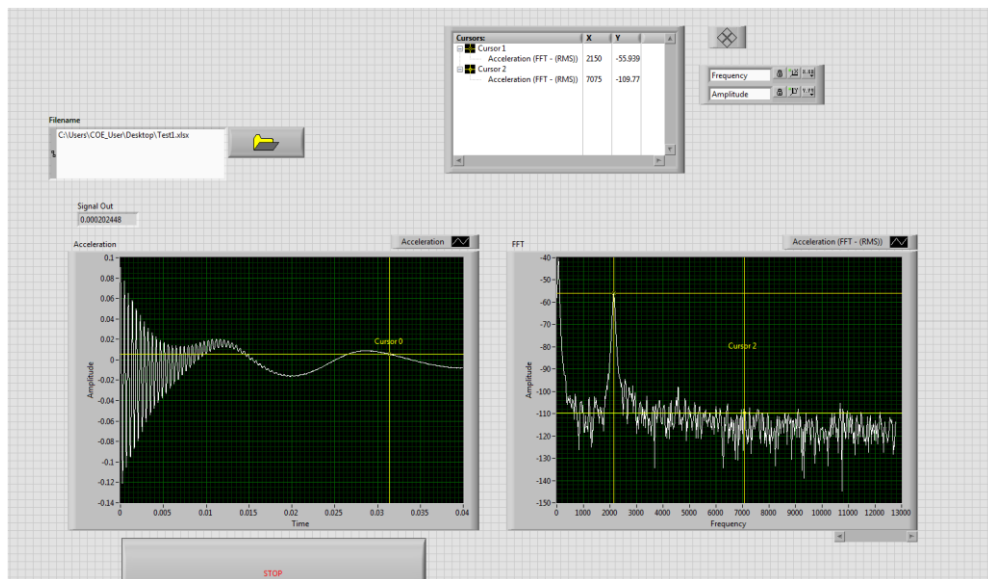


Figure: 6.6 Dynamic frequency readout of sample 1.80.24.2 prior to freeze thaw cycling.

6.6.1 Testing Procedure Calibration

In order to prepare for the testing procedures and prevent any unforeseen obstacles, the series of samples cured at 140°F (60°C) were tested in order to calibrate the testing procedure. During this procedure, it was determined that the water pressure changes from the freezing to thawing cycles was significant enough that some water bath containers longer than the desired length at sixteen (16) inches could not be used. These water bath containers had a wood block placed at the desired location sealed with caulk. However, the combination of the water pressure and insufficient strength of the caulk, the walls failed and the water leveled out in the entire container. A second problem found during this preliminary testing involved the fan in the chamber which caused some significant evaporation of water during the testing cycles leaving the top surfaces with less water than required. In this case, plexiglass covers were selected to cover the samples and prevent evaporation of water in between cycles. As a result of these two issues, the containers selected for use were custom made from stainless steel boxes of dimensions 3¼”x3¼”x3¼”x12¼” (82.5mm x 82.5mm x 82.5mm x 311.15 mm). The stainless steel was selected to avoid rusting of the boxes over time.

6.6.2 Freeze Thaw Cycles and Measurements

Once the sample and chamber set up was established to meet ASTM guidelines, the freezing and thawing cycle was initiated by placing samples in the chamber at the beginning of the thawing cycle. Six samples were placed in the chamber on the first day of testing. These samples were all of the 158°F (70°C) curing temperature, 24 hour curing duration series. The next day the samples of the 158°F (70°C) curing temperature, 48 hour curing duration series were placed in the chamber. A week later the 176°F

(80°C) curing temperature, 24 hour curing sample series samples were placed in the chamber and the following day the 176°F (80°C) curing temperature, 48 hour curing duration series. Each of these series had two samples of the same design, as shown in Table: 6.1. The iterative starting of the sample testing was designed to avoid having too many samples ready for removal at a time which could increase the time a sample would be waiting to be tested or to begin the freeze thaw cycling.

As previously noted, samples were cycled from a freezing temperature of 0°F (-18°C) to a thawing temperature of 40°F (4°C). ASTM C666 (2008) requires that cycling occur over a time period of 5 hours where freezing takes up 25% of the time and thawing takes up the remaining time. The calibration of the chamber, as previously noted in Section 7.4.1 explains the process of preparing the chamber for testing. Once the chamber was adequately programmed to cycle, six samples were placed in the chamber to begin testing. At this time, additional concrete mass was placed in the chamber to *hold* the space for future samples. The next day another six samples were placed in the chamber followed by the same pattern a week later for the remaining twelve samples. The samples were divided into sets of six by the curing temperature and curing duration i.e. samples cured at 158°F (70°C) for forty-eight hours were tested together.

Once samples were in the chamber, thirty-three freeze thaw cycles occurred before measurements were taken. The weight, dimensions, and transverse frequencies were measured and noted at each testing and used to track the changes of the samples. The testing period of thirty-three cycles per week required approximately ten weeks to complete testing to the ASTM prescribed 300 total cycles. The collected raw data can be found in Appendix D.



Figure: 6.7 Samples after being removed from environmental chamber.



Figure: 6.8 Sample weight measurement following removal from environmental chamber.

Table: 6.1 Freeze thaw sample series and quantities.

Day	Samples	Number of Samples
1	1.70.24	2
	2.70.24	2
	3.70.24	2
2	1.70.48	2
	2.70.48	2
	3.70.48	2
8	1.80.24	2
	2.80.24	2
	3.80.24	2
9	1.80.48	2
	2.80.48	2
	3.80.48	2

6.6.3 Calculations

The following section outlines the calculations per ASTM C215 (2008) and ASTM C666 (2008) used to calculate the durability factor of the concrete.

$$P_c = \left(\frac{n_1^2}{n^2} \right) \times 100 \quad \text{Equation (6.1)}$$

P_c = relative dynamic modulus of elasticity, after c cycles of freezing and thawing, percent

n = fundamental transverse frequency at 0 cycles of freezing and thawing

n_1 = fundamental transverse frequency after c cycles of freezing and thawing

$$DF = PN/M \quad \text{Equation (6.2)}$$

P = relative dynamic modulus of elasticity at N cycles, percent

N = number of cycles at which P reaches the specified minimum value for discontinuing the test or the specified number of cycles at which the exposure is to be terminate, whichever is less

M = specified number of cycles at which the exposure is to be terminated

$$\text{Dynamic } E = CMn^2 \quad \text{Equation (6.3)}$$

M = mass of specimen (kg)

n = fundamental transverse frequency (Hz)

$C = 0.9464 (L^3T/bt^3)$, m^{-1} for a prism

L = length of specimen, m

d = diameter of specimen, m

t, b = dimensions of cross section of prism, m (t , is in the direction in which impact is driven)

T = correction factor that depends on the ratio of the radius of gyration

$K = t/3.464$, radius of gyration for a prism

6.7 Air Content: Additional Testing

Critical to the freeze thaw durability of concrete is the air content of the samples. As previously outlined in Section 6.2, the amount of air voids in a concrete sample can greatly contribute to the freeze thaw capability. Per the guidelines stated in Section 6.2.1 and Section 6.2.2, a durability factor of 80 or greater is deemed “good” and this value is strongly associated with the air content of a sample, as shown in Figure: 6.2. Typically, air content values greater than 4% have a better probability of achieving *good* durability parameters (FHWA 2006). The air content measured for the freeze thaw samples was originally measured for the fresh concrete and the results can be found in Section 3.6.3. In this testing, the air content ranged from 1.5% to 4% with no specific outcome for the three mixture designs. The concrete with the least amount of water did no better than the sample with the most water indicating little difference between the mixes. In order to more accurately determine the air content of the samples a second series of air content testing was performed per ASTM C457 (2012) “Standard Test Method for Microscopical Determination of Parameters of the Air-Void System in Hardened Concrete.”

Testing Procedure B: Modified Point Count Method was selected for the analysis of the air content. The procedure required hardened samples with a polished surface of four inches by four inches. The samples sit on a table with a pre-calibrated movement in the lateral and transverse directions. The movement allows for a grid analysis to take place across the surface of the sample. With a stereoscopic microscope the sample is analyzed at every point in the east-west direction and then adjusted in the north-south direction to cover the entire sample surface. At each stop along the surface, a record is

taken based on if the stop is an air void, paste, coarse aggregate, or fine aggregate. These results are shown in Table: 6.2, per the calculations detailed below.

Table: 6.2 Recorded count values for air content analysis.

			S_p	S_a	S_t
Sample	C. Agg.	F. Agg.	Paste	Void/Air	Total
1.70.24	455	158	443	28	1084
1.80.24	376	207	409	30	1022
1.80.48	395	274	369	22	1060
2.60.48	368	211	417	28	1024
2.70.24	465	188	400	31	1084
2.80.48	348	215	477	25	1065
3.60.24	406	138	441	14	999
3.70.24	414	222	417	32	1085
3.70.48	436	210	405	31	1082

Outlined below are the calculations used to determine the air content per ASTM

C457 (2012) with the following notation definitions:

N = total number of voids intersected

S_t = total number of stops

S_a = number of stops in air voids

S_p = number of stops in paste

$l = 0.125 \text{ in.}$ = the east-west translation distance between stops

Total Traverse Length (ASTM C457)

$$T_t = S_t \times l \quad \text{Equation 6.4}$$

Air Content (ASTM C457)

$$A = \frac{S_a \times 100}{S_t} \quad \text{Equation 6.5}$$

Void Frequency (ASTM C457)

$$n = \frac{N}{T_t} \quad \text{Equation 6.6}$$

Total Traverse Length (ASTM C457)

$$n = \frac{N}{T_t} \quad \text{Equation 6.7}$$

Paste Content (ASTM C457)

$$p = \frac{S_p \times 100}{S_t}$$

Equation 6.8

Paste-Air Ratio (ASTM C457)

$$\frac{P}{A} = \frac{S_p}{S_a}$$

Equation 6.9

Average Chord Length (ASTM C457)

$$l = \frac{A}{100n}$$

Equation 6.10

Specific Surface (ASTM C457)

$$a = \frac{4}{l}$$

Equation 6.11

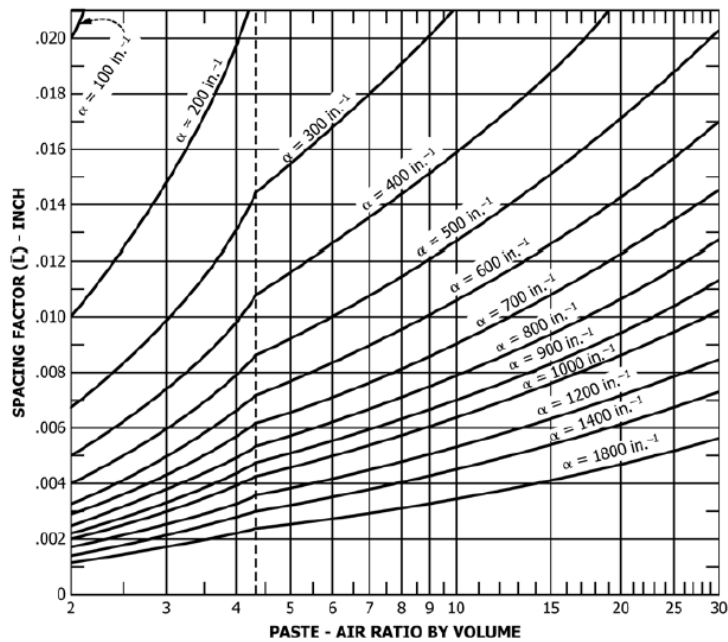


Figure: 6.9 Chart used to find spacing factor per ASTM C457 (2012).

Table: 6.3 ASTM C457 calculated values for air content of selected samples.

Sample	Total traverse length	Air Content	Void Frequency	Paste content	Paste to Air Ratio	Avg. chord length	Specific Surface	Spacing factor, Fig. 7.11 estimate
	T_t , in	A, %						
1.70.24	135.50	2.58	3.476	40.870	15.841	0.00742	538.9	0.0170
1.80.24	127.75	2.94	3.436	40.020	13.612	0.00856	467.5	0.0170
1.80.48	132.50	2.08	2.951	34.810	16.736	0.00705	567.5	0.0135
2.60.48	128.00	2.73	3.477	40.720	14.916	0.00785	509.5	0.0175
2.70.24	135.50	2.86	3.181	36.900	12.902	0.00899	444.9	0.0158
2.80.48	133.13	2.35	3.771	44.790	19.060	0.00623	641.9	0.0130
3.60.24	124.88	1.40	3.644	44.140	31.529	0.00384	1041.1	0.0095
3.70.24	135.63	2.95	3.311	38.430	13.027	0.00891	448.9	0.0170
3.70.48	135.25	2.87	3.224	37.430	13.042	0.00890	449.3	0.0170

6.8 Results

The following sections outline the results for the freeze-thaw study. The data is subdivided into physical changes and the durability factor calculations. The section on physical changes outlines the physical deterioration of the samples and the mass changes of the samples. The durability factor section outlines the results of the frequency testing, dynamic modulus calculations, and durability factor calculations.

6.8.1 Physical Deterioration

Figure: 6.10 and Figure: 6.11 provide images of samples after cycling prior to ending of the freeze-thaw testing. Additional images can be found in Appendix E.



Figure: 6.10 Sample 3.80.48.2 at 66 of 132 cycles.



Figure: 6.11 Sample 3.80.48.2 at 132 of 132 cycles.

6.8.2 Mass Change

The following tables and figures provide data for the mass change of samples over time.

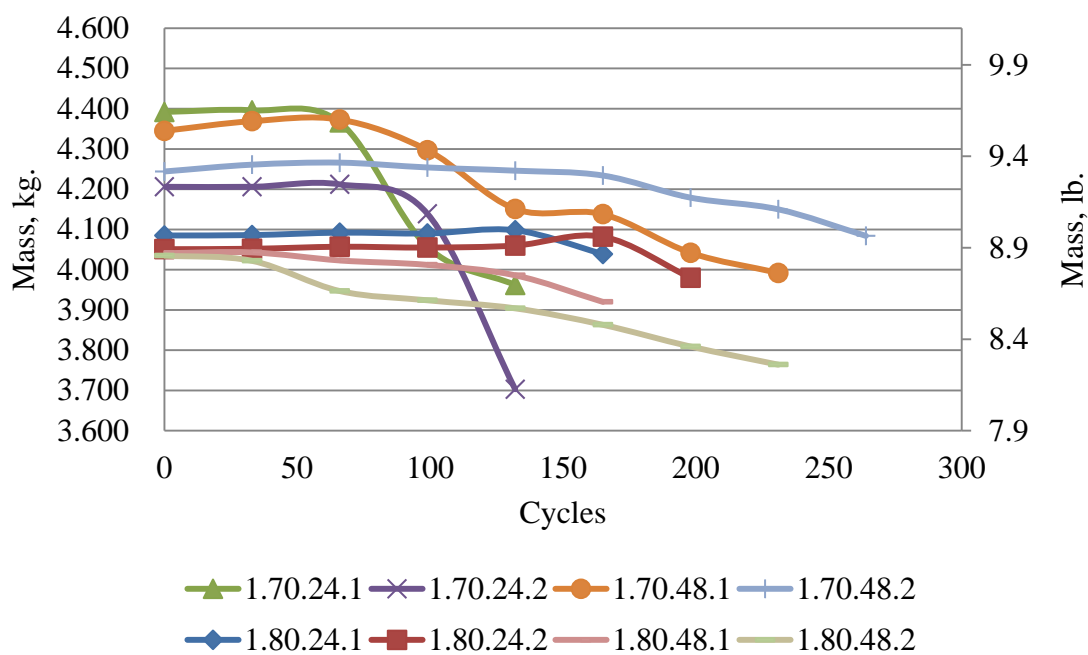


Figure: 6.12 Mass change chart of $w/cm: 1$ samples.

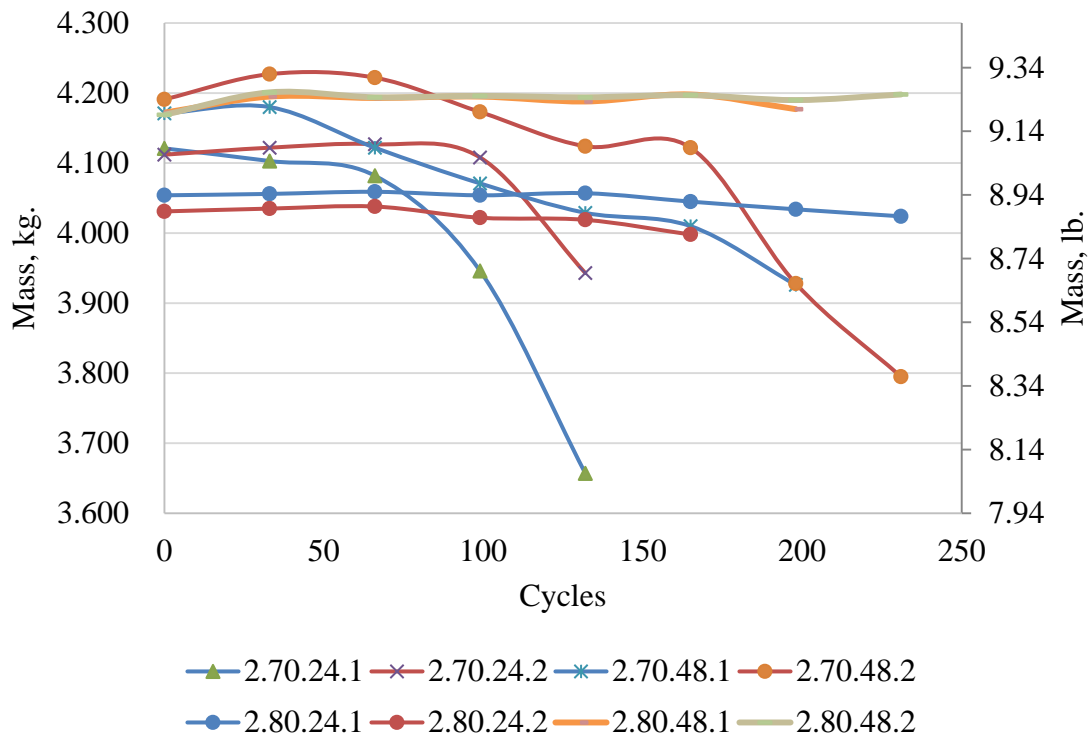


Figure: 6.13 Mass change chart of *w/cm*: 2 samples.

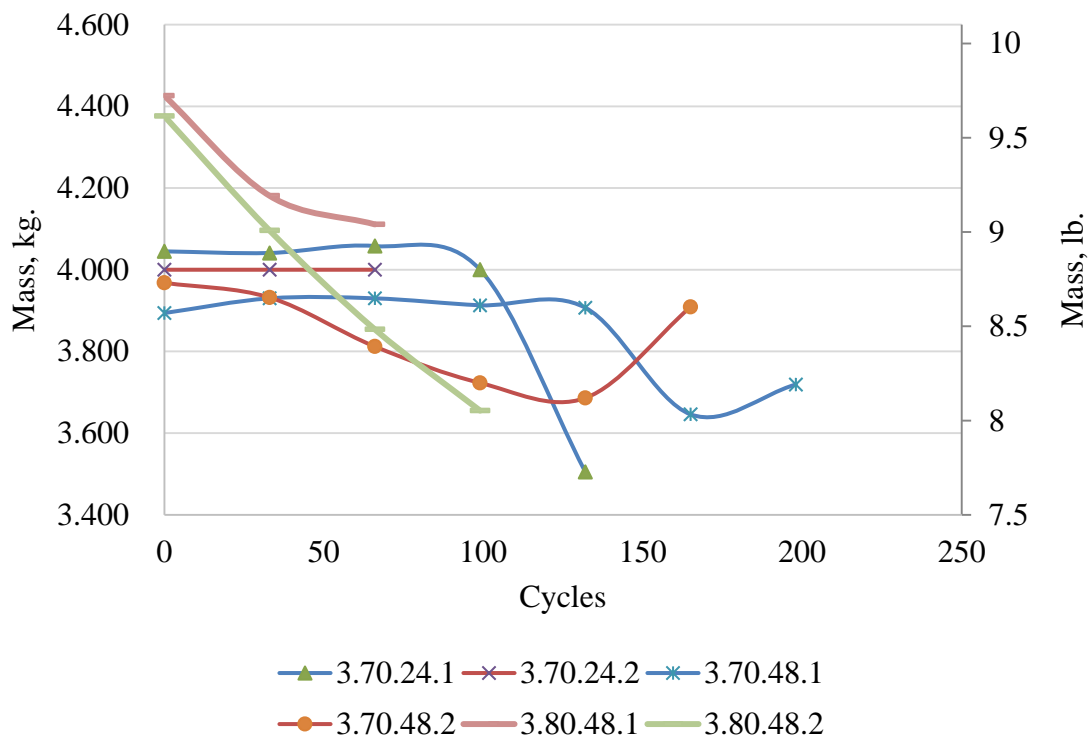


Figure: 6.14 Mass change chart of *w/cm* 3 samples.

6.8.3 Mechanical and Durability Properties

The results and measurements of the tests are presented in the following tables and figures. These outline the compressive strength of the samples at the start of freeze-thaw testing, the recorded transverse frequency, and calculated dynamic modulus and durability factors for each sample.

Table: 6.4 Average compressive strength of freeze thaw specimens (psi, MPa).

Sample	f'_c	
	psi	MPa
1.70.24	5,089	35.09
1.70.48	5,833	40.22
2.70.24	4,409	30.40
2.70.48	4,996	34.44
3.70.24	4,573	31.53
3.70.48	5,133	35.39
1.80.24	5,086	35.07
1.80.48	4,904	33.81
2.80.24	5,234	36.09
2.80.48	5,232	36.07
3.80.24	4,999	34.47
3.80.48	5,319	36.67

Table: 6.5 Calculated values per ASTM C666 (2008) and ASTM C215 (2008) including final durability factors.

Batch Label	n _c , Hz.	n, Hz.	P _c	P	N	M	DF	Avg. DF	Std. Dev	Range
1.70.24.1	1550	2230	48	48	66	66	48	42.5	7.8	11
1.70.24.2	1350	2230	37	37	66	66	37			
2.70.24.1	1580	2180	53	53	66	66	53	51	2.8	4
2.70.24.2	1500	2150	49	49	132	132	49			
3.70.24.1	1000	2050	24	24	66	66	24	36.5	17.7	25
3.70.24.2	1400	2000	49	49	66	66	49			
1.70.48.1	1750	2300	58	58	297	297	58	60	2.8	4
1.70.48.2	1750	2230	62	62	264	264	62			
2.70.48.1	1350	2200	38	38	198	198	38	49	15.6	22
2.70.48.2	1730	2230	60	60	132	132	60			
3.70.48.1	1500	2050	54	54	99	99	54	54	0	0
3.70.48.2	1500	2050	54	54	165	165	54			
1.80.24.1	1500	2200	46	46	165	165	46	51.5	7.8	11
1.80.24.2	1630	2150	57	57	198	198	57			
2.80.24.1	1630	2200	55	55	231	231	55	54.5	0.7	1
2.80.24.2	1600	2180	54	54	165	165	54			
1.80.48.1	1500	2080	52	52	165	165	52	50.5	2.1	3
1.80.48.2	1500	2150	49	49	231	231	49			
2.80.48.1	1400	2130	43	43	198	198	43	49.5	9.2	13
2.80.48.2	1600	2130	56	56	231	231	56			
3.80.48.1	1600	2200	53	53	66	66	53	48.5	6.4	9
3.80.48.2	1550	2330	44	44	66	66	44			

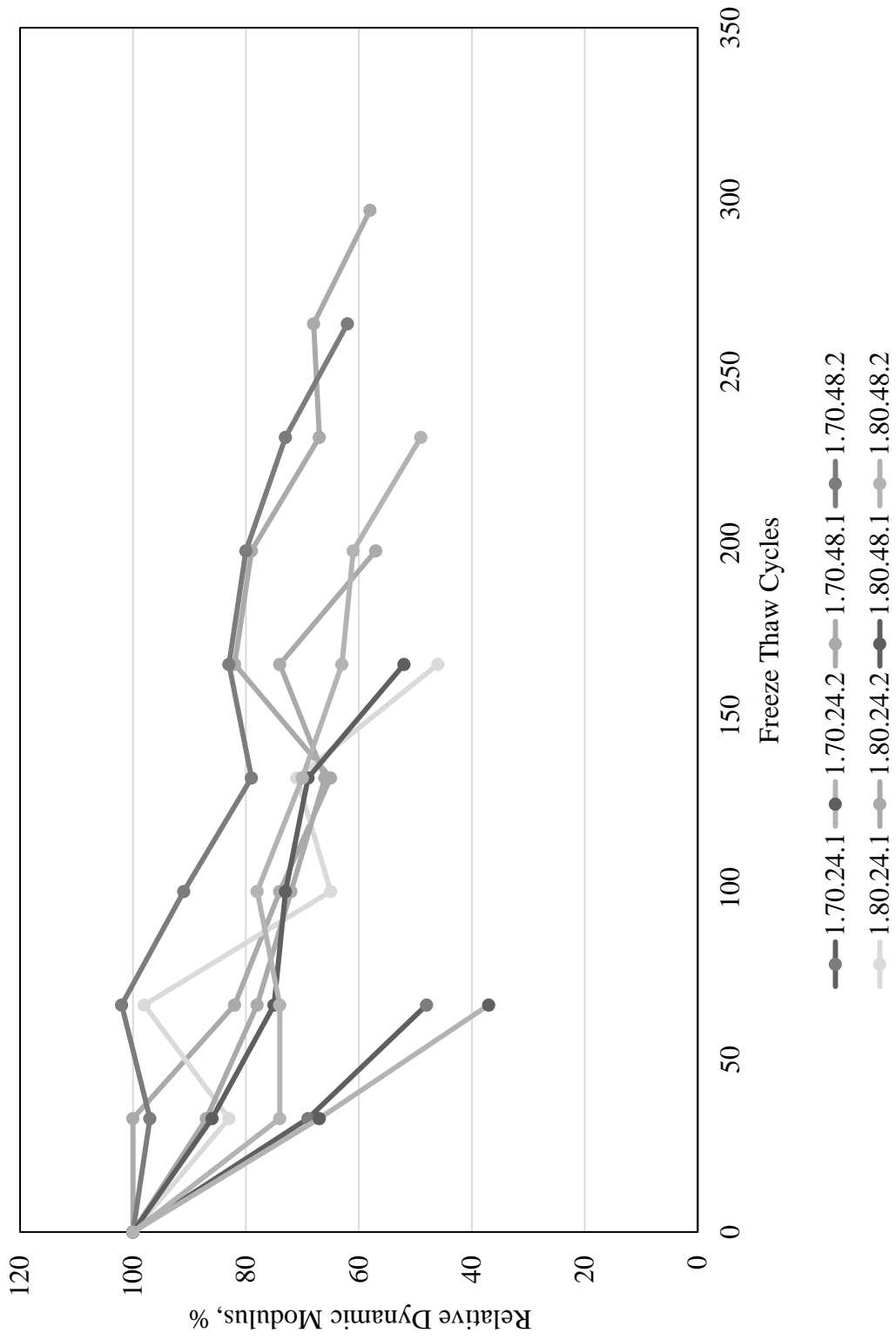


Figure: 6.15 Relative dynamic modulus of samples with the base water content in the mixture design, notated as Series 1.

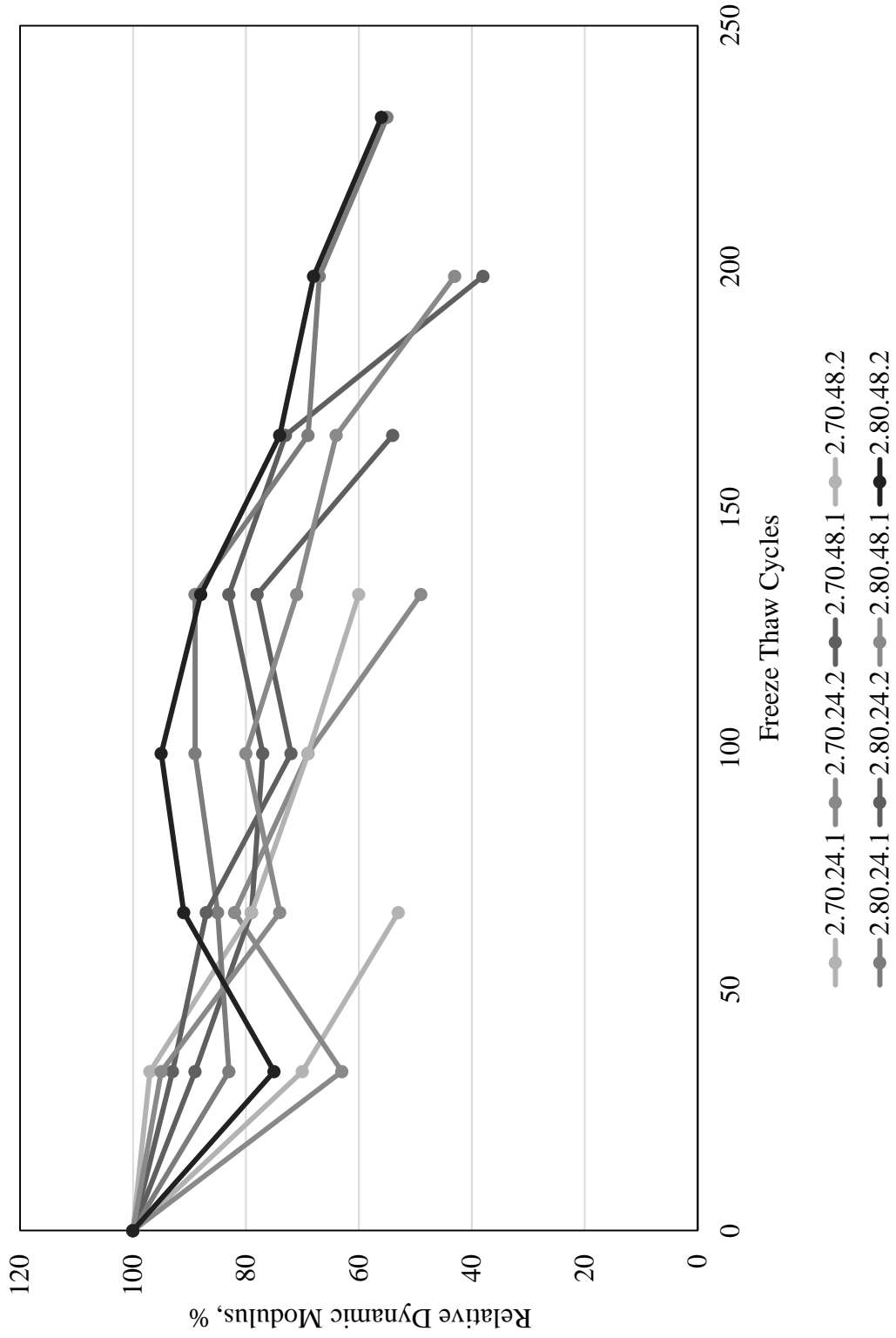


Figure: 6.16 Relative dynamic modulus of samples with a 10% water content increase in the mixture design, notated as Series 2.

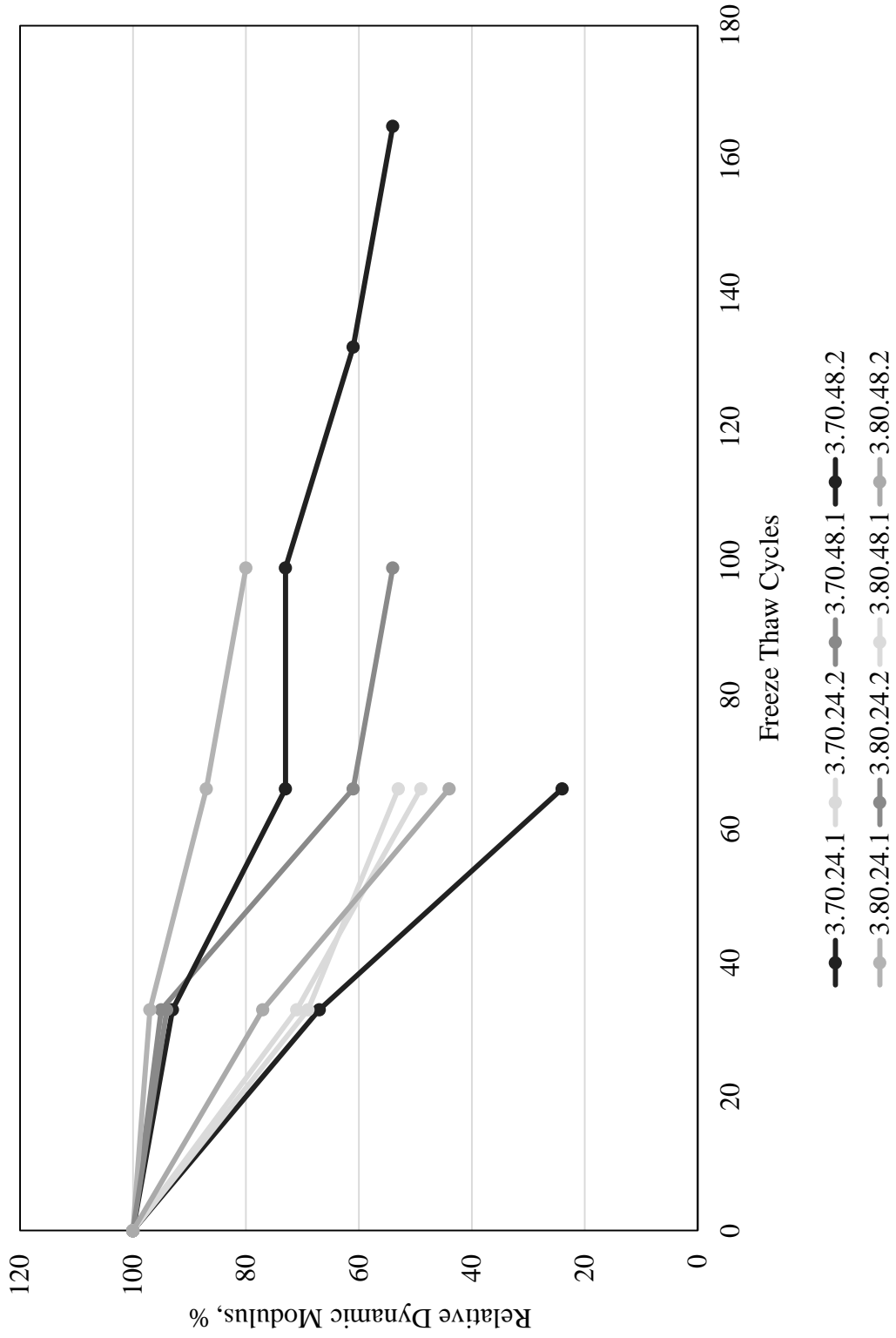


Figure: 6.17 Relative dynamic modulus of samples with a 20% water content increase in the mixture design, notated as Series 3.

6.9 Discussion

As there are multiple levels of data presented in this portion of the study, the discussion is divided first by comparing the samples of the same mixture design type by water content series followed by a comparison of durability factors. Reference will be made to the tables and figures shown in Section 6.8.

Figure: 6.15 through Figure: 6.17 show the relative dynamic modulus of the samples grouped by w/cm . Overall, the relative dynamic modulus declines more slowly in samples with less water since these samples endured more freeze thaw cycles before dropping below the 60% of initial dynamic modulus threshold, which caused test cessation. The endurance of samples with less water could partially be attributed to higher mechanical strength of the concrete. However, the inconsistency between samples that were cured at 176° F (80°C) for 48 hours versus those cured at 158°F (70°C) for 24 hours does not confirm the theory. The samples cured at 176° F (80°C) for 48 hours generally had a higher compressive strength than the samples cured at 158°F (70°C) for 24 hours and if the theory was applicable then the samples cured at higher temperatures and for a longer duration would have continuously resulted in higher durability factors. It is not probable that the mechanical strength of these samples adds to the relationships between the relative dynamic modulus and durability factors to the mixture design.

The more probable relationship lies in the air content of the concrete and the resulting durability factors and rate of change of the relative dynamic modulus. As discussed in Section 3.6.3 and Section 6.7, the air content ranges are between 1% and 4% for the fresh concrete and between 1.4% and 2.95% for the hardened concrete. The resulting durability factors for the samples ranged from 24 to 62, all falling below the

good durability designation with no particular distribution based on the water content. The air content also had no significant distribution based on the water content as shown in Table: 6.3 the values do not indicate a higher air content with a higher water content or a lower air content with a lower water content as would theoretically be expected. Notably, the range of air contents for the selected samples tested for freeze thaw (as shown in Table: 6.3) is very small, a 1% difference. Most samples tested for freeze thaw durability ranged between 2% and 3%, further restricting the boundaries of the test results as compared to Figure: 6.2 which shows that *good durability* more frequently occurs in concrete with air contents greater than 4%. Given the boundary for the air content, the durability factors more appropriately indicate an average durability factor of 45 for air content ranges between 2% and 3%. The overall performance of the mixture designs is positive in that the majority of samples resulted in a better durability factor than is typically expected with PCC as shown in Figure: 6.2, which shows that most concretes with an air content below 3% result in a durability factor of 40 or lower. Figure: 6.18 and Figure: 6.19 show a summary of the air content to durability factor results. Based on the guidelines presented in Section 6.2.1, it should be noted that no samples achieved the recommended guidelines for durable concrete. Figure: 6.19 illustrates the relationship between the three test methods used to measure the fresh concrete air content and hardened concrete air content.

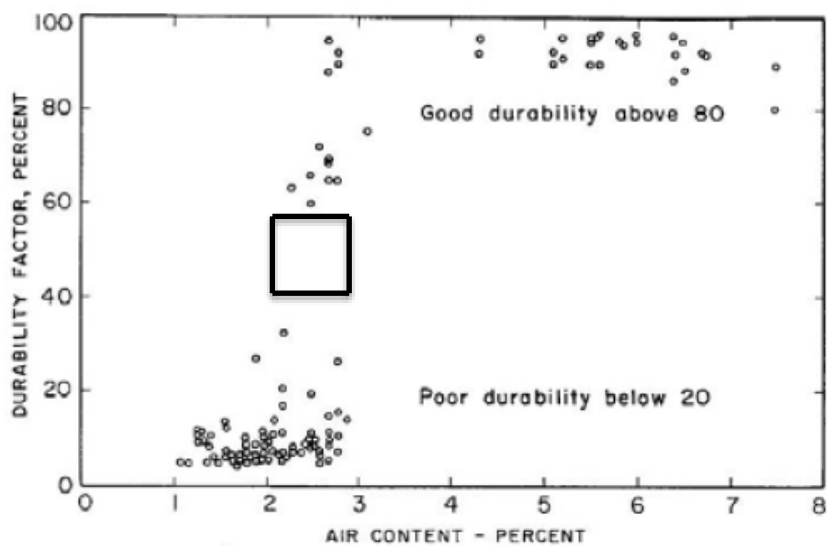


Figure: 6.18 Freeze-thaw durability factor parameters against total air content (Cordon and Merrill 1963) with results from study shown in box.

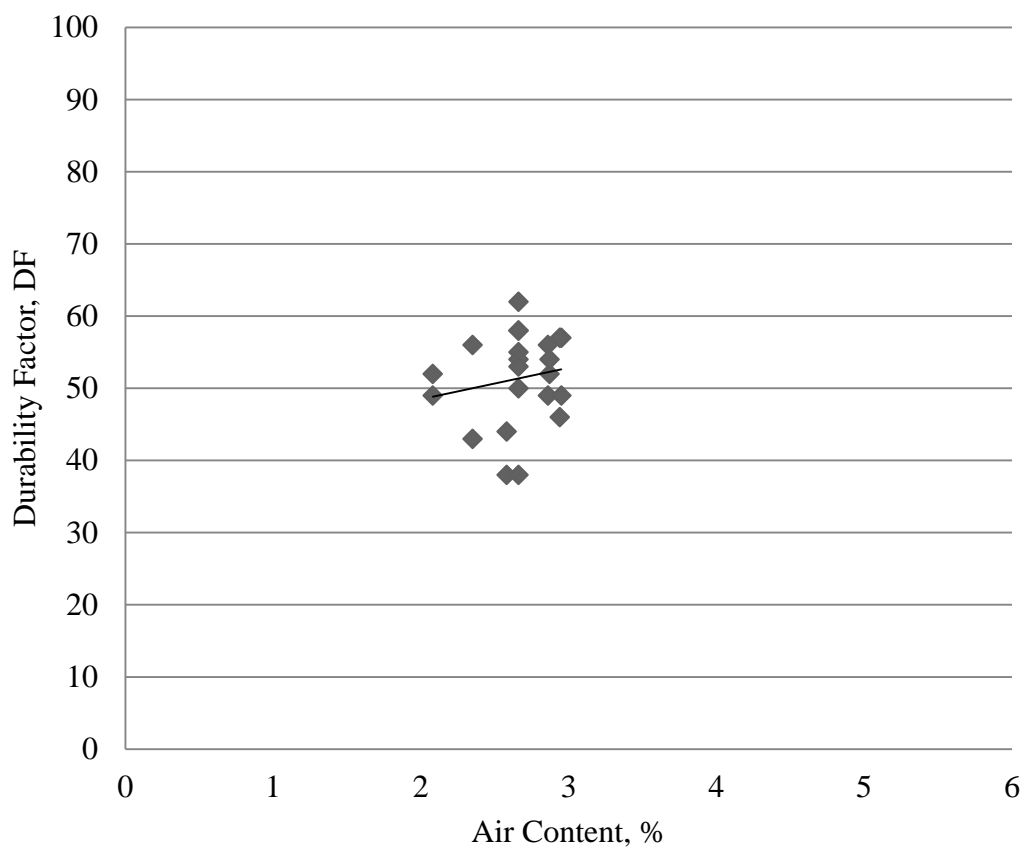


Figure: 6.19 Summary Durability Factors against air content of samples with a linear trend line applied.

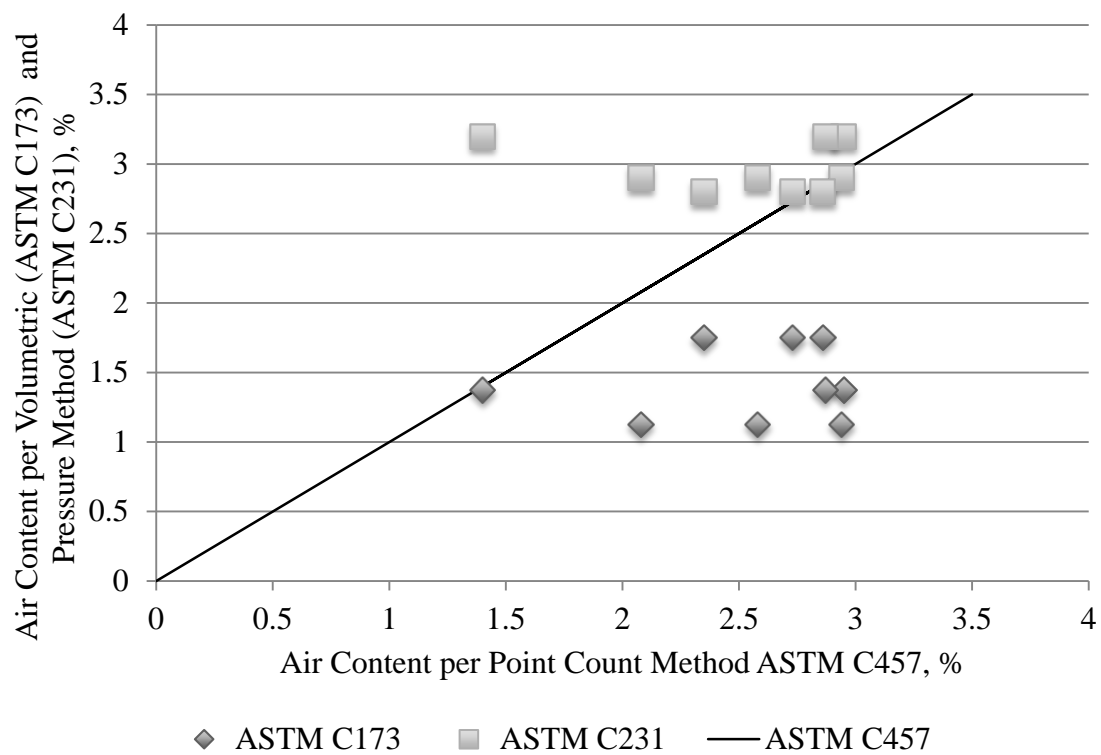


Figure: 6.20 Summary of measured air content per ASTM C173, ASTM C231, and ASTM C457.

Table: 6.6 Summary of measured and calculated values associated with the freeze-thaw durability of the samples.

Sample	ASTM C457 Air Content	Void Frequency N, in ⁻¹	specific surface a, in ² /in ³	Spacing factor, Fig. 4 estimate L, in	Avg. DF	Compressive Strength		ASTM C173 Air Content	ASTM C231 Air Content
	A, %					psi	MPa		
1.70.24	2.58	3.476	538.9	0.0170	42.5	5,089	35.09		
1.80.24	2.94	3.436	467.5	0.0170	51.5	5,086	35.07		
1.80.48	2.08	2.951	567.5	0.0135	50.5	4,904	33.81	1.13%	2.90%
2.70.24	2.86	3.181	444.9	0.0158	51.0	4,409	30.40		
2.80.48	2.35	3.771	641.9	0.0130	49.5	5,232	36.07	1.75%	2.80%
3.70.24	2.95	3.311	448.9	0.0170	36.5	4,573	31.53		
3.70.48	2.87	3.224	449.3	0.0170	54.0	5,133	35.39	1.38%	3.20%

CHAPTER 7: CONCLUSIONS

GCC is among the many novel types of concretes being researched worldwide. Within the GCC research there exist many source material options for preparing GCC, however fly ash has become a popular one due to its status as an abundant waste material. Although, the quantity of carbon dioxide emissions associated with fly ash based GCC are disputed amongst researchers, it is clear that the use of fly ash is viable (if not preferable) to the sustainability interests in construction industries.

The most currently appropriate application for GCC has been determined to be in the precast concrete industry. The precast concrete factories provide a controlled environment for quality control purposes and uses common mixing techniques. However, GCC production does require a slightly different set of methods and tolerances, primarily in the curing process, which requires high heat curing for the entire product. The following were the main goals of this study:

- Determine the relationship between each production variable on the mechanical properties of GCC
- Determine if a co-relationship exists between production variables and their impact on the mechanical properties of GCC
- Analyze the freeze thaw durability of two mixture designs with varying curing temperatures and curing durations

The following main conclusions have been made as a result of this study:

- Improvements in workability were found in Mixture design 3 with a 20% increase in water to Mixture design 1.
- The increased water typically reduced the compressive strength by approximately 500 psi (3.45 MPa).
- Samples cured at temperatures above 158°F (70°C) produced improved mechanical properties compared to those cured at 140°F (60°C).
- Freeze thaw durability of samples cured at 158°F (70°C) and 176°F (80°C) fell below the *good durability* classification.
- GCC samples with an air content between 2% and 3% produced higher durability factors than is typically expected of their PCC counterparts.

The mixture design of GCC plays a significant role in the predicting its final mechanical properties. A proper balance of the necessary quantities of aggregates, fly ash, water, and activating solution are key, however, these results have shown that the curing regimen may be of greater importance within some ranges. Although this study does not propose tolerances for these characteristics, it is apparent that an eventual specification would include some policy for water additions as well as curing temperature and duration.

The study described in this thesis employed precursor materials from only one source. In particular, the single source of fly ash may not be representative of the performance of other ashes from other coal plants due to the great variability of this material. As such, the ash composition and quality is also a production variable but one that cannot be controlled as easily as those discussed in this paper. Because of this aspect of GCC production, an eventual standard will most likely be largely performance based.

The variables considered also did not leave a constrained range set by the research team. Only ranges that were known to produce acceptable workability and compressive strength results were attempted. One might expect greater non-linearity outside of these ranges. Nevertheless, the proposed combinations of production variables are limited in that this study only presents the optimization within the specified production ranges and has not concluded by determining the absolute optimum value for any production variable. Namely, the minimum value of any of the production variables can be offset by a maximum value of another production variable. Hence, an optimized curing temperature, curing duration, or water content value is not set but the value in having the design capability to adjust according to the production conditions is strongly highlighted.

The industrial application of GCC is in the early stages of development and requires studies in other areas of durability and mechanical property characterizations. At this time, further testing will be required in order to adequately qualify GCC in the workability spectrum. While GCC fell within the accepted ranges of SCC, it does not behave exactly like SCC as it does not flow easily and fluidly. As such, a second form of measuring the workability may be required. The practical application of GCC also requires strict attention to high heat curing as higher compressive strengths are achieved with higher heat application. In environments where high heat is a deterrent for casting PCC, GCC may provide the market an opportunity for alternative.

In order to produce a performance based specification and characterize a wider range of mechanical and durability properties for GCC, the following recommendations are made for future research:

- A greater range of w/cm should be analyzed in order to determine if the rates of change in compressive strength become more or less significant outside of the ranges. Furthermore, this study is limited to a 20% change in w/cm and has resulted in a very small air content variation which
- Additional durability testing should be performed, including chloride permeability of a concrete mass and testing of the alkali silica reaction of the GCC.
- Additional research on the use of air-entraining admixtures should be performed in order to assess if any improvement in durability factors can be achieved.

REFERENCES

- ACI (2014). "Building Code Requirements for Structural Concrete (ACI 318-14)." 8.5 *Modulus of Elasticity*, American Concrete Institute, Farmington Hills, MI.
- Aldred, J., and Day, J. "Is geopolymer concrete a suitable alternative to traditional concrete." *Proc., 37th Conference on our world in concrete & structures, Singapore*, 29-31.
- Alonso, S., and Palomo, A. (2001). "Alkaline activation of metakaolin and calcium hydroxide mixtures: influence of temperature, activator concentration and solids ratio." *Materials Letters*, 47(1-2), 55-62.
- ASTM (2008). "ASTM C215 Standard Test Method for Fundamental Transverse, Longitudinal, and Torsional Resonant Frequencies of Concrete Specimens." ASTM International, West Conshohocken, PA.
- ASTM (2008). "ASTM C666 Standard Test Method for Resistance of Concrete to Rapid Freezing and Thawing." ASTM International West Conshohocken, PA.
- ASTM (2010). "ASTM C78 Flexural Strength of Concrete (Using Simple Beam with Third-Point Loading)." ASTM International, West Conshohocken, PA.
- ASTM (2012). "ASTM C457 Standard Test Method for Microscopical Determination of Parameters of the Air-Void System in Hardened Concrete." ASTM International West Conshohocken, PA.
- ASTM (2013). "ASTM C618 Standard Specification for Coal Fly Ash and Raw or Calcined Natural Pozzolan for Use in Concrete." *ASTM Standard C618, 2012a*, ASTM International, West Conshohocken, PA.
- ASTM (2014). "ASTM C173 Standard Test Method for Air Content of Freshly Mixed Concrete by the Volumetric Method." ASTM International West Conshohocken, PA.
- ASTM (2014). "ASTM C231 Standard Test Method for Air Content of Freshly Mixed Concrete by the Pressure Method." ASTM International, West Conshohocken, PA.

- ASTM (2014). "ASTM C1611 Standard Test Method for Slump Flow of Self-Consolidating Concrete." ASTM International.
- ASTM (2014). "Standard Test Method for Air Content of Freshly Mixed Concrete by the Volumetric Method ", ASTM International, West Conshohocken, PA.
- ASTM (2015). "C39 Standard Test Method for Compressive Strength of Cylindrical Concrete Specimens." ASTM International West Conshohocken, PA.
- Bligh, R., and Glasby, T. (2014). "Geopolymer Precast Floor Panels." *Structure Magazine*, 30-32.
- Cordon, W. A., and Merrill, D. (1963). "Requirements for Freezing and Thawing Durability for Concrete." *ASTM*, 63, 1026-1036.
- Davidovits, J. (2013). "Geopolymer Cement: A Review." Institut Geopolymere, 1-11.
- Fernández-Jiménez, A., and Palomo, A. (2003). "Characterisation of fly ashes. Potential reactivity as alkaline cements☆." *Fuel*, 82(18), 2259-2265.
- Fernández-Jiménez, A., and Palomo, A. (2005). "Composition and microstructure of alkali activated fly ash binder: Effect of the activator." *Cement and Concrete Research*, 35(10), 1984-1992.
- FHWA (2006). "Freeze Thaw Resistance of Concrete with Marginal Air Content." U.S. Department of Transportation, Federal Highway Administration.
- Hardjito, D., and Rangan, B. V. (2005). "Development and Properties of Low-Calcium Fly Ash-Based Geopolymer Concrete."
- Hardjito, D., Wallah, S. E., Sumajouw, D. M. J., and Rangan, B. V. (2004). "Factors Influencing the Compressive Strength of Fly Ash-Based Geopolymer Concrete." *Civil Engineering Dimension*, 6(2), 88-93.
- Hasanbeigi, A., Price, L., and Lin, E. (2012). "Emerging energy-efficiency and CO2 emission-reduction technologies for cement and concrete production: A technical review." *Renewable and Sustainable Energy Reviews*, 16(8), 6220-6238.

- Heath, A., Paine, K., Goodhew, S., Ramage, M., and Lawrence, M. (2013). "The potential for using geopolymer concrete in the UK." *Proceedings of the Institution of Civil Engineers: Construction Materials*, 166(4), 195-203.
- Khale, D., and Chaudhary, R. (2007). "Mechanism of geopolymerization and factors influencing its development: a review." *J Mater Sci*, 42(3), 729-746.
- Kosmatka, S. H., and Wilson, M. L. (2011). *Design and Control of Concrete Mixtures*, PCA, USA.
- McLellan, B. C., Williams, R. P., Lay, J., van Riessen, A., and Corder, G. D. (2011). "Costs and carbon emissions for geopolymer pastes in comparison to ordinary portland cement." *Journal of Cleaner Production*, 19(9–10), 1080-1090.
- Mindness, S., Young, F. J., and Darwin, D. (2002). *Concrete*, Prentice Hall, Upper Saddle River, NJ.
- NRMCA (2008). "Concrete CO2 Fact Sheet." NRMCA, ed., National Ready Mixed Concrete Association
- PPG-Industries (2011). "Product Stewardship Summary: PELS Anhydrous Caustic Beads."
- Tempest, B., Gergely, J., and Skipper, A. (2016). "Reinforced geopolymer cement concrete in flexure: A closer look at stress-strain performance and equivalent stress-block parameters." *PCI Journal*(November-December).
- Tempest, B., Snell, C., Gentry, T., Trejo, M., and Isherwood, K. (2015). "Manufacture of full-scale geopolymer cement concrete components: A case study to highlight opportunities and challenges." *PCI Journal*(November-December).
- Turner, L. K., and Collins, F. G. (2013). "Carbon dioxide equivalent (CO₂-e) emissions: A comparison between geopolymer and OPC cement concrete." *Construction and Building Materials*, 43(0), 125-130.
- Univar (2013). "Material Safety Data Sheet: Sodium Silicate N."

Van Deventer, J. S. J., Provis, J. L., and Duxson, P. (2012). "Technical and commercial progress in the adoption of geopolymer cement." *Minerals Engineering*, 29(0), 89-104.

Vora, P. R., and Dave, U. V. (2013). "Parametric Studies on Compressive Strength of Geopolymer Concrete." *Procedia Engineering*, 51(0), 210-219.

APPENDIX A: INTERVIEW TRANSCRIPT

Question: Did you think the production of GCC (geopolymer concrete) would succeed?

Responses:

1: “No, you guys were like gonna totally fail.”

2: “Yes. Yes, of course. That’s why you’re doing this. So, that you aren’t going to waste time if it’s not going to function.”

3: “I figured you guys would succeed cause you were dedicated to it and worked hard.”

4: “After the first test down there, I had serious doubts.”

Question: What were your first impressions when working with GCC (geopolymer concrete)?

Responses:

1: “What y’all were pouring it wasn’t really mud.”

2: “It’s just something new, different. I was interested, excited.”

3: “I thought oh no, not this.”

Question: What aspect of GCC (geopolymer concrete) should be improved?

Responses:

1: “Mostly just the workability.” “I’ve been working in concrete for 35 years and it’s hard to surprise us with anything.”

2: “Go back to the lab and work on workability.”

Question: How would you feel about seeing GCC (geopolymer concrete) in a plant setting?

Responses:

1: “At this stage, I don’t know.”

2: “I want to know how to get a better finish on top of it. It would definitely be a challenge for me.”

3: “I couldn’t deal with that everyday.”

4: “It worked out fine after you all worked out the kinks in it. It might just be something we can work on and see what we can do with it.”

APPENDIX B: COMPRESSIVE STRENGTH DATA

Table: B.1 Compressive strength data of samples.

W/C ratio	Curing Temperature (°C)	Batch Label	Curing Time	Test Period	Peak Load, lb.	Peak Load, psi	Average, psi
1	60	C	12	0-day	18,550	1,477	
1	60	C	12	0-day	19,354	1,541	1,506
1	60	C	12	0-day	18,826	1,499	
1	60	C	12	14-day	28,643	2,280	
1	60	C	12	14-day	31,100	2,476	2,378
1	60	C	12	14-day	29,879	2,379	
1	60	C	24	0-day	33,620	2,677	
1	60	C	24	0-day	34,133	2,718	2,715
1	60	C	24	0-day	34,545	2,750	
1	60	C	24	14-day	43,047	3,427	
1	60	C	24	14-day	43,541	3,467	3,426
1	60	C	24	14-day	42,518	3,385	
1	60	B	36	0-day	31,303	2,492	
1	60	B	36	0-day	32,365	2,577	2,601
1	60	B	36	0-day	34,328	2,733	
1	60	B	36	14-day	37,322	2,971	
1	60	B	36	14-day	37,024	2,948	3,016
1	60	B	36	14-day	39,317	3,130	
1	60	B	36	28-day	41,159	3,277	
1	60	B	36	28-day	41,327	3,290	3,298
1	60	B	36	28-day	41,780	3,326	
1	60	B	48	0-day	40,012	3,186	
1	60	B	48	0-day	39,843	3,172	3,136
1	60	B	48	0-day	38,318	3,051	
1	60	B	48	14-day	41,187	3,279	
1	60	B	48	14-day	42,174	3,358	3,413
1	60	B	48	14-day	45,256	3,603	
1	60	B	48	28-day	47,662	3,795	
1	60	B	48	28-day	47,823	3,808	3,751
1	60	B	48	28-day	45,851	3,651	
1	70	C	12	0-day	30,115	2,398	
1	70	C	12	0-day	27,019	2,151	2,387

W/C ratio	Curing Temperature (°C)	Batch Label	Curing Time	Test Period	Peak Load, lb.	Peak Load, psi	Average, psi
1	70	C	12	0-day	32,820	2,613	
1	70	C	12	14-day	33,768	2,689	
1	70	C	12	14-day	40,384	3,215	3,000
1	70	C	12	14-day	38,886	3,096	
1	70	C	12	28-day	40,932	3,259	
1	70	C	12	28-day	38,668	3,079	3,250
1	70	C	12	28-day	42,870	3,413	
1	70	C	24	0-day	52,176	4,154	
1	70	C	24	0-day	50,137	3,992	4,074
1	70	C	24	0-day	51,202	4,077	
1	70	C	24	14-day	60,601	4,825	
1	70	C	24	14-day	53,094	4,227	4,660
1	70	C	24	14-day	61,908	4,929	
1	70	C	24	28-day	62,628	4,986	
1	70	C	24	28-day	57,880	4,608	4,763
1	70	C	24	28-day	58,987	4,696	
1	70	B	36	0-day	57,799	4,602	
1	70	B	36	0-day	56,545	4,502	4,541
1	70	B	36	0-day	56,745	4,518	
1	70	B	36	14-day	67,671	5,388	
1	70	B	36	14-day	66,821	5,320	5,561
1	70	B	36	14-day	75,035	5,974	
1	70	B	36	28-day	67,867	5,403	
1	70	B	36	28-day	67,313	5,359	5,517
1	70	B	36	28-day	72,725	5,790	
1	70	B	48	0-day	63,024	5,018	
1	70	B	48	0-day	65,561	5,220	5,168
1	70	B	48	0-day	66,131	5,265	
1	70	B	48	14-day	72,718	5,790	
1	70	B	48	14-day	77,563	6,175	5,938
1	70	B	48	14-day	73,469	5,849	
1	70	B	48	28-day	73,086	5,819	
1	70	B	48	28-day	77,093	6,138	6,008
1	70	B	48	28-day	76,219	6,068	
1	80	C	12	0-day	42,361	3,373	
1	80	C	12	0-day	42,938	3,419	3,418
1	80	C	12	0-day	43,473	3,461	
1	80	C	12	14-day	49,342	3,929	
1	80	C	12	14-day	52,684	4,195	3,983

W/C ratio	Curing Temperature (°C)	Batch Label	Curing Time	Test Period	Peak Load, lb.	Peak Load, psi	Average, psi
1	80	C	12	14-day	48,045	3,825	
1	80	C	24	0-day	58,148	4,630	
1	80	C	24	0-day	58,001	4,618	4,611
1	80	C	24	0-day	57,587	4,585	
1	80	C	24	14-day	61,976	4,934	
1	80	C	24	14-day	60,202	4,793	4,867
1	80	C	24	14-day	61,216	4,874	
1	80	B	36	0-day	66,341	5,282	
1	80	B	36	0-day	68,808	5,478	5,210
1	80	B	36	0-day	61,179	4,871	
1	80	B	36	14-day	71,199	5,669	
1	80	B	36	14-day	72,727	5,790	5,730
1	80	B	36	14-day	71,974	5,730	
1	80	B	48	0-day	70,163	5,586	
1	80	B	48	0-day	69,596	5,541	5,618
1	80	B	48	0-day	71,924	5,726	
1	80	B	48	14-day	68,753	5,474	
1	80	B	48	14-day	70,508	5,614	5,675
1	80	B	48	14-day	74,551	5,936	
2	60	C	12	0-day	13,774	1,097	
2	60	C	12	0-day	13,297	1,059	1,120
2	60	C	12	0-day	15,140	1,205	
2	60	C	12	14-day	20,868	1,661	
2	60	C	12	14-day	21,186	1,687	1,679
2	60	C	12	14-day	21,198	1,688	
2	60	C	24	0-day	26,099	2,078	
2	60	C	24	0-day	24,293	1,934	2,004
2	60	C	24	0-day	25,129	2,001	
2	60	C	24	14-day	31,476	2,506	
2	60	C	24	14-day	32,381	2,578	2,558
2	60	C	24	14-day	32,549	2,591	
2	60	B	36	0-day	27,672	2,203	
2	60	B	36	0-day	29,345	2,336	2,278
2	60	B	36	0-day	28,831	2,295	
2	60	B	36	14-day	34,554	2,751	
2	60	B	36	14-day	34,102	2,715	2,713
2	60	B	36	14-day	33,579	2,673	
2	60	B	36	28-day	35,903	2,859	
2	60	B	36	28-day	36,723	2,924	2,892

W/C ratio	Curing Temperature (°C)	Batch Label	Curing Time	Test Period	Peak Load, lb.	Peak Load, psi	Average, psi
2	60	B	36	28-day	-	-	
2	60	B	48	0-day	34,652	2,759	
2	60	B	48	0-day	34,669	2,760	2,769
2	60	B	48	0-day	35,009	2,787	
2	60	B	48	14-day	39,289	3,128	
2	60	B	48	14-day	38,405	3,058	3,148
2	60	B	48	14-day	40,919	3,258	
2	60	B	48	28-day	43,195	3,439	
2	60	B	48	28-day	41,984	3,343	3,358
2	60	B	48	28-day	41,360	3,293	
2	70	B	36	0-day	50,244	4,000	
2	70	B	36	0-day	51,767	4,122	4,005
2	70	B	36	0-day	48,892	3,893	
2	70	B	36	14-day	59,138	4,708	
2	70	B	36	14-day	58,184	4,632	4,711
2	70	B	36	14-day	60,185	4,792	
2	70	B	36	28-day	63,335	5,043	
2	70	B	36	28-day	62,134	4,947	5,038
2	70	B	36	28-day	64,356	5,124	
2	70	B	48	0-day	60,992	4,856	
2	70	B	48	0-day	58,497	4,657	4,748
2	70	B	48	0-day	59,410	4,730	
2	70	B	48	14-day	62,879	5,006	
2	70	B	48	14-day	61,812	4,921	4,935
2	70	B	48	14-day	61,265	4,878	
2	70	B	48	28-day	65,195	5,191	
2	70	B	48	28-day	66,245	5,274	5,231
2	70	B	48	28-day	65,678	5,229	
2	80	C	12	0-day	36,538	2,909	
2	80	C	12	0-day	36,759	2,927	2,937
2	80	C	12	0-day	37,352	2,974	
2	80	C	12	14-day	42,838	3,411	
2	80	C	12	14-day	45,460	3,619	3,529
2	80	C	12	14-day	44,663	3,556	
2	80	C	24	0-day	48,854	3,890	
2	80	C	24	0-day	49,479	3,939	3,898
2	80	C	24	0-day	48,561	3,866	
2	80	C	24	14-day	52,894	4,211	
2	80	C	24	14-day	56,070	4,464	4,307

W/C ratio	Curing Temperature (°C)	Batch Label	Curing Time	Test Period	Peak Load, lb.	Peak Load, psi	Average, psi
2	80	C	24	14-day	53,340	4,247	
3	60	C	12	0-day	7,101	565	
3	60	C	12	0-day	5,138	409	532
3	60	C	12	0-day	7,829	623	
3	60	C	12	14-day	12,026	957	
3	60	C	12	14-day	12,183	970	957
3	60	C	12	14-day	11,843	943	
3	60	C	12	28-day	12,996	1,035	
3	60	C	12	28-day	12,620	1,005	1,048
3	60	C	12	28-day	13,865	1,104	
3	60	C	24	0-day	17,034	1,356	
3	60	C	24	0-day	16,190	1,289	1,335
3	60	C	24	0-day	17,065	1,359	
3	60	C	24	14-day	23,926	1,905	
3	60	C	24	14-day	23,040	1,834	1,806
3	60	C	24	14-day	21,095	1,680	
3	60	C	24	28-day	25,298	2,014	
3	60	C	24	28-day	25,459	2,027	1,954
3	60	C	24	28-day	22,889	1,822	
3	60	B	36	0-day	24,998	1,990	
3	60	B	36	0-day	25,044	1,994	1,969
3	60	B	36	0-day	24,159	1,923	
3	60	B	36	14-day	28,422	2,263	
3	60	B	36	14-day	29,083	2,316	2,278
3	60	B	36	14-day	28,341	2,256	
3	60	B	36	28-day	31,639	2,519	
3	60	B	36	28-day	31,102	2,476	2,511
3	60	B	36	28-day	31,893	2,539	
3	60	B	48	0-day	28,793	2,292	
3	60	B	48	0-day	29,067	2,314	2,305
3	60	B	48	0-day	28,991	2,308	
3	60	B	48	14-day	35,007	2,787	
3	60	B	48	14-day	35,320	2,812	2,736
3	60	B	48	14-day	32,753	2,608	
3	60	B	48	28-day	36,538	2,909	
3	60	B	48	28-day	34,376	2,737	2,859
3	60	B	48	28-day	36,808	2,931	
3	70	C	12	0-day	26,686	2,125	
3	70	C	12	0-day	29,009	2,310	2,189

W/C ratio	Curing Temperature (°C)	Batch Label	Curing Time	Test Period	Peak Load, lb.	Peak Load, psi	Average, psi
3	70	C	12	0-day	26,776	2,132	
3	70	C	12	14-day	33,607	2,676	
3	70	C	12	14-day	35,933	2,861	2,816
3	70	C	12	14-day	36,563	2,911	
3	70	C	24	0-day	38,922	3,099	
3	70	C	24	0-day	41,012	3,265	3,129
3	70	C	24	0-day	37,984	3,024	
3	70	C	24	14-day	49,606	3,950	
3	70	C	24	14-day	49,539	3,944	3,947
3	70	B	36	0-day	44,731	3,561	
3	70	B	36	0-day	40,761	3,245	3,402
3	70	B	36	0-day	42,721	3,401	
3	70	B	36	14-day	45,940	3,658	
3	70	B	36	14-day	48,464	3,859	3,725
3	70	B	36	14-day	45,957	3,659	
3	70	B	36	28-day	51,121	4,070	
3	70	B	36	28-day	49,214	3,918	3,973
3	70	B	36	28-day	49,356	3,930	
3	70	B	48	0-day	47,699	3,798	
3	70	B	48	0-day	47,637	3,793	3,800
3	70	B	48	0-day	47,826	3,808	
3	70	B	48	14-day	52,026	4,142	
3	70	B	48	14-day	51,067	4,066	4,065
3	70	B	48	14-day	50,092	3,988	
3	70	B	48	28-day	56,097	4,466	
3	70	B	48	28-day	55,839	4,446	4,443
3	70	B	48	28-day	55,487	4,418	
3	80	C	12	0-day	38,160	3,038	
3	80	C	12	0-day	40,030	3,187	3,171
3	80	C	12	0-day	41,298	3,288	
3	80	C	12	14-day	42,782	3,406	
3	80	C	12	14-day	45,521	3,624	3,567
3	80	C	12	14-day	46,109	3,671	
3	80	C	24	0-day	49,202	3,917	
3	80	C	24	0-day	51,285	4,083	4,047
3	80	C	24	0-day	51,995	4,140	
3	80	C	24	14-day	55,306	4,403	
3	80	C	24	14-day	52,209	4,157	4,230
3	80	C	24	14-day	51,862	4,129	

W/C ratio	Curing Temperature (°C)	Batch Label	Curing Time	Test Period	Peak Load, lb.	Peak Load, psi	Average, psi
2	60	C	12	28-day	26,443	2,105	
2	60	C	12	28-day	26,878	2,140	2,148
2	60	C	12	28-day	27,625	2,199	
1	60	C	12	28-day	33,188	2,642	
1	60	C	12	28-day	35,583	2,833	2,715
1	60	C	12	28-day	33,529	2,670	
2	60	C	24	28-day	32,986	2,626	
2	60	C	24	28-day	33,794	2,691	2,631
2	60	C	24	28-day	32,353	2,576	
1	60	C	24	28-day	44,916	3,576	
1	60	C	24	28-day	44,598	3,551	3,554
1	60	C	24	28-day	44,407	3,536	
3	70	C	12	28-day	35,184	2,801	
3	70	C	12	28-day	38,908	3,098	2,950
3	70	C	24	28-day	53,725	4,277	
3	70	C	24	28-day	53,004	4,220	4,149
3	70	C	24	28-day	49,604	3,949	
1	80	B	36	28-day	73,995	5,891	
1	80	B	36	28-day	74,209	5,908	5,843
1	80	B	36	28-day	71,964	5,730	
1	80	C	12	28-day	64,210	5,112	
1	80	C	12	28-day	64,624	5,145	5,153
1	80	C	12	28-day	65,327	5,201	
2	80	C	12	28-day	41,817	3,329	
2	80	C	12	28-day	44,138	3,514	3,481
2	80	C	12	28-day	45,207	3,599	
3	80	C	12	28-day	45,277	3,605	
3	80	C	12	28-day	47,859	3,810	3,691
3	80	C	12	28-day	45,926	3,657	
1	80	B	48	28-day	70,498	5,613	
1	80	B	48	28-day	71,280	5,675	5,772
1	80	B	48	28-day	75,718	6,029	
1	80	C	24	28-day	64,210	5,112	
1	80	C	24	28-day	64,264	5,117	5,143
1	80	C	24	28-day	65,327	5,201	
2	80	C	24	28-day	56,525	4,500	
2	80	C	24	28-day	53,584	4,266	4,347
2	80	C	24	28-day	53,679	4,274	
3	80	C	24	28-day	56,503	4,499	

W/C ratio	Curing Temperature (°C)	Batch Label	Curing Time	Test Period	Peak Load, lb.	Peak Load, psi	Average, psi
3	80	C	24	28-day	54,178	4,314	4,397
3	80	C	24	28-day	54,995	4,379	
2	70	C	12	0-day	23,485	1,870	
2	70	C	12	0-day	28,361	2,258	2,083
2	70	C	12	0-day	26,651	2,122	
2	70	C	24	0-day	37,460	2,982	
2	70	C	24	0-day	40,587	3,231	3,195
2	70	C	24	0-day	42,367	3,373	
3	80	B	48	0-day	55,883	4,449	
3	80	B	48	0-day	61,412	4,889	4,669
2	80	B	48	0-day	65,481	5,213	5,213
2	70	C	24	14-day	48,932	3,896	
2	70	C	24	14-day	49,653	3,953	3,955
2	70	C	24	14-day	50,429	4,015	
3	80	B	36	14-day	54,051	4,303	4,359
3	80	B	36	14-day	55,445	4,414	
3	80	B	48	14-day	52,564	4,185	4,401
3	80	B	48	14-day	57,983	4,616	
2	80	B	36	14-day	60,165	4,790	4,923
2	80	B	36	14-day	63,498	5,056	
2	80	B	48	14-day	62,763	4,997	4,953
2	80	B	48	14-day	61,655	4,909	
2	70	C	12	28-day	36,533	2,909	
2	70	C	12	28-day	37,892	3,017	2,965
2	70	C	12	28-day	37,308	2,970	
2	70	C	24	28-day	49,374	3,931	
2	70	C	24	28-day	47,064	3,747	3,904
2	70	C	24	28-day	50,671	4,034	
3	80	B	36	28-day	68,889	5,485	5,485
2	80	B	36	28-day	59,225	4,715	4,622
2	80	B	36	28-day	56,882	4,529	
3	80	B	48	28-day	55,664	4,432	4,446
3	80	B	48	28-day	56,002	4,459	
2	80	B	48	28-day	67,913	5,407	5,407
2	80	B	36	0-day	51,924	4,134	
2	80	B	36	0-day	54,440	4,334	4,234
3	80	B	36	0-day	47,567	3,787	
3	80	B	36	0-day	48,569	3,867	3,827
2	70	C	12	14-day	32,494	2,587	

W/C ratio	Curing Temperature (°C)	Batch Label	Curing Time	Test Period	Peak Load, lb.	Peak Load, psi	Average, psi
2	70	C	12	14-day	38,371	3,055	2,821

APPENDIX C: SENSITIVITY ANALYSIS

Parameters						
Response	Goal	Lower	Target	Upper	Weight	Importance
Compressive Strength, psi	Maximum	409	5726		1	1
Solutions						
Solution	Water:Solids Ratio	Temperature, C	Curing Time, hr.	Compressive Strength, psi Fit	Composite Desirability	
1	0.0954	80	48	5670.50	0.989562	
2	0.0954	79.9550	48	5669.34	0.989343	
3	0.107346	77.8731	46.7954	4754.15	0.817219	
4	0.113925	80	48	4542.25	0.777366	
5	0.0954	73.3608	29.4809	4492.63	0.768033	
6	0.0954	80	17.4464	3979.99	0.671618	
7	0.113249	68.9613	45.8782	3734.11	0.625374	
8	0.104749	69.5146	29.3593	3573.85	0.595233	
9	0.114270	79.7647	17.8934	3321.46	0.547764	

Figure: C.1 Optimization analysis output of samples tested at 0-days.

Parameters						
Response	Goal	Lower	Target	Upper	Weight	Importance
Compressive Strength, psi	Maximum	943	6175		1	1
Solutions						
Solution	Water:Solids Ratio	Temperature, C	Curing Time, hr.	Compressive Strength, psi Fit	Composite Desirability	
1	0.0954	77.9798	48	5872.64	0.942209	
2	0.0954	79.6255	48	5853.21	0.938496	
3	0.0966826	76.0222	47.7868	5756.16	0.919946	
4	0.0954	72.2052	25.8223	4893.58	0.755081	
5	0.113225	79.4789	47.4705	4573.93	0.693984	
6	0.0954	79.3941	17.8230	4508.78	0.681533	
7	0.111458	70.5472	46.7370	4371.34	0.655263	
8	0.104653	69.6078	29.7648	4369.22	0.654859	
9	0.113410	79.1913	18.3938	3739.23	0.534448	

Figure: C.2 Optimization analysis output of samples tested at 14-days.

Parameters						
Response	Goal	Lower	Target	Upper	Weight	Importance
Compressive Strength, psi	Maximum	1005	6138		1	1

Solutions						
Solution	Water:Solids		Curing Time, hr.	Compressive Strength, psi		Composite Desirability
	Ratio	Temperature, C		Fit		
1	0.0954	78.7879	48	6036.49	0.980224	
2	0.0954	77.4460	48	6026.41	0.978260	
3	0.0954	66.2734	45.5503	5093.05	0.796426	
4	0.114147	79.7554	48	4935.75	0.765781	
5	0.0954	70.0944	21.7122	4719.34	0.723619	
6	0.102069	76.1997	23.2406	4669.69	0.713947	
7	0.113754	69.3226	46.7293	4415.15	0.664358	
8	0.104552	69.5	29.4001	4350.03	0.651671	
9	0.113920	79.5987	17.8155	3826.13	0.549606	

Figure: C.3 Optimization analysis output of samples tested at 28-days.

Parameters						
Response	Goal	Lower	Target	Upper	Weight	Importance
Compressive Strength, psi	Maximum	409	6175		1	1

Solutions						
Solution	Water:Solids		Curing Time, hr.	Compressive Strength, psi		Composite Desirability
	Ratio	Temperature, C		Fit		
1	0.0954	79.5960	48	5863.36	0.945951	
2	0.0954	78.6184	48	5858.44	0.945098	
3	0.0964725	77.3555	47.2976	5732.32	0.923226	
4	0.113918	79.9254	48	4658.79	0.737042	
5	0.0954	79.9120	16.4886	4371.07	0.687143	
6	0.0954	69.5954	22.9098	4295.40	0.674021	
7	0.104652	69.5410	29.5083	4074.31	0.635677	
8	0.113339	68.6790	46.0232	4019.06	0.626095	
9	0.102235	76.5770	12.1360	3553.10	0.545283	

Figure: C.4 Optimization analysis output of all samples tested.

APPENDIX D: FREEZE THAW DATA

Table: D.1 Recorded and calculated freeze thaw data of sample 1.70.24.1.

Cumulative Cycle	Mass, kg	n, Hz	C, m ⁻¹	L, m	b, m	t, m	T	K	K/L	Poisson's Ratio	Dynamic E, Gpa	RDM, %
0	4.392	2230	1011.73	0.31	0.078	0.079	1.38	0.0228	0.0735	0.2	22.000	100
33	4.396	1850	1031.43	0.312	0.078	0.079	1.38	0.0228	0.0731	0.2	15.500	69
66	4.366	1550	1061.34	0.311	0.078	0.078	1.38	0.0225	0.0723	0.2	11.000	48
99	4.057	2050	998.92	0.31	0.079	0.079	1.38	0.0228	0.0735	0.2	17.000	85
132	3.962	1380	1001.97	0.309	0.078	0.079	1.38	0.0228	0.0738	0.2	7.500	38

Table: D.2 Recorded and calculated freeze thaw data of sample 1.70.24.2.

Cumulative Cycle	Mass, kg	n, Hz	C, m ⁻¹	L, m	b, m	t, m	T	K	K/L	Poisson's Ratio	Dynamic E, Gpa	RDM, %
0	4.206	2230	1058.06	0.308	0.076	0.078	1.38	0.0225	0.0731	0.2	22.000	100
33	4.206	1830	1114.48	0.308	0.078	0.076	1.38	0.0219	0.0711	0.2	15.500	67
66	4.212	1350	1054.52	0.309	0.077	0.078	1.38	0.0225	0.0728	0.2	8.000	37
99	4.139	2080	1068.4	0.309	0.076	0.078	1.38	0.0225	0.0728	0.2	19.000	87
132	3.703	1480	1528.43	0.308	0.076	0.069	1.38	0.0199	0.0646	0.2	12.500	44

Table: D.3 Recorded and calculated freeze thaw data of sample 2.70.24.1.

Cumulative Cycle	Mass, kg	n, Hz	C, m ⁻¹	L, m	b, m	t, m	T	K	K/L	Poisson's Ratio	Dynamic E, Gpa	RDM, %
0	4.121	2180	1110.71	0.305	0.076	0.076	1.38	0.0219	0.0718	0.2	22.000	100
33	4.103	1830	1107.1	0.306	0.077	0.076	1.38	0.0219	0.0716	0.2	15.000	70
66	4.082	1580	1078.53	0.306	0.076	0.077	1.38	0.0222	0.0725	0.2	11.000	53
99	3.946	1930	1043.79	0.304	0.077	0.077	1.38	0.0222	0.073	0.2	15.500	78
132	3.657	1630	1223.55	0.301	0.069	0.075	1.38	0.0217	0.0721	0.2	12.000	56

Table: D.4 Recorded and calculated freeze thaw data of sample 2.70.24.2.

Cumulative Cycle	Mass, kg	n, Hz	C, m ⁻¹	L, m	b, m	t, m	T	K	K/L	Poisson's Ratio	Dynamic E, Gpa	RDM, %
0	4.112	2150	1110.71	0.305	0.076	0.076	1.38	0.0219	0.0718	0.2	21.000	100
33	4.122	1700	1110.71	0.305	0.076	0.076	1.38	0.0219	0.0718	0.2	13.000	63
66	4.127	1950	1121.67	0.306	0.076	0.076	1.38	0.0219	0.0716	0.2	17.500	82
99	4.108	1780	1078.53	0.306	0.076	0.077	1.38	0.0222	0.0725	0.2	14.000	69
132	3.943	1500	1074.99	0.307	0.077	0.077	1.38	0.0222	0.0723	0.2	9.500	49

Table: D.5 Recorded and calculated freeze thaw data of sample 3.70.24.1.

Cumulative Cycle	Mass, kg	n, Hz	C, m ⁻¹	L, m	b, m	t, m	T	K	K/L	Poisson's Ratio	Dynamic E, Gpa	RDM, %
0	4.045	2050	1078.53	0.306	0.076	0.077	1.38	0.0222	0.0725	0.2	18.500	100
33	4.041	1680	1064.52	0.306	0.077	0.077	1.38	0.0222	0.0725	0.2	12.000	67
66	4.058	1000	1107.1	0.306	0.077	0.076	1.38	0.0219	0.0716	0.2	4.500	24
99	4.000	1780	1024.1	0.306	0.077	0.078	1.38	0.0225	0.0735	0.2	13.000	75
132	3.505	1550	1272.98	0.305	0.069	0.075	1.38	0.0217	0.0711	0.2	10.500	57

Table: D.6 Recorded and calculated freeze thaw data of sample 3.70.24.2.

Cumulative Cycle	Mass, kg	n, Hz	C, m ⁻¹	L, m	b, m	t, m	T	K	K/L	Poisson's Ratio	Dynamic E, Gpa	RDM, %
0	4.00	2000	1110.71	0.305	0.076	0.076	1.38	0.0219	0.0718	0.2	18.000	100
33	4.00	1680	1054.12	0.305	0.077	0.077	1.38	0.0222	0.0728	0.2	12.000	71
66	4.00	1400	1107.1	0.306	0.077	0.076	1.38	0.0219	0.0716	0.2	8.500	49

Table: D.7 Recorded and calculated freeze thaw data of sample 1.70.48.1.

Cumulative Cycle	Mass, kg	n, Hz	C, m ⁻¹	L, m	b, m	t, m	T	K	K/L	Poisson's Ratio	Dynamic E, Gpa	RDM, %
0	4.345	2300	971.15	0.307	0.076	0.08	1.38	0.0231	0.0752	0.2	22.500	100
33	4.369	2300	932.52	0.308	0.077	0.081	1.38	0.0234	0.076	0.2	21.500	100
66	4.373	2080	1086.61	0.308	0.08	0.076	1.38	0.0219	0.0711	0.2	20.500	82
99	4.297	1980	944.79	0.308	0.076	0.081	1.38	0.0234	0.076	0.2	16.000	74
132	4.151	1850	944.79	0.308	0.076	0.081	1.38	0.0234	0.076	0.2	13.500	65
165	4.138	2080	935.62	0.307	0.076	0.081	1.38	0.0234	0.0762	0.2	17.000	82
198	4.042	2050	935.62	0.307	0.076	0.081	1.38	0.0234	0.0762	0.2	16.000	79
231	3.992	1880	957.39	0.308	0.075	0.081	1.38	0.0234	0.076	0.2	13.500	67
264	3.938	1900	1143.8	0.308	0.076	0.076	1.38	0.0219	0.0711	0.2	16.500	68
297	3.738	1750	938.86	0.306	0.075	0.081	1.38	0.0234	0.0765	0.2	10.500	58

Table: D.8 Recorded and calculated freeze thaw data of sample 3.70.48.2.

Cumulative Cycle	Mass, kg	n, Hz	C, m ⁻¹	L, m	b, m	t, m	T	K	K/L	Poisson's Ratio	Dynamic E, Gpa	RDM, %
0	4.244	2230	1100.37	0.308	0.079	0.076	1.38	0.0219	0.0711	0.2	23.000	100
33	4.261	2200	980.67	0.308	0.076	0.08	1.38	0.0231	0.075	0.2	20.000	97
66	4.266	2250	993.74	0.308	0.075	0.08	1.38	0.0231	0.075	0.2	21.500	102
99	4.254	2130	990.25	0.309	0.076	0.08	1.38	0.0231	0.0748	0.2	19.000	91
132	4.246	1980	1111.12	0.309	0.079	0.076	1.38	0.0219	0.0709	0.2	18.500	79
165	4.234	2030	977.39	0.309	0.077	0.08	1.38	0.0231	0.0748	0.2	17.000	83
198	4.179	2000	990.25	0.309	0.076	0.08	1.38	0.0231	0.0748	0.2	16.500	80
231	4.150	1900	990.25	0.309	0.076	0.08	1.38	0.0231	0.0748	0.2	15.000	73
264	4.084	1750	1028.33	0.309	0.076	0.079	1.38	0.0228	0.0738	0.2	13.000	62

Table: D.9 Recorded and calculated freeze thaw data of sample 2.70.48.1.

Cumulative Cycle	Mass, kg	n, Hz	C, m ⁻¹	L, m	b, m	t, m	T	K	K/L	Poisson's Ratio	Dynamic E, Gpa	RDM, %
0	4.171	2200	1074.99	0.307	0.077	0.077	1.38	0.0222	0.0723	0.2	21.500	100
33	4.180	2080	989.28	0.309	0.079	0.079	1.38	0.0228	0.0738	0.2	18.000	89
66	4.122	1950	1044.31	0.308	0.077	0.078	1.38	0.0225	0.0731	0.2	16.500	79
99	4.071	1930	1044.31	0.308	0.077	0.078	1.38	0.0225	0.0731	0.2	16.000	77
132	4.029	2000	1058.06	0.308	0.076	0.078	1.38	0.0225	0.0731	0.2	17.000	83
165	4.010	1880	980.67	0.308	0.076	0.08	1.38	0.0231	0.075	0.2	14.000	73
198	3.926	1350	1058.06	0.308	0.076	0.078	1.38	0.0225	0.0731	0.2	7.500	38

Table: D.10 Recorded and calculated freeze thaw data of sample 3.70.48.2.

Cumulative Cycle	Mass, kg	n, Hz	C, m ⁻¹	L, m	b, m	t, m	T	K	K/L	Poisson's Ratio	Dynamic E, Gpa	RDM, %
0	4.191	2230	1061.21	0.307	0.078	0.077	1.38	0.0222	0.0723	0.2	22.000	100
33	4.227	2200	1074.99	0.307	0.077	0.077	1.38	0.0222	0.0723	0.2	22.000	97
66	4.222	1980	1061.21	0.307	0.078	0.077	1.38	0.0222	0.0723	0.2	17.500	79
99	4.173	1850	1058.05	0.308	0.079	0.077	1.38	0.0222	0.0721	0.2	15.000	69
132	4.124	1730	1092.91	0.306	0.078	0.076	1.38	0.0219	0.0716	0.2	13.500	60

Table: D.11 Recorded and calculated freeze thaw data of sample 3.70.48.1.

Cumulative Cycle	Mass, kg	n, Hz	C, m ⁻¹	L, m	b, m	t, m	T	K	K/L	Poisson's Ratio	Dynamic E, Gpa	RDM, %
0	3.894	2050	1110.71	0.305	0.076	0.076	1.38	0.0219	0.0718	0.2	18.000	100
33	3.930	2000	1110.71	0.305	0.076	0.076	1.38	0.0219	0.0718	0.2	17.500	95
66	3.930	1600	1167.13	0.306	0.076	0.075	1.38	0.0217	0.0709	0.2	11.500	61
99	3.913	1500	1110.71	0.305	0.076	0.076	1.38	0.0219	0.0718	0.2	10.000	54
132	3.907	1800	1110.71	0.305	0.076	0.076	1.38	0.0219	0.0718	0.2	14.000	77
165	3.646	1780	1117.99	0.307	0.077	0.076	1.38	0.0219	0.0713	0.2	13.000	75
198	3.719	1480	1175.95	0.304	0.077	0.074	1.38	0.0214	0.0704	0.2	9.500	52

Table: D.12 Recorded and calculated freeze thaw data of sample 3.70.48.2.

Cumulative Cycle	Mass, kg	n, Hz	C, m ⁻¹	L, m	b, m	t, m	T	K	K/L	Poisson's Ratio	Dynamic E, Gpa	RDM, %
0	3.968	2050	1125.52	0.305	0.075	0.076	1.38	0.0219	0.0718	0.2	19.000	100
33	3.932	1980	1078.53	0.306	0.076	0.077	1.38	0.0222	0.0725	0.2	16.500	93
66	3.812	1750	1103.52	0.303	0.075	0.076	1.38	0.0219	0.0723	0.2	13.000	73
99	3.723	1750	1262.06	0.303	0.074	0.073	1.38	0.0211	0.0696	0.2	14.500	73
132	3.686	1600	1175.33	0.304	0.074	0.075	1.38	0.0217	0.0714	0.2	11.000	61
165	3.909	1500	1061.08	0.303	0.075	0.077	1.38	0.0222	0.0733	0.2	9.500	54

Table: D.13 Recorded and calculated freeze thaw data of sample 1.80.24.1.

Cumulative Cycle	Mass, kg	n, Hz	C, m ⁻¹	L, m	b, m	t, m	T	K	K/L	Poisson's Ratio	Dynamic E, Gpa	RDM, %
0	4.085	2200	1064.52	0.306	0.077	0.077	1.38	0.0222	0.0725	0.2	21.000	100
33	4.086	2000	1014.1	0.305	0.077	0.078	1.38	0.0225	0.0738	0.2	16.500	83
66	4.092	2180	1107.1	0.306	0.077	0.076	1.38	0.0219	0.0716	0.2	21.500	98
99	4.090	1780	1107.1	0.306	0.077	0.076	1.38	0.0219	0.0716	0.2	14.500	65
132	4.098	1850	1064.52	0.306	0.077	0.077	1.38	0.0222	0.0725	0.2	15.000	71
165	4.039	1500	1064.52	0.306	0.077	0.077	1.38	0.0222	0.0725	0.2	9.500	46

Table: D.14 Recorded and calculated freeze thaw data of sample 1.80.24.2.

Cumulative Cycle	Mass, kg	n, Hz	C, m ⁻¹	L, m	b, m	t, m	T	K	K/L	Poisson's Ratio	Dynamic E, Gpa	RDM, %
0	4.051	2150	1078.53	0.306	0.076	0.077	1.38	0.0222	0.0725	0.2	20.000	100
33	4.052	2000	1107.1	0.306	0.077	0.076	1.38	0.0219	0.0716	0.2	18.000	87
66	4.057	1900	1107.1	0.306	0.077	0.076	1.38	0.0219	0.0716	0.2	16.000	78
99	4.055	1830	1107.1	0.306	0.077	0.076	1.38	0.0219	0.0716	0.2	15.000	72
132	4.060	1750	1050.88	0.306	0.078	0.077	1.38	0.0222	0.0725	0.2	13.000	66
165	4.082	1850	1064.52	0.306	0.077	0.077	1.38	0.0222	0.0725	0.2	15.000	74
198	3.980	1630	1030.4	0.304	0.078	0.077	1.38	0.0222	0.073	0.2	11.000	57

Table: D.15 Recorded and calculated freeze thaw data of sample 2.80.24.1.

Cumulative Cycle	Mass, kg	n, Hz	C, m ⁻¹	L, m	b, m	t, m	T	K	K/L	Poisson's Ratio	Dynamic E, Gpa	RDM, %
0	4.054	2200	1027.44	0.305	0.076	0.078	1.38	0.0225	0.0738	0.2	20.000	100
33	4.056	2000	1096.28	0.305	0.077	0.076	1.38	0.0219	0.0718	0.2	18.000	83
66	4.059	2030	1110.71	0.305	0.076	0.076	1.38	0.0219	0.0718	0.2	18.500	85
99	4.054	2080	1024.1	0.306	0.077	0.078	1.38	0.0225	0.0735	0.2	18.000	89
132	4.057	2080	1014.1	0.305	0.077	0.078	1.38	0.0225	0.0738	0.2	18.000	89
165	4.045	1830	1054.12	0.305	0.077	0.077	1.38	0.0222	0.0728	0.2	14.500	69
198	4.034	1800	1096.28	0.305	0.077	0.076	1.38	0.0219	0.0718	0.2	14.500	67
231	4.024	1630	1064.52	0.306	0.077	0.077	1.38	0.0222	0.0725	0.2	11.500	55

Table: D.16 Recorded and calculated freeze thaw data of sample 2.80.24.2.

Cumulative Cycle	Mass, kg	n, Hz	C, m ⁻¹	L, m	b, m	t, m	T	K	K/L	Poisson's Ratio	Dynamic E, Gpa	RDM, %
0	4.031	2180	1067.99	0.305	0.076	0.077	1.38	0.0222	0.0728	0.2	20.500	100
33	4.035	2100	1107.1	0.306	0.077	0.076	1.38	0.0219	0.0716	0.2	19.500	93
66	4.038	2030	1107.1	0.306	0.077	0.076	1.38	0.0219	0.0716	0.2	18.500	87
99	4.022	1850	1064.52	0.306	0.077	0.077	1.38	0.0222	0.0725	0.2	14.500	72
132	4.019	1930	1064.52	0.306	0.077	0.077	1.38	0.0222	0.0725	0.2	16.000	78
165	3.998	1600	1096.28	0.305	0.077	0.076	1.38	0.0219	0.0718	0.2	11.000	54

Table: D.17 Recorded and calculated freeze thaw data of sample 1.80.48.1.

Cumulative Cycle	Mass, kg	n, Hz	C, m ⁻¹	L, m	b, m	t, m	T	K	K/L	Poisson's Ratio	Dynamic E, Gpa	RDM, %
0	4.041	2080	1054.12	0.305	0.077	0.077	1.38	0.0222	0.0728	0.2	18.500	100
33	4.043	1930	1064.52	0.306	0.077	0.077	1.38	0.0222	0.0725	0.2	16.000	86
66	4.023	1800	1078.53	0.306	0.076	0.077	1.38	0.0222	0.0725	0.2	14.000	75
99	4.012	1780	1054.12	0.305	0.077	0.077	1.38	0.0222	0.0728	0.2	13.500	73
132	3.986	1730	1067.99	0.305	0.076	0.077	1.38	0.0222	0.0728	0.2	12.500	69
165	3.920	1500	1199.31	0.306	0.077	0.074	1.38	0.0214	0.0699	0.2	10.500	52

Table: D.18 Recorded and calculated freeze thaw data of sample 1.80.48.2.

Cumulative Cycle	Mass, kg	n, Hz	C, m ⁻¹	L, m	b, m	t, m	T	K	K/L	Poisson's Ratio	Dynamic E, Gpa	RDM, %
0	4.035	2150	1014.1	0.305	0.077	0.078	1.38	0.0225	0.0738	0.2	19.000	100
33	4.022	1850	1107.1	0.306	0.077	0.076	1.38	0.0219	0.0716	0.2	15.000	74
66	3.947	1850	1110.71	0.305	0.076	0.076	1.38	0.0219	0.0718	0.2	15.000	74
99	3.924	1900	1067.99	0.305	0.076	0.077	1.38	0.0222	0.0728	0.2	15.000	78
132	3.904	1800	1191.42	0.304	0.076	0.074	1.38	0.0214	0.0704	0.2	15.000	70
165	3.863	1700	1155.73	0.305	0.076	0.075	1.38	0.0217	0.0711	0.2	13.000	63
198	3.809	1680	1144.4	0.304	0.076	0.075	1.38	0.0217	0.0714	0.2	12.500	61
231	3.764	1500	1099.82	0.304	0.076	0.076	1.38	0.0219	0.072	0.2	9.500	49

Table: D.19 Recorded and calculated freeze thaw data of sample 2.80.48.1.

Cumulative Cycle	Mass, kg	n, Hz	C, m ⁻¹	L, m	b, m	t, m	T	K	K/L	Poisson's Ratio	Dynamic E, Gpa	RDM, %
0	4.172	2130	1005.16	0.308	0.077	0.079	1.38	0.0228	0.074	0.2	19.000	100
33	4.195	2080	1058.05	0.308	0.079	0.077	1.38	0.0222	0.0721	0.2	19.000	95
66	4.193	1830	1068.39	0.309	0.079	0.077	1.38	0.0222	0.0718	0.2	15.000	74
99	4.195	1900	1058.05	0.308	0.079	0.077	1.38	0.0222	0.0721	0.2	16.000	80
132	4.188	1800	1058.05	0.308	0.079	0.077	1.38	0.0222	0.0721	0.2	14.500	71
165	4.198	1700	1018.38	0.308	0.076	0.079	1.38	0.0228	0.074	0.2	12.500	64
198	4.177	1400	1014.98	0.309	0.077	0.079	1.38	0.0228	0.0738	0.2	8.500	43

Table: D.20 Recorded and calculated freeze thaw data of sample 2.80.48.2.

Cumulative Cycle	Mass, kg	n, Hz	C, m ⁻¹	L, m	b, m	t, m	T	K	K/L	Poisson's Ratio	Dynamic E, Gpa	RDM, %
0	4.169	2130	1058.05	0.308	0.079	0.077	1.38	0.0222	0.0721	0.2	20.000	100
33	4.201	1850	1017.88	0.308	0.079	0.078	1.38	0.0225	0.0731	0.2	14.500	75
66	4.194	2030	1061.21	0.307	0.078	0.077	1.38	0.0222	0.0723	0.2	18.500	91
99	4.196	2080	1047.78	0.307	0.079	0.077	1.38	0.0222	0.0723	0.2	19.000	95
132	4.194	2000	1058.05	0.308	0.079	0.077	1.38	0.0222	0.0721	0.2	17.500	88
165	4.197	1830	982.64	0.307	0.078	0.079	1.38	0.0228	0.0743	0.2	14.000	74
198	4.190	1750	967.93	0.308	0.077	0.08	1.38	0.0231	0.075	0.2	12.500	68
231	4.198	1600	979.71	0.308	0.079	0.079	1.38	0.0228	0.074	0.2	10.500	56

Table: D.21 Recorded and calculated freeze thaw data of sample 3.80.48.1.

Cumulative Cycle	Mass, kg	n, Hz	C, m ⁻¹	L, m	b, m	t, m	T	K	K/L	Poisson's Ratio	Dynamic E, Gpa	RDM, %
0	4.426	2200	932.52	0.308	0.077	0.081	1.38	0.0234	0.076	0.2	20.000	100
33	4.181	1830	948.1	0.307	0.075	0.081	1.38	0.0234	0.0762	0.2	13.500	69
66	4.111	1600	938.86	0.306	0.075	0.081	1.38	0.0234	0.0765	0.2	10.000	53

Table: D.22 Recorded and calculated freeze thaw data of sample 3.80.48.2.

Cumulative Cycle	Mass, kg	n, Hz	C, m ⁻¹	L, m	b, m	t, m	T	K	K/L	Poisson's Ratio	Dynamic E, Gpa	RDM, %
0	4.376	2330	954.03	0.309	0.076	0.081	1.38	0.0234	0.0757	0.2	22.500	100
33	4.096	2050	1013.23	0.31	0.075	0.08	1.38	0.0231	0.0745	0.2	17.500	77
66	3.854	1550	1061.75	0.307	0.075	0.078	1.38	0.0225	0.0733	0.2	10.000	44
99	3.655	1880	1145.01	0.304	0.073	0.076	1.38	0.0219	0.072	0.2	15.000	65
132	3.343	1650	1560.52	0.306	0.067	0.071	1.38	0.0205	0.067	0.2	14.000	50

APPENDIX E: FREEZE THAW SAMPLE PICTURES



Figure: E.1 Sample 1.70.24.2 at 66 of 132 cycles.

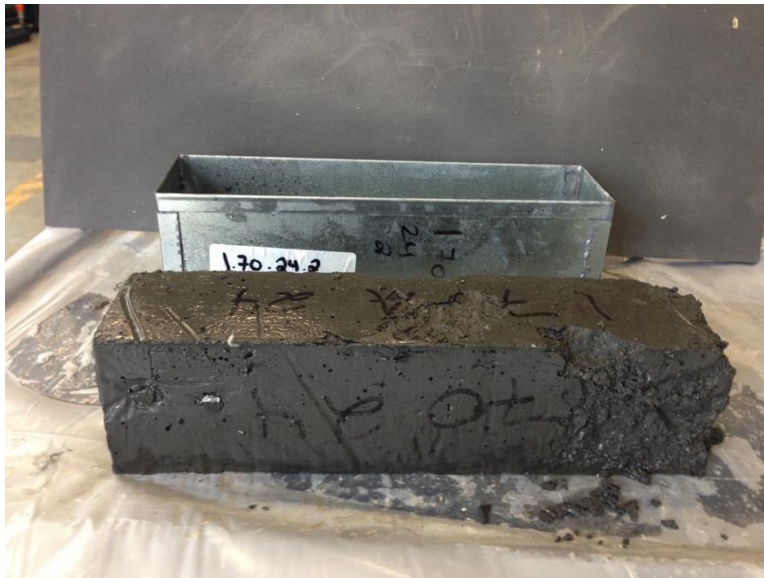


Figure: E.2 Sample 1.70.24.2 at 99 of 132 cycles.

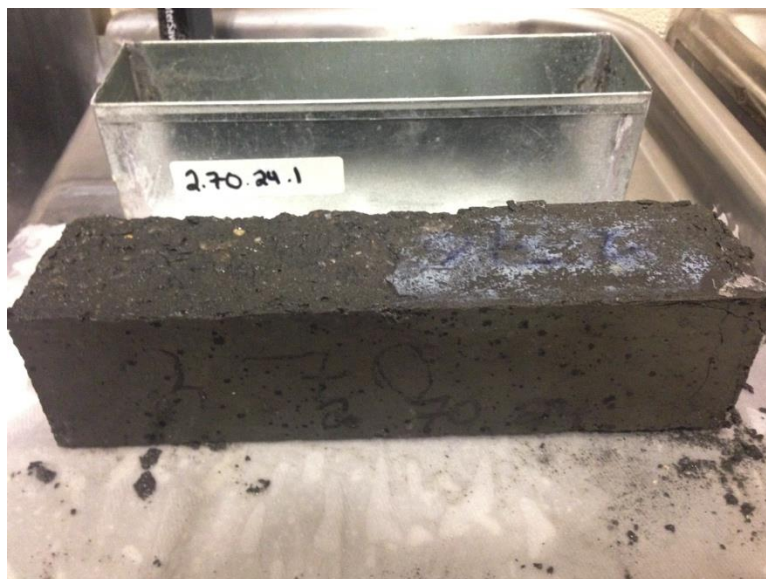


Figure: E.3. Sample 2.70.24.1 at 66 of 132 cycles.



Figure: E.4. Sample 2.70.24.1 at 99 of 132 cycles.

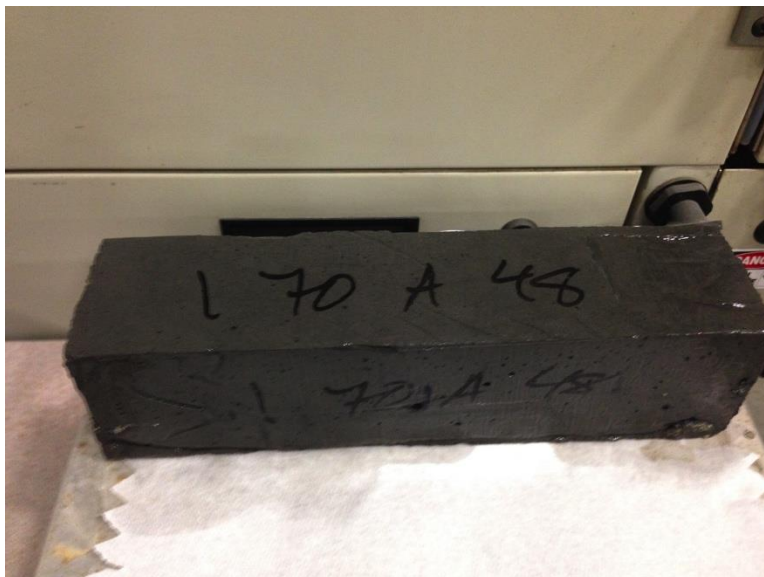


Figure: E.5 Sample 1.70.48.2 at 66 of 264 cycles.



Figure: E.6 Sample 1.70.48.2 at 99 of 264 cycles.

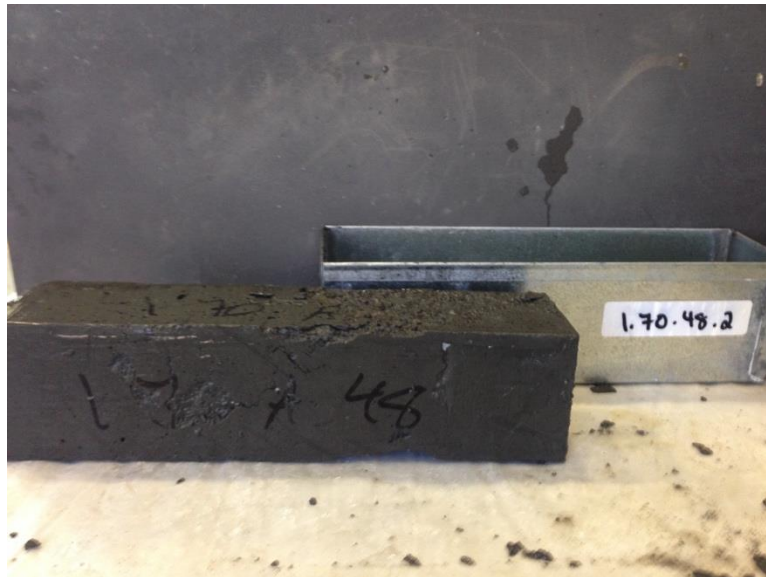


Figure: E.7 Sample 1.70.48.2 at 198 of 264 cycles.



Figure: E.8 Sample 1.70.48.2 at 264 of 264 cycles.

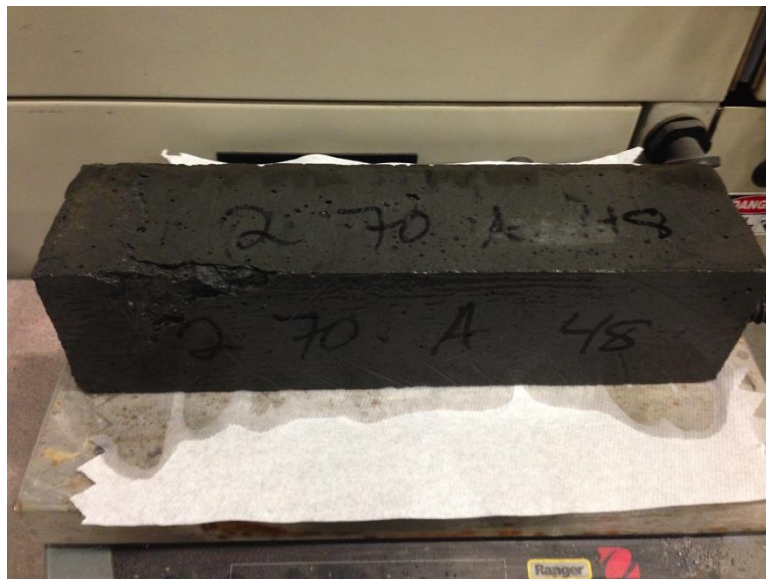


Figure: E.9 Sample 2.70.48.1 at 66 of 132 cycles.



Figure: E.10 Sample 2.70.48.1 at 165 of 198 cycles.



Figure: E.11 Sample 2.70.48.1 at 198 of 198 cycles.

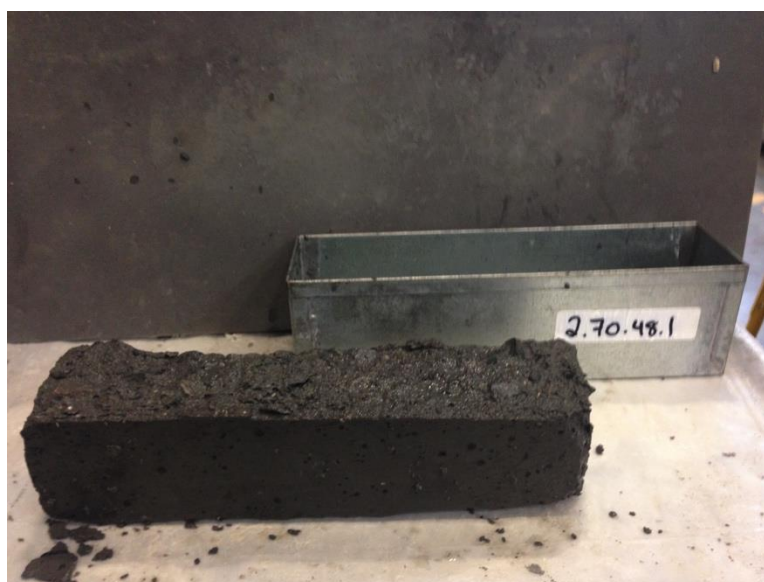


Figure: E.12 Sample 2.70.48.1 at 264 cycles, 66 cycles past the 60% of initial dynamic modulus.



Figure: E.13 Sample 3.70.48.2 at 198 of 198 cycles.



Figure: E.14 Sample 2.80.24.1 at 33 of 231 cycles.



Figure: E.15 Sample 2.8.0.24.1 at 99 of 231 cycles.



Figure: E.16 Sample 2.80.24.1 at 231 of 231 cycles.



Figure: E.17 Sample 1.80.48.2 at 33 of 231 cycles.



Figure: E.18 Sample 1.80.48.2 at 66 of 231 cycles.



Figure: E.19 Sample 1.80.48.2 at 231 of 231 cycles.



Figure: E.20 Sample 2.80.48.1 at 33 of 198 cycles.



Figure: E.21 Sample 2.80.48.1 at 198 of 198 cycles.



Figure: E.22 Sample 3.80.48.2 at 33 of 132 cycles.